Dipl.-Ing. Marie-Luise Lechner

Synthesis and characterization of organotin compounds

Dissertation

zur Erlangung des akademischen Grades eines Doktor der technischen Wissenschaften

erreicht an der

Technischen Universität Graz

Univ.-Prof. Dipl.-Chem. Dr.rer.nat. Frank Uhlig
Institut für Anorganische Chemie

Technische Universität Graz

2010

'if it was so, it might be; and if it were so, it would be; but as it isn't, it ain't. That's logic.'

Lewis Carroll

Acknowledgment

I acknowledge Evelyne Maier, Helmar Wiltsche, Andreas Ranz, Xinghua Guo and Herbert Motter for their analytical support.

I also acknowledge the work group of Prof. Uhlig at the Departement of Inorganic Chemistry.

Special thanks to Monika and Babsi for their support and friendship. Also thanks for constantly supplying me with books, chocolate and maths problems.

Special thanks to Roland for helping ideas, discussion, the NMR support, the crystal structure solving and your hardly ever ending patience.

I acknowledge Jörg Albering for crystal structure measurement.

I acknowledge the Paul Smith group in Zürich for their warm welcoming and their support. 'Merci vielmals' to Walter Caseri, Markus Trummer and Stefan Busato for their helping hand and discussion. I also acknowledge Doris Sutter for NMR measurement.

Thanks to all the students who worked for me during their lab courses.

Special thanks for Claudia. I would not have been able to do the whole work without your helping hands and it would have been half the fun.

Also special thanks to Michael Scherzer for becoming my first Bacchelor student.

Special thanks to my supervisor Frank Uhlig. I am grateful for your encouragement and support. I also appreciated the freedom you gave me and the relaxed work atmosphere.

I acknowledge the 'FORTE Wissenschaftlerinnen College' for their financial support.

Contents

Chapter 2

Introduction

Tin has been known for over 5000 years when people discovered that alloying copper with tin gives a hard alloy. This period is known as the Bronze Age. Today tin still is of great industrial importance. Half of the produced tin is used in solders successively replacing lead. Further uses are tin plates, glass coatings, alloys and chemicals[10].

Due to the high toxicity organotin compounds were abandoned in the past. The use as ship anti fouling agent was, for instance, shut out due to the toxic effects on the marine life. Today however the possible applications and analytical techniques of organotin Chemistry are growing fast. In addition to X-ray and ESR methods, new NMR and Computational methods have been established. Thus a large variety of organotin structures could be determined.

The main application for organotin compounds is used as a stabilizer for PVC. Due to the toxiticity of some organotin compounds they are also used in larvicides, insecticides and fungicides. Furthermore, organotin compounds are considered as anti tumor agents and as ionopores in sensors.

In addition, organotin compounds provide a variety of application in Organic Chemistry. They are used for cross coupling reaction such as Stille coupling or esterification. In addition organotin compounds can be used as catalysts in the formation of urethanes from isocyanates and a hydroxyl compound. In order to avoid toxic byproducts, attempts to bind organotin compounds to a solid matrix were made[10].

The aim of this thesis was to investigate the formation of tin tin, as well as tin-metal bonds, and to characterize the resulting products by state of the art analytical methods. The formation of tin tin bonds can be done through three different pathways. When using chlorinated monostannanes (R_3SnCl or R_2SnCl_2) as starting materials bond formation can be done with alkaline[46] or earth alkaline metals[6](figure 2.1). These Wurtz or Wurtz-like reactions are the most common reactions for tin tin coupling. In general, these methods lead to a high percentage of

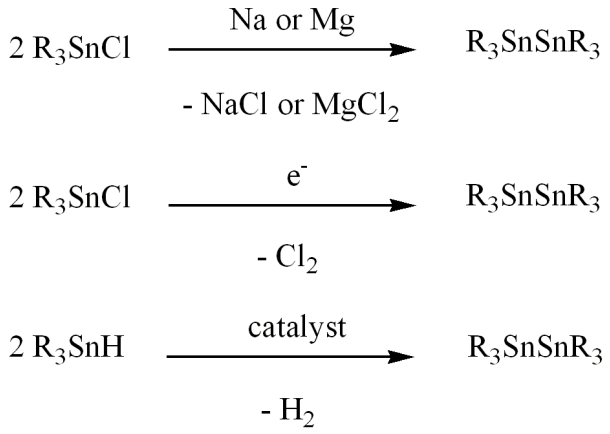

Figure 2.1: Possible methods for Sn Sn bond formation

cyclic products, which can be isolated with high yields. Electrochemical reactions in which chlorine is eliminated, are far less common[39] (figure 2.1).

Tin tin bonds can also be established by starting with tin hydrides(figure 2.1). Different transition metal catalysts are used for such dehydrogenating coupling[1]. Nowadays, also rare earth metal catalysts are quite common[9]. However, only a few tin tin coupling of reactions using a base as catalyst are described by Davies[9] or Neumann et al.[38]. These reactions generally result in a mixture of cyclic and linear tin poly- and oligomers. The product contribution is highly dependent on the reaction conditions.

The polymerisation of dialkylstannanes is well known. Among the products. polydibutylstannane has been very well characterized by several authors[10]. On the contrary diarylpolystannanes gained little attention in literature[29]. One reason for that could be the bad solubility of these substances that impedes characterization methods like NMR measurements or GPC analysis.

1. In the first part of this thesis unknown or just partly described diaryldichlorostannanes will be presented. Structural data, as well as, NMR shifts will be discussed. These compounds were also used as educts for different further on reactions.

2. In the following part the formation of tin tin bonds starting from different dichloromonostannanes using magnesium will be described. Using *di^{t}butyldichlorostannane* as educt a monofunctionalized tetrastannacyclobutane was formed. In addition a series of derivatisation reactions of the resulting product carried out.

3. In a last part TMEDA was used to fulfill the role as catalytic base to form tin bonds in a dehydrogenative coupling on th one hand. On the other hand

it functioned as stabilization reagent when used in combination with dialkylmagnesium or -zinc compounds. These methods and the corresponding products will be described and compared.

Chapter 3

Diaryldichlorstannanes

3.1 Introduction

The first *diaryldichlorostannanes* where described in the 1930s by Kocheskov et al[23]. Among them where *diphenyldichlorostannane*, *di-o-tolyldichlorostannane*, *di-m-tolyldichlorostannane* and *di-p-tolyldichlorostannane*. Only *diphenyldichlorostannane* has been structurally described so far[21]. In addition, crystal structures of *dimesityl-dichlorostannane*[5], *bis*(*triisopropylphenyl*)-*dichlorostannane* [45], as well as, *disupermesityldichlorostannane*[51] were reported.

Table 3.1: List of educts for polymerization described by Tilley et al.[29] [28]

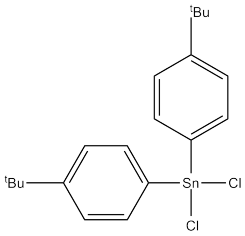	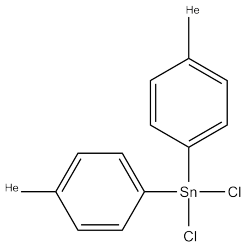	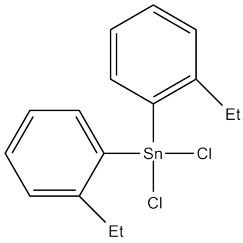	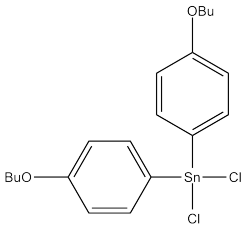
bis-p- (^{t}*butylphenyl*)- *dichlorostannane*	*bis-p-* (^{n}*hexylphenyl*)- *dichlorostannane*	*bis-o-* (*ethylphenyl*)- *dichlorostannane*	*bis-p-* (*butoxyphenyl*)- *dichlorostannane*
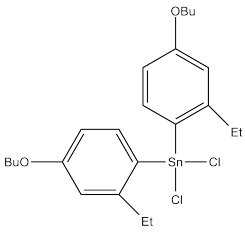	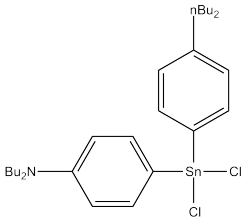	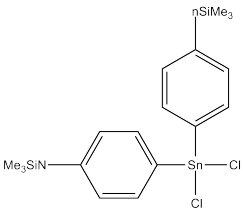	
bis-(4-*butoxy-* 2-*ethylphenyl*)- *dichlorostannane*	*bis-*(N, N- *dibutylaniline*)- *dichlorostannane*	*bis-*(N, N- *bistrimethylsilylanyline*)- *dichlorostannane*	

Due to simple synthesis, *diphenyldichlorostannane* is the most used diaryldichlorostannane. Nowadays however the interest in different diaryldichlorostannes and diaryldihydrostannanes (further on only named diarylstannanes) is increasing. Most of them are used as educts for polymerization as described by Tilly et al.[29] [28] (see table 3.1). Bulkier aryl substituents as *triisopropylphenyl*[36] or *supermesityl*[51] are used in stannylene synthesis.

3.2 General remarks

Table 3.2: List of diaryldichlorostannanes synthesized in this thesis

name	description	ref
diphenyldichlorostannane **42**	white crystals	[23]
di-o-tolyldichlorostannane **53**	colorless liquid	[23]
di-m-tolyldichlorostannane **51**	brownish solid	[23]
di-p-tolyldichlorostannane **48**	colorless liquid	[23]
bis-(p-butylphenyl)stannane **56**	light yellow liquid	*
bis-(3, 5-*dimethylphenyldichlorostannane* **59**	white solid	*

* diaryldichlorostannane first described in this thesis

In this thesis different types of diarylstannanes were synthesized out of the corresponding diaryldichlorostannanes(see table 3.2). The former were used as educts for polymerization reaction. Furthermore, they reacted with either *dibutylmagnesium* or *diethylzinc* to from tin metal bonds.

Attempts to synthesize *bis-*(3, 5-*dimethylphenyl)dichlorostannane* **59** were made. Instead of the disubstituted product the mono substituted (3, 5-*dimethyl-phenyl)trichlorostannane* **60** crystallized as *acetone* adduct out of the reaction mixture. **59** could only be obtained in a second attempt. In addition, also single crystals of *di-m-tolyldichlorostannane* **51** and *di-p-tolyldichlorostannane* **48** could be isolated.

3.3 Discussion of the crystal structure

3.3.1 Comparison of *di-p-tolyldichlorostannane* 48 and *di-m-tolyldichlorostannane* 51

As *di-p-tolyldichlorostannane* **48** and *di-m-tolyldichlorostannane* **51** only differ in the position of the methyl group on the ligand they were expected to have similar

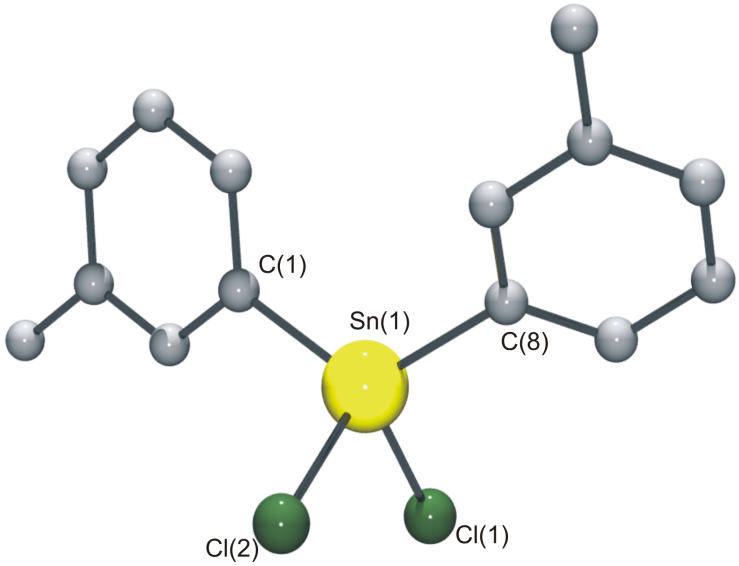

Figure 3.1: Crystal structure of **51** (Hydrogen atoms omitted for clarity) Selected bond lengths [Å] and angles [°] for **51**: Sn-Cl(1): 2.3362(7); Sn-Cl(2):2.3516(7); Sn-C(1):2.106(2); Sn-C(8):2.107(2); Cl(1)-Sn-Cl(2):100.68(3); C(1)-Sn-C(8):122.15(10); Cl(1)-Sn-C(1):108.35(7); Cl(1)-Sn-C(8):107.80(7); Cl(2)-Sn-C(1):107.26(7); Cl(2)-Sn-C(8):108.50(7);

physical properties. Their physical appearance however is quite different. **48** is a colorless liquid which solidifies at about 6°C to form white crystals. These crystals are in the monoclinic space group C2/c with 8 molecules in the unit cell. On the contrary, **51** is a light brownish solid consisting of small needle like crystals. This substance crystallizes in the orthorhombic space group Pbca with also 8 molecules in the unit cell.

However, the structural characteristics of **48** and **51** are quite similar. Sn-C distances range for both molecules from 2.1 Å onwards, which corresponds to the average Sn-C distance. Also Sn-Cl distances range from 2.336 Å to 2.352 Å. The four ligands are arranged around the tin atom to form a tetrahedral coordination sphere. However, the C-Sn-C angle is over 10° larger than the expected tetrahedral angle. This is most probably due to the steric demand of the *m-tolyl* as well as the *p-tolyl* group.

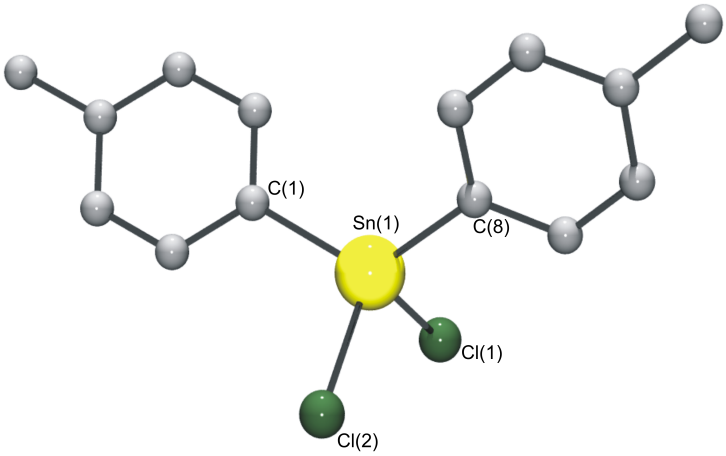

Figure 3.2: Crystal structure of **48** (Hydrogen atoms omitted for clarity) Selected bond lengths [Å] and angles [°] for **48**: Sn-Cl(1): 2.3391(7); Sn-Cl(2):2.3440(7); Sn-C(1):2.101(3); Sn-C(8):2.105(3); Cl(1)-Sn-Cl(2):101.18(3); C(1)-Sn-C(8):121.78(14);Cl(1)-Sn-C(1):109.58(8); Cl(1)-Sn-C(8):106.15(10); Cl(2)-Sn-C(1):105.74(9); Cl(2)-Sn-C(8):110.53(7);

3.3.2 Discussion of the structure of $3,5$-*dimethylphenyltrichlorostannane*acetone* **60**

$3,5$-*Dimethylphenyldichlorostannane*acetone* **60** crystallizes in the monoclinic space group P2(1)¸ There are 4 identical molecules in the unit cell. Due to the coordination of the *acetone* molecule, the Sn atom is penta coordinated and the molecule forms a trigonal bi pyramidal structure with Cl(3) and the *acetone* in axial position and the other Cl atoms, as well as, the aryl group in the planar position. Sn-Cl distances range from 2.325 to 2.389 Å. The bonding between Sn and Cl(3) (2.389 Å) is somewhat larger than the other Sn-Cl distances, which fall from 2.33 to 2.39 Å. This is due to the bi pyramidal coordination sphere. The Sn-C bonding is 2.109 Å which is about the common Sn-C distance. The Sn-O distance is 2.372 Å which is also somewhat larger than a normal Sn-O bonding.

The angles vary in a way that is expected for a trigonal bi pyramidal structure. The Cl(1)-Sn-Cl(2) angle is 114.81°. Two Cl-Sn-C angles vary from 117.81° to

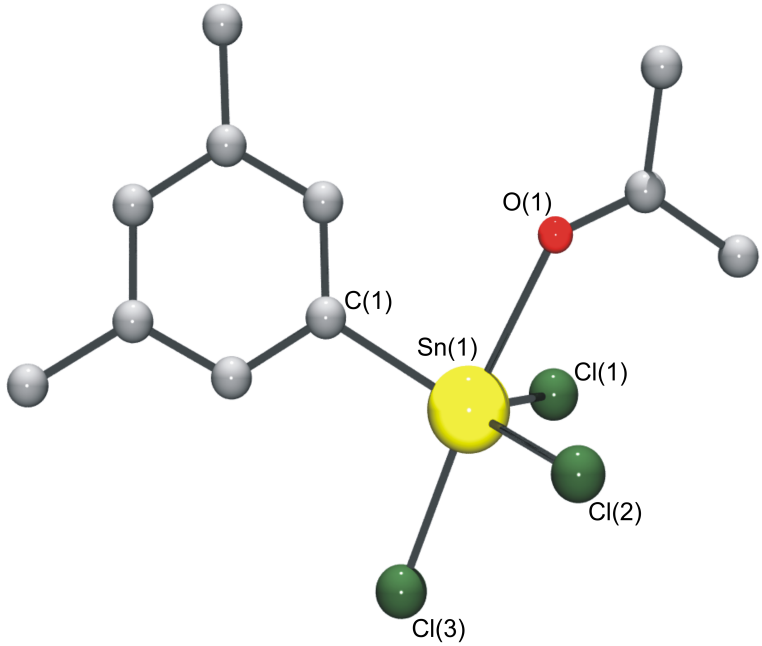

Figure 3.3: Crystal structure of **60** (Hydrogen atoms omitted for clarity) Selected bond lengths [Å] and angles [°] for **60**: Sn-Cl(1):2.3346(4); Sn-Cl(2):2.3891(5); Sn-Cl(3):2.3251(5); Sn-O:2.3721(13); Sn-C(1):2.1086(16); Cl(1)-Sn-Cl(2):93.712(17); Cl(1)-Sn-Cl(3):114.812(19); Cl(1)-Sn-O:81.23(3); Cl(1)-Sn-C(1):123.95(5); Cl(2)-Sn-Cl(3):94.738(18); Cl(2)-Sn-O:173.66(3); Cl(2)-Sn-C(1):100.58(5); Cl(3)-Sn-O:84.02(3); Cl(3)-Sn-C(1):117.52(5); O-Sn-C(1):85.47(5);

123.95°. The difference is most probably due to the sterical demand of the aryl group. The O-Sn-Cl(3) angle (173.66°) is to some extent smaller than 180°.

3.3.3 Comparison with diaryldichlorostannane described in literature

The most characteristic features of the structures are their tetrahedral angles. In general, the C-Sn-C angle is to some extend larger than the Cl-Sn-Cl angle. This is due to the sterical demand of the aryl group. However, the difference between the C-Sn-C angle of the different diaryldichlorostannane is not dependent on the bulkiness of the substituent. On the contrary the C-Sn-C angle of $Supmes_2SnCl_2$ is 116.96°, which is the smallest angle of the literature known compounds.

Table 3.3: Structural characteristics of *di-m-tolyldichlorostannane*, *di-p-tolyldichlorostannane* and 3, 5-*dimethylphenyldichlorostannane*acetone* in comparison to literature known diaryldichlorostannanes

name	bonding [Å]		angles [°]		torsion between the aryl groups [°]	ref
	Sn-C	Sn-Cl	C-Sn-C	Cl-Sn-Cl		
Ph_2SnCl_2	2.112-2.117	2.337-2.357	126.95	97.87	45.60	[21]
$(iPr_3)Ph_2SnCl_2$	2.146	2.352	120.40	98.06	60.51	[45]
Mes_2SnCl_2	2.117	2.414	119.71	100.28	99.01	[36]
$Supmes_2SnCl_2$	2.194-2.202	2.370-2.371	116.96	94.48	78.22	[51]
$m\text{-}Tol_2SnCl_2$	2.105-2.107	2.336-2.352	122.15	100.68	30.78	*
$p\text{-}Tol_2SnCl_2$	2.101-2.105	2.339-2.344	121.77	101.18	46.11	*
$(Me_2Ph)SnCl_3$* *acetone*	2.109	2.325-2.389		93.71-114.81		*

*Crystal structures first described in this thesis.

In order to get a convenient arrangement of the bulkier substituents the aryl groups tend to twist. Larger torsion angles between the plane of the aryl groups of the bulkier subtituents could be observed (60.51°-99.01°), whereas smaller substituents have torsion angles between 30.78° to 46.11°. (See table 3.3)

3.4 Discussion of the NMR data

3.4.1 Comparison of the ^{119}Sn NMR shift of different diaryldichlorostannane

The ^{119}Sn NMR shifts of the different diaryldichlorostannanes are listed in table 3.4.

3.4.2 Influence of concentration and solvents on the ^{119}Sn NMR shift of different diaryldichlorostannane

Part of this section was done in a Bachelor thesis carried out by Michael Scherzer.

The influence of the concentration and different solvents on the ^{119}Sn NMR shift of selected diaryldichlorostannane were investigated. The diaryldichlorostannane used are listed in table 3.4. The *di^{t}butyldichlorostannane* was measured as reference.

Table 3.4: Diaryldichlorostannane used for NMR data comparison

name	^{119}Sn NMR shift in $CDCl_3$
diphenyldichlorostannane **42**	-45 ppm
di-m-tolyldichlorostannane **51**	-42 ppm
di-p-tolyldichlorostannane **48**	-35 ppm
bis-(3,5-dimethylphenyl)dichlorostannane **59**	-26 ppm

Concentration: The diaryldichlorostannanes were measured at 5 different concentrations ranging from 0.2 to 0.0125 mol l^{-1}. The results are listed in table 3.5. For each diarylstannane a small shift to low field of the signal could be observed. However, the difference is below 3 ppm which is too small to be worth mentioned.

Table 3.5: ^{119}Sn NMR data of different diaryldichlorostannane at different concentrations

	0.2 mol l^{-1}	0.1 mol l^{-1}	0.05 mol l^{-1}	0.025 mol l^{-1}	0.0125 mol l^{-1}
Ph_2SnCl_2 **42** [ppm]	-44.6	-45.5	-47.2	-47.5	-49.7
δ ppm	0	-0.9	-2.5	-2.9	-5.0
m-Tol_2SnCl_2 **51** [ppm]	-41.7	-43.1	-43.5	-43.9	-44.2
δ ppm	0	-1.4	-1.8	-2.2	-2.5
p-Tol_2SnCl_2 **48** [ppm]	-34.7	-36.4	-37.0	-36.6	*
δ ppm	0	-1.7	-2.3	-1.9	
$(3,5\text{-}Me_2Ph)_2SnCl_2$ **59** [ppm]	-32.4	-33.5	-38.6	-36.5	-36.5
δ ppm	0	-	-	-	
$^tBu_2SnCl_2$ **35** [ppm]	54.3	53.6	53.3	53.3	53.6

*Due to the high dilusion no signal could be obtained.

Non coordinating solvents: The influence of the solvent's polarity was tested. Weak coordinating solvents were used in order to eliminate coordination effects such as pentane, chloroform, toluene. All data is listed in table 3.6.

Table 3.6: NMR data of different diaryldichlorostannane solved in selected non coordinating solvents

	pentane	toluene	chloroform
dipole moment [D]	0		1.01
Ph_2SnCl_2 **42** [ppm]	- 26.5	-28.2	-44.7
δ ppm	0	-1.7	-18.2
m-Tol_2SnCl_2 **51** [ppm]	-25.1	-26.2	-41.7
δ ppm	0	-1.1	-16.6
p-Tol_2SnCl_2 **48** [ppm]	-20.1	-20.7	-34.8
δ ppm	0	-0.6	-14.7
$(3,5\text{-}Me_2Ph)_2SnCl_2$ **59** [ppm]	-24.4	-24.9	-32.4
δ ppm	0	-0.5	-6.0
$^tBu_2SnCl_2$ **35** [ppm]	54.8	54.5	54.3

Hardly any shift differences between the pentane samples and the toluene samples could be found. However, differences up to 18 ppm were found between pentane samples and chloroform samples. Thus no linear correlation between polarity and ^{119}Sn NMR shift could be observed. The shift differences of $(3,5\text{-}Me_2Ph)_2SnCl_2$ **59** measured in pentane and measured in chloroform is the lowest. The larger sterical shielding of the tin atoms with bulkier substituents might be the reason.

Coordinating solvent: THF was successively added to a solution of diaryldichlorostannane in chloroform. After every addition, NMR samples were made. All data is listed in table 3.7. As the amount of compound and the amount of THF were minor, larger errors are expected. Therefore, the obtained results can only be seen as estimation.

However, the data clearly shows that even addition of small amounts of THF result in large shifts differences up to -50 ppm. Lowest shift differences were obtained for $(3,5\text{-}Me_2Ph)_2SnCl_2$ **59**. Again sterical shielding might be the reason.

Most NMR data of pure compounds were measured in deuterated chloroform. However, samples of reaction solution contain various types of solvents. The obtained results for non coordinating and coordinating solvents clearly shows that polarity as well as coordination ability of the solvent has to be considered when interpreting ^{119}Sn NMR spectra of reaction solutions.

Table 3.7: NMR data of selected diaryldichlorostannane with different compound to THF ratios

Compound:THF	1:0	1:1	1:2	1:5
Ph_2SnCl_2 **42** [ppm]	-45.1	-55.6	-66.0	-91.5
δ ppm	0	-11	-21	-46
m-Tol_2SnCl_2 **51** [ppm]	-38.9	-40.2	-43.0	-73.6
δ ppm	0	-1	-4	-35
p-Tol_2SnCl_2 **48** [ppm]	-34.8	-72.4	-81.3	-87.8
δ ppm	0	-38	-47	-53
$(3,5\text{-}Me_2Ph)_2SnCl_2$ **59** [ppm]	-32.4	-39.0	-47.5	-63.8
δ ppm	0	-7	-15	-31
${}^tBu_2SnCl_2$ **35** [ppm]	54.3	53.8	53.3	53.6

Chapter 4

Monofunctionalized four membered tin ring systems

4.1 Introduction

Four membered tin ring Parts of this chapter were published in the Journal of Organometallic Chemistry[27].

Different types of four membered tin ring systems are described in literature. The ring size of cyclostannanes is dependent on the bulkiness of the substituent. So only four membered ring systems with large substituents such as $^{t}butyl$, or larger aromatic systems are known. In 1964 Farrar et al.[19] published a synthesis, leading to *octa-*^{t}*butyltetrastannacyclobutane*. It was not until twenty years later when Puff et al.[41] fully characterized this product. Puff et al. also presented the crystal structure of *octa-*^{t}*amyltetrastannacyclobutane*[41].

Neumann et al.[37] analyzed different types of perphenantryl substituted cyclostannanes. Among them was *octa-phenantryltetrastannacyclobutane*, being the only structurally described fully aryl substituted four membered tin ring so far. Also *octa-phenyltetrastannacyclobutane*[4], as well as *octa-methyltetrastannacyclobutane*[2] were postulated. However, as their structures have never been proved by XRD analysis, their existences is quite unlikely.

There are also tetrastannanes with silicon containing substituents. *Octakis-((trimethylsilyl)-methyl)- tetrastannacyclobutane*[3] was structurally described.

Few functionalized cyclotetrastannanes are known. Mallela et al.[31] reported on the synthesis and structure of $1,2,3,4$-*tetra-chloro*-$1,2,3,4$-*tetrakis-(tris-(tri methylsilyl)- silyl)tetra-stannacyclobutane* as well as the germanium containing analog cyclotetrastannane: $1,2,3,4$-*tetra-chloro*-$1,2,3,4$-*tetrakis-(tris-(trimethylsilyl)- germyl)tetrastannacyclobutane*.

1-*Bromo*-$1,2,2,3,3,4,4$-*heptakis-*$(2,6-$*diethylphenyl*$)$-[7] and $1,1,2,2,3,3,4$-*heptakis-* $(2,6-$*diethylphenyl*$)$-*tetrastannacyclobutane*[46] have been the only iso-

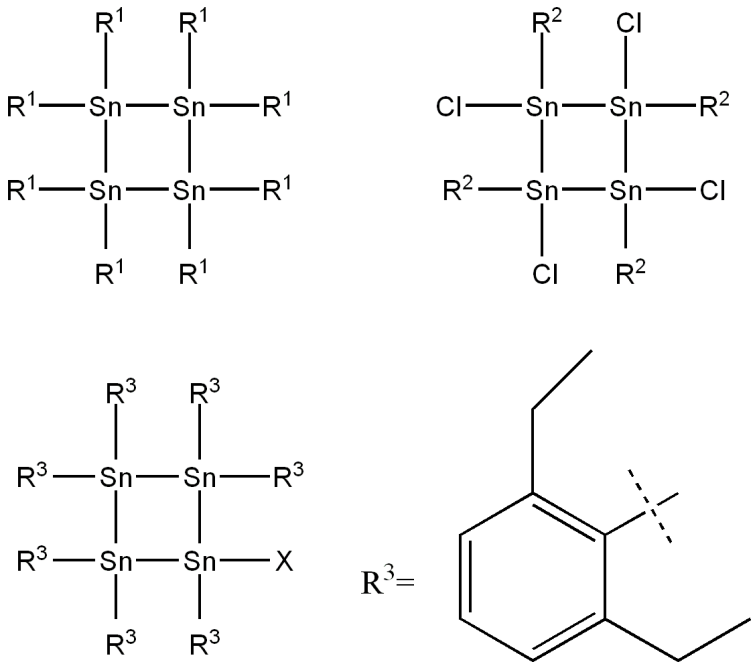

Figure 4.1: Different tetrastannacyclobutanes known in literature: R^1=$^t Bu$[19], $^t amyl$[41], *phen*[37], *Me*[2], *Ph*[4]; R^2=$(Me_3Si)_3Si$, $(Me_3Si)_3Ge$[31]; X= Br[7], H[46];

lated and structurally characterized monofunctionalized tetrastannacyclobutanes so far. In addition, a possible mechanism of the formation of the latter was described, postulating an anionic monofunctionalized four membered tin ring as an intermediate. However, neither the existence of this intermediate could be proved by spectroscopic methods, nor could it be isolated.

Decker described in her PhD thesis[11] that stirring 1, 4-*dichloro*-1, 1, 2, 2, 3, 3, 4, 4-*octa*-^{t}*butyltetra-stannane* in the presence of excess magnesium leads to a dark read solution. This solution was characterized by NMR clearly displacing three signals with 1 : 2 : 1 ratio in ^{119}Sn NMR. Due to the coupling pattern she concluded that the main product was a monofunctionalized four membered tin ring: 1, 1, 2, 2, 3, 3, 4-*hepta*-^{t}*butyl*-4-*chloromagnesiotetrastannacyclobutane* **62**.

In order to prove the identity of this four membered ring by reactivity, a couple of derivatisation reactions were carried out and the corresponding product were investigated with ^{119}Sn NMR. The conversion of **62** with alkylhalogenides (MeI and EtBr) leads to the corresponding alkyl substituated four membered tin rings: 1, 1, 2, 2, 3, 3, 4-*hepta*-^{t}*butyl*-4-*methyltetrastannacyclobutane* and 1, 1, 2, 2, 3, 3, 4-*hepta*-^{t}*butyl*-4-*ethyltetrastannacyclobutane*. Chloroform was added to **62**, too. This lead to 1-*chloro*-1, 2, 2, 3, 3, 4, 4-*hepta*-^{t}*butyltetrastannacyclobutane*. However, none of these monofunctionalized tin ring systems were structurally characterized by XRD measurement.

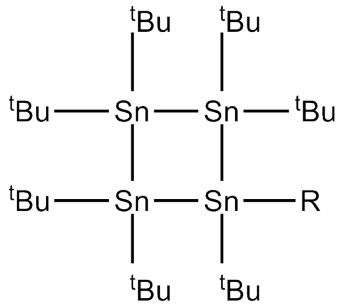

Figure 4.2: Monofunctionalized tetrastannacyclobutanes described by Katharina Decker: R=MgCl, Me, Et, Cl[11]

Other tin ring systems There are also a couple of six and five membered tin ring system with less bulkier substituents. However, only *dodeca-phenylhexastannacyclohexane*, as well as *dodeca-benzylhexastannacyclohexane* were structurally characterized by Puff et al.[40] in 1984. No crystal structure of any five membered tin ring system has been reported so far. *Dodeca-methylhexastannacyclohexane*, *dodeca-ethylhexastannacyclohexane*, *dodeca-octylhexastannacyclohexane* as well as *decabutyl-pentastannacyclopentane* were postulated. But as all tin atoms in one ring system are structurally equal, they all result in just on signal in ^{119}Sn NMR. Therefore, no solid prove of the presence of a five or a six membered tin ring can be provided.

4.2 Reaction pathway

Reacting *di^{t}butyldichlorostannane* **35** with an excess of magnesiums also leads to a dark red solution. The ^{119}Sn NMR displayed three NMR signals confirming the formation of 1, 1, 2, 2, 3, 3, 4-*hepta-^{t}butyl-4-chloromagnesiotetrastannacyclobutane* **62**. A ^{119}Sn NMR investigation showed the presence of a reaction cascade as shown in figure 4.3.

In a first step (A) all monostannane is converted into distannane. As a next step, the precipitation of a yellow solid could be observed (B). This yellow precipitate was later identified as *octa-^{t}butyltetrastannacyclobutane* **61**. Finally the precipitate disappears again. Simultaneously, the solution turns dark red and **62** is formed (C).

A mechanism for this last step was proposed as shown in figure 4.4. A Grignard reagent reacts with one *^{t}butyl* group of **61** and abstracts one hydrogen. Thus isobutane and isobutene is formed. At the same time a tin magnesium bond is established. Head space analysis of the gas phase above the reaction was done. An equal amount of isobutane and isobutene was found which confirms this theory.

Until now it is unclear weather *^{t}butylmagnesiumchloride* is formed by some

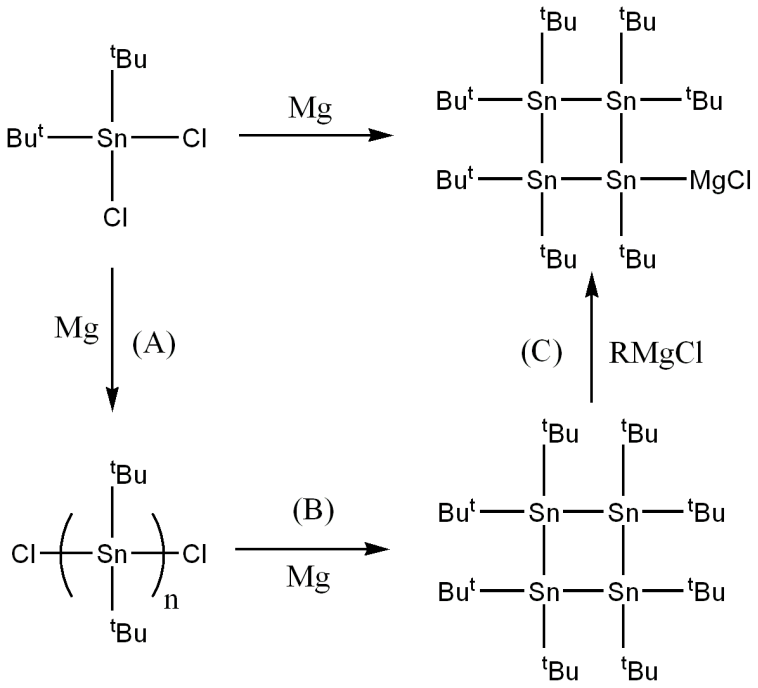

Figure 4.3: Reaction cascade leading to **62**

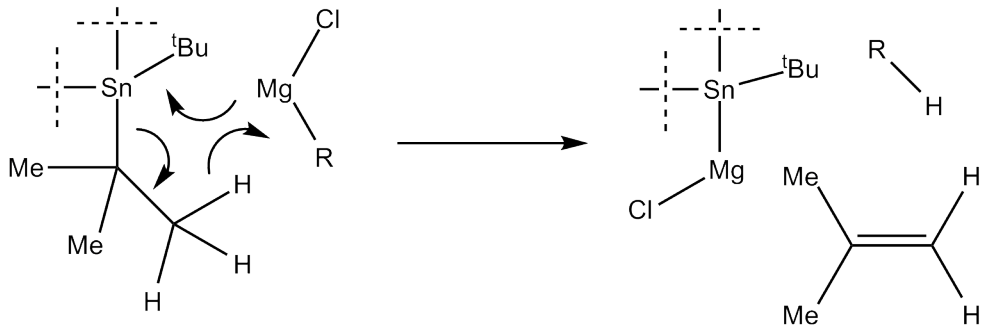

Figure 4.4: Proposed mechanism of the last step (C)

kind of decomposition of the educt in the first place that than reacts with **61**. Alternatively, a Gringard type tin compound could react with the $^{t}butyl$ group and decompose afterwards to form butane and a tin(II) compound. However, the presence of a Grignard reagent is necessary as **61** reacts with activated magnesium and $^{t}BuCl$ to form **62**. But stirring with only magnesium at 30°C does not show any reaction at all.

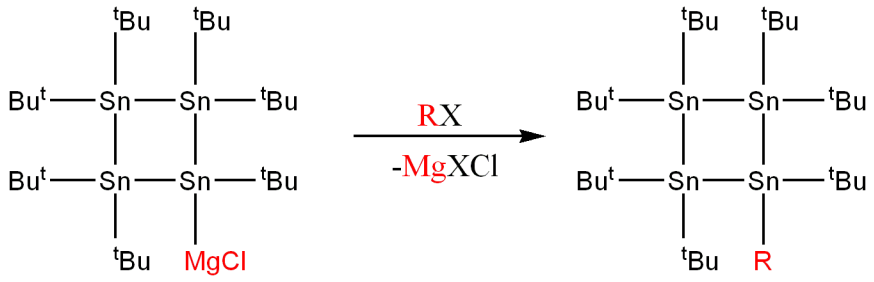

Figure 4.5: Reaction of **62** with alkylhalogenes

4.3 Derivatisation reactions

4.3.1 Reaction with alkylhalogenides

As described in the introduction chapter 4.1 **62** reacts with alkylhalogenides to form the corresponding alkyl substituted monofunctionalised four membered tin ring. Besides methylation and ethylation also the reaction with *propylchloride* was performed. The latter reaction clearly proves that alkylation is possible with every kind of halogenides.

Methylation was also observed while reacting **62** with *dimethylsulfate*. $1,1,2,2,3,3,4$-*hepta*-^{t}*butyl*-4-*methyltetrastannacyclobutane* **64** could be recrystallized out of THF providing the first structural prove of this monofunctionalised tin rings. In addition, also single crystals of the ethylated or propylated compound could be isolated. Due to high disorder of the ^{t}*butyl* groups in the crystal lattice no reliable crystal structure could be obtained.

This high disorder is most probably caused by the high crystallization rate. The *propyl* and *ethyl* group interacts in all directions in the same way by weak van-der-Waals-interactions. For the molecular packing it does not really matter in which direction the groups assemble.

4.3.2 Reaction with dihalogenalkyles

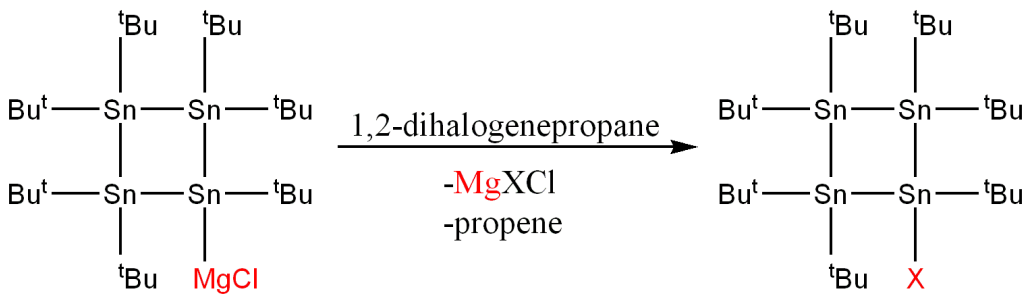

Figure 4.6: Reaction of **62** with 1,2-dihalogenepropanes

Derivatisations with dihalogenalkyles were also investigated. The reaction with 1, 2-*dibromoethane* is hardly controllable. Generally, the ring structure is decomposed and 1, 2-*dibromo*-1, 1, 2, 2-*tetra*-^{t}*butyldistannane* is formed. Also the formation of 1-*bromo*-1, 2, 2, 3, 3, 4, 4-*hepta*-^{t}*butyltetrastannacyclobutane* **72** could be observed, however.

1, 2-*Dibromopropane* also reacted with **62**. Although ^{119}Sn NMR signals showed a high number of peaks, **72** was identified as main product. The reaction was redone with 1, 2-*dichloropropane* as reagent. ^{119}Sn NMR showed the formation of the corresponding chlorinated product: 1-*chloro*-1, 2, 2, 3, 3, 4, 4-*hepta*-^{t}*butyltetrastannacyclobutane* **71**. Both products could be reacrystalized out of THF.

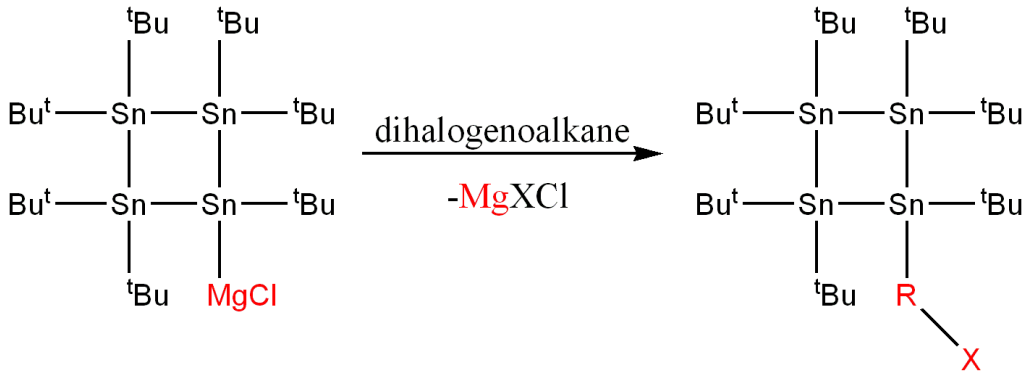

Figure 4.7: Reaction of **62** with dihalogenealkanes

The reaction of **62** with 1, 3-*chloropropane* leads to the formation of 1, 1, 2, 2, 3, 3,-4-*hepta*-^{t}*butyl*-4-(3-*chloropropyl*)*tetrastannacyclobutane* **67**. The structure of this compound could be proved by XRD measurement. The conversion was repeated with 1, 5-*dichloropentane* resulting in the corresponding halogenealkyl substituted four membered tin ring. However, the reaction with 1, 6-*dibromohexane* gave three pairs of ^{119}Sn NMR signals. This suggests a mixture of *bromohexyl* substituted four membered tin ring and the dimeric structure that originates of the reaction of **62** with $1, 1, 2, 2, 3, 3, 4-hepta-^t butyl-4-(6-bromohexyl)-tetrastannacyclobutane$ **69**(figure 4.8).

Also the reaction of **62** with 1, 4-*dichlorobutine* was carried out. However, the product was not stable and decomposed. Traces of **71** could be found in the ^{119}Sn NMR spectra. Other side products could not be identified.

4.3.3 Further derivatisation

A solution of **62** was added to elemental sulfur and elemental tellurium. Corresponding tristannadichalcogenocyclopentanes (figure 4.9) were formed and identified by ^{119}Sn NMR. These five membered rings have already been described by Puff

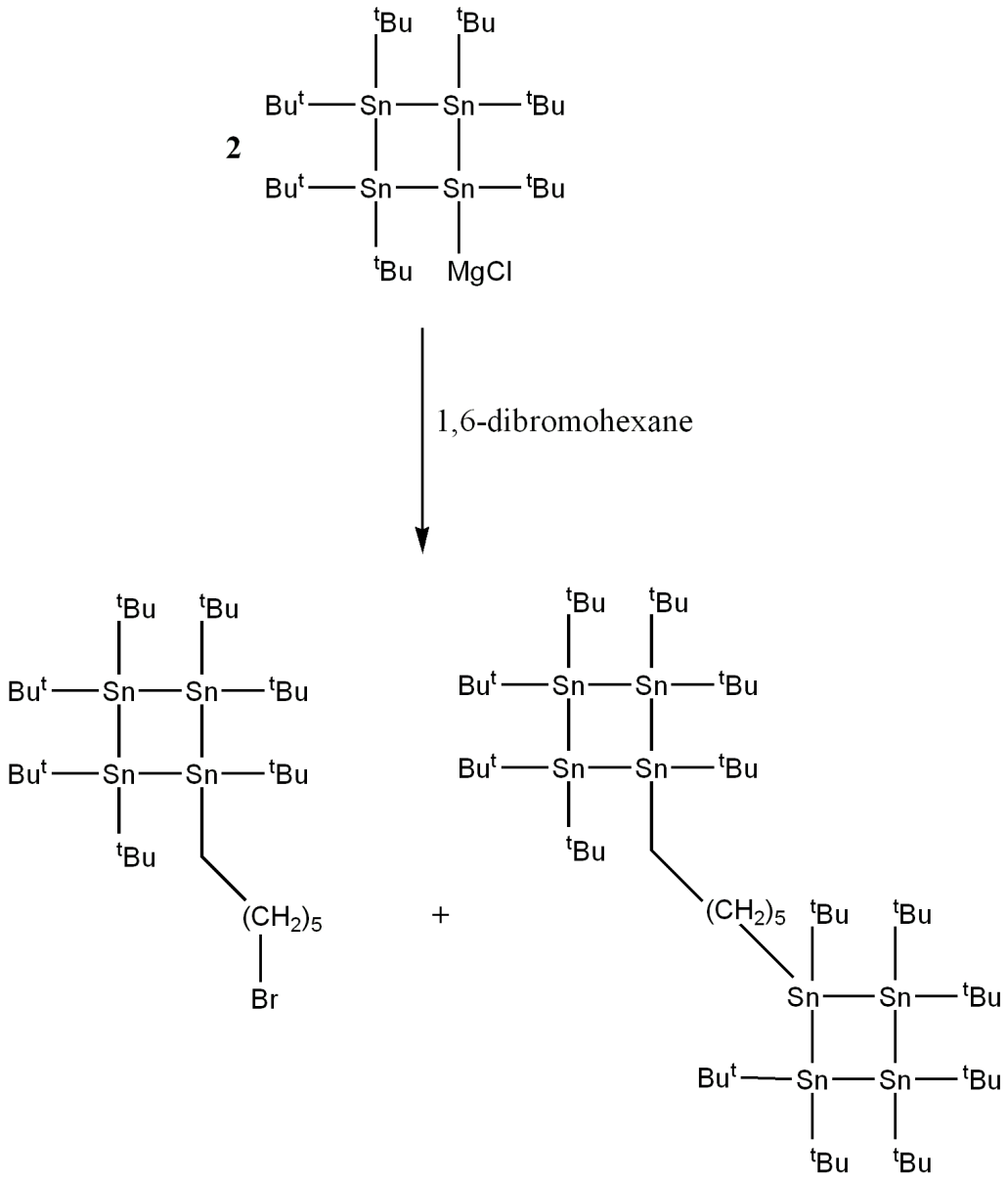

Figure 4.8: Possible products of the reaction of $1,6-$ *dibromohexane* with **62**

et al. while performing similar reactions with *octa-^{t}butyltetrastannacyclobutane* and the 16th group's elements[42].

4.3.4 Cleavage of the ring system

The cleavage of *octa-^{t}butyltetrastannacyclobutane* with halogenes lead to $1,4$-*dihalogene*-$1,1,2,2,3,3,4,4$-*octa^{t}butyltetrastannane*[43]. Also smaller chains were obtained as side products.

Attemps to cleave $1,1,2,2,3,3,4$-*hepta-^{t}butyl*-4-*methyltetrastannacyclobutane* **64** were made, while adding chlorine in 1:1 ratio. However, to provide the exact amount of the chlorine was difficult and according to ^{119}Sn NMR *di^{t}butyldichloro-*

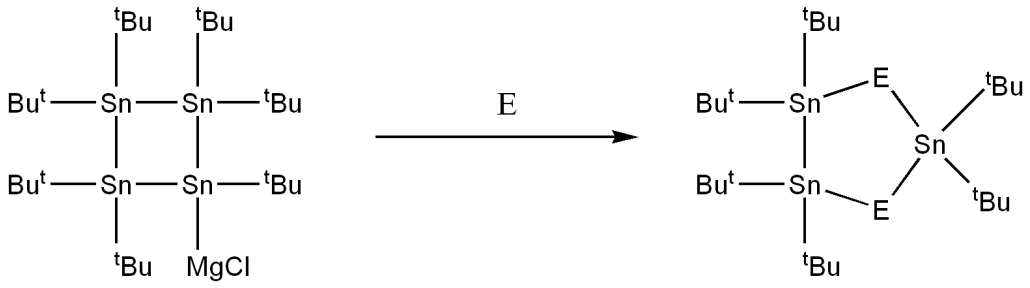

Figure 4.9: Tristannadichalcogenocyclopentanes: E= S, Te

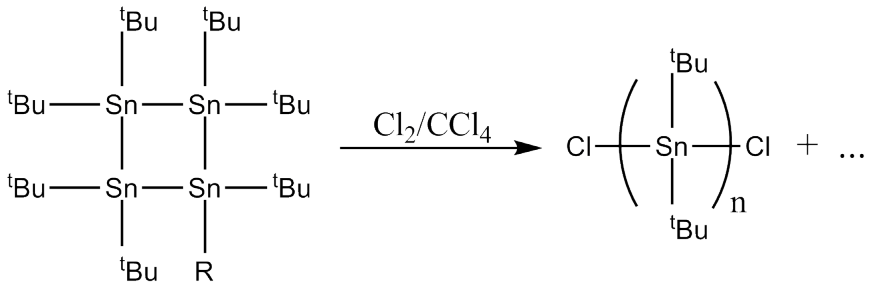

Figure 4.10: Cleavage of the ring systems: R=^{t}Bu[43],Me

stannane **35** was found as major product. Next to the signal for **35**, different signals which represent presumable tri- and tetrastannanes were found. Thus no systematic cleavage next to the methyl group was obtained.

4.4 Discussion of the crystal structures

4.4.1 Crystal structure of $1,1,2,2,3,3,4$-*hepta*-^{t}*butyl*-4-*methyl*-*tetrastannacyclobutane* **64**

$1,1,2,2,3,3,4$-*Hepta*-^{t}*butyl*-4-*methyltetrastannacyclobutane* **64** crystallizes in the triclinic space group P-1. There are 6 molecules in the unit cell. However, they are arranged in three independent but almost identical couples. These small differences are only due to packing modes of the ^{t}*butyl* groups resulting in crystallographic independent molecules. When this structure is later compared with other crystal structure or calculated structure the average of the bonds and angles of these three molecules will be used.

The Sn-Sn bond lengths range from 2.8107(3)Å to 2.8834(3)Å which falls in between the average Sn-Sn distance. The tin tin distances between the monofunctionalised Sn(1) tin and the symmetric Sn(2/4) tins is to some extend shorter than the corresponding distances between Sn(3) and Sn (2/4). This is most probably due to the bulky ^{t}*butyl* group which are sterically more demanding than the *methyl*

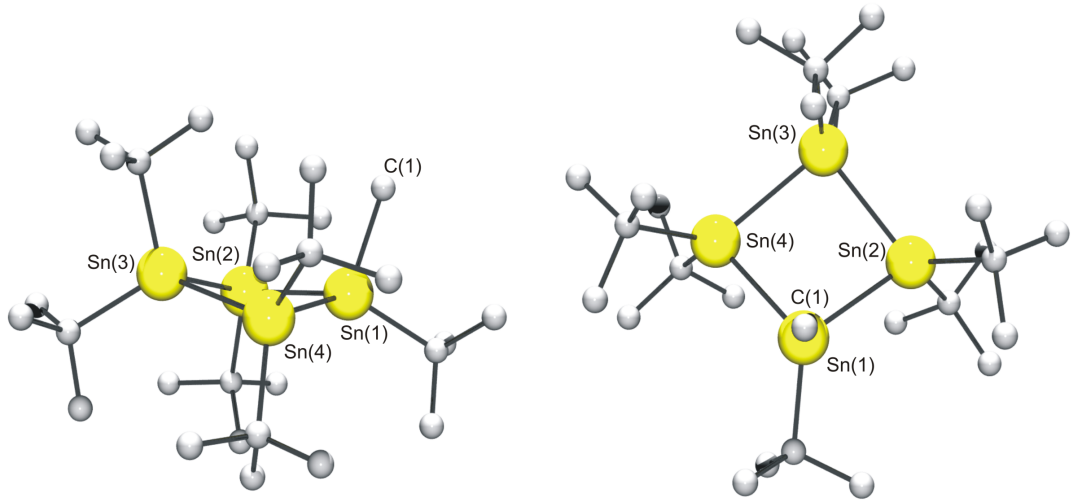

Figure 4.11: Crystal structure of **64** (Hydrogen atoms omitted for clarity) Selected bond lengths [Å] and angles [°] for **64**:Sn(1)-C(1):2.178(3); Sn(1)-C(2):2.206(3); Sn(1)-Sn(2):2.8194(3); Sn(1)-Sn(4):2.8127(3); Sn(2)-Sn(3):2.8788(3); Sn(3)-Sn(4):2.8838(3); Sn(4)-Sn(1)-Sn(2):92.369(10); Sn(1)-Sn(2)-Sn(3):87.033(9); Sn(2)-Sn(3)-Sn(4):89.694(9); Sn(1)-Sn(4)-Sn(3):87.063(9); C(1)-Sn(1)-C(2):101.61(14);

group.

Sn-C distances between the tin atoms and the ^{t}*butyl* group ranges from 2.204(3) to 2.241(4)Å. Again due to the less sterically demand the Sn-C bond between Sn(1) and the *methyl* group is considerably shorter (2.178(3) – 2.180(3) Å).

The inner cyclic Sn-Sn-Sn angles range from about 90° (86.333(9)° to 92.757(10)°). For the methyl substituted tin centre larger angles are observed as consequence of the shorter distances. Likewise smaller angles are found for the more crowded tin atoms.

4.4.2 Crystal structure of 1, 1, 2, 2, 3, 3, 4-*hepta*-^{t}*butyl*-4-(3-*chloropropyl*)-*tetrastannacyclobutane* **67**

1, 1, 2, 2, 3, 3, 4-*Hepta*-^{t}*butyl*-4-(3-*chloropropyl*)*tetrastannacyclobutane* **67** crystallizes in the monoclinic space group P2(1)/n, containing 4 identical molecules in the unit cell. Otherwise the structural characteristics are similar to **64**. Sn-Sn bonding ranges from 2.8321(4) Å to 2.8923(4)Å. Distances between the *chloropropyl* substituted Sn(1) to Sn(2/4) are considerably shorter than the Sn(3) to Sn(2/4) distances. Likewise, Sn-C bonds between the *chloropropyl* group and Sn(1) ranges from 2.199(4)Å and is therefore shorter than the tin bonds between tin atoms and the ^{t}*butyl* groups ranging from 2.213Å to 2.236Å.

The inner cyclic angles are around 90°. Same as in **64**, the angle between Sn(2)-

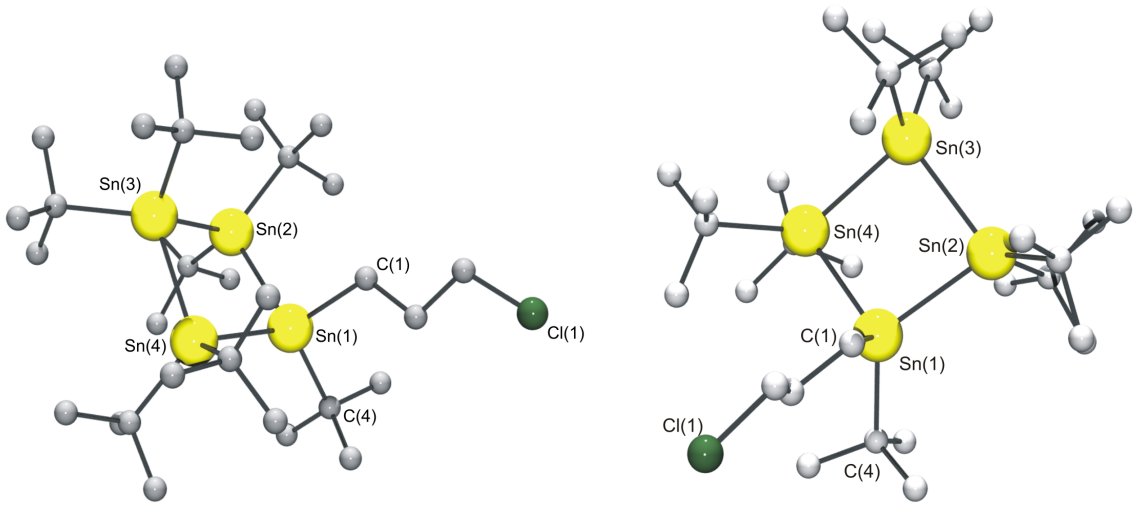

Figure 4.12: Crystal structure of **67** (Hydrogen atoms omitted for clarity) Selected bond lengths [Å] and angles [°] for **67**:Sn(1)-C(1):2.199(4); Sn(1)-Sn(2):2.8424(4); Sn(1)-Sn(4):2.8321(4); Sn(2)-Sn(3):2.8923(4); Sn(3)-Sn(4):2.8877(4); Sn(4)-Sn(1)-Sn(2):91.962(11); Sn(1)-Sn(2)-Sn(3):86.656(10); Sn(4)-Sn(3)-Sn(2):89.818(10); Sn(1)-Sn(4)-Sn(3):86.938(10); C(1)-Sn(1)-C(4):105.36(15);

Sn(1)-Sn(4) is larger with a value of 91.962(11)°. The other inner cyclic Sn-Sn-Sn angles range from 86.656(19)° to 89.818(10)°.

The tin to chlorine distance is 5.970Å. This is considerably longer than the average distance between a tin atom and a proton on the ^{t}*butyl* group which ranges 3.97Å. So the chlorine functionality is not shielded and further reaction can take place. However, 1,3-*dichloropropane* does not bridge two ring systems, as the distance is to short to avoid the interference of the ^{t}*butyl* groups. Simulations of the sterical demand of the ^{t}*butyl* groups based on the crystal structure data clearly show that a chain with at least five carbon atoms is needed, in order to avert the tangency of the substituents on two bridged four membered rings.

It is for the same reason that it is not before using 1,6-*dibromohexane* for derivatisation reactions to get the first hints of a dimeric structure as described above. Also a dimeric structure of 1,1,2,2,3,3,4-*hepta*-^{t}*butyl*-4-*chloromagnesio-tetrastannacyclobutane* **62** is considered as being very unlikely.

4.4.3 Crystal structure of 1-*halogeno*-1,2,2,3,3,4,4-*hepta*-^{t}*butyl-tetrastannacyclobutane* (Cl: 71 and Br: 72)

The crystal structure of 1-*chloro*-1,2,2,3,3,4,4-*hepta*-^{t}*butyltetrastannacyclobutane* **71** is very similar to the crystal structure of 1-*bromo*-1,2,2,3,3,4,4-*hepta*-^{t}*butyltetra-stannacyclobutane* **72**. They both crystallize in a monoclinic space group P21, with two identical molecules in the unit cell.

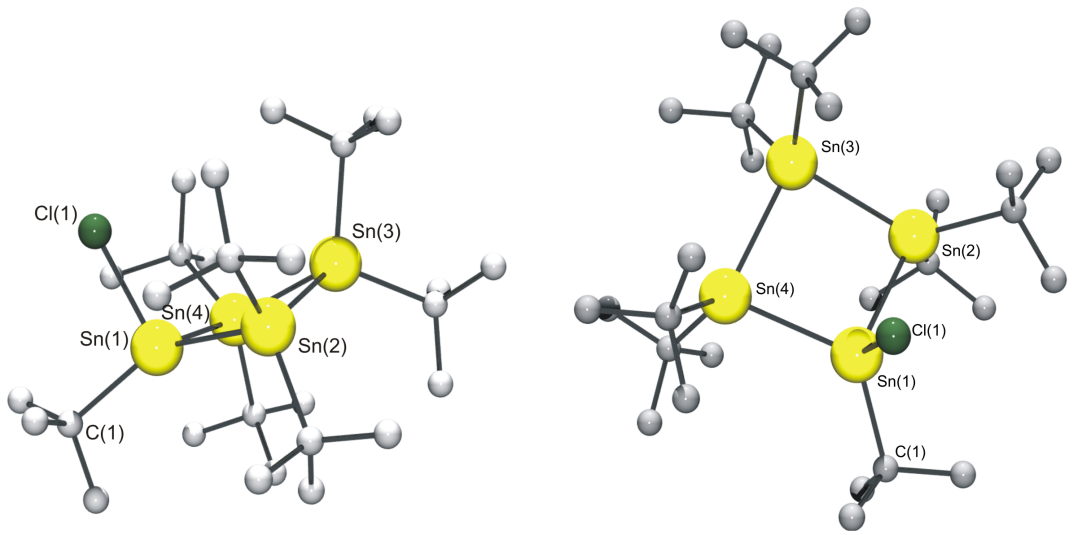

Figure 4.13: Crystal structure of **71** (Hydrogen atoms omitted for clarity) Selected bond lengths [Å] and angles [°] for **71**:Sn(1)-Cl:2.4624(6); Sn(1)-C(1):2.202(3); Sn(1)-Sn(2):2.8132(3); Sn(1)-Sn(4):2.8168(3); Sn(2)-Sn(3):2.9122(3); Sn(3)-Sn(4):2.8868(4); Sn(4)-Sn(1)-Sn(2):94.362(7); Sn(1)-Sn(2)-Sn(3):85.666(7); Sn(2)-Sn(3)-Sn(4):90.816(7); Sn(1)-Sn(4)-Sn(3):86.082(7); C(1)-Sn(1)-Cl:99.49(8);

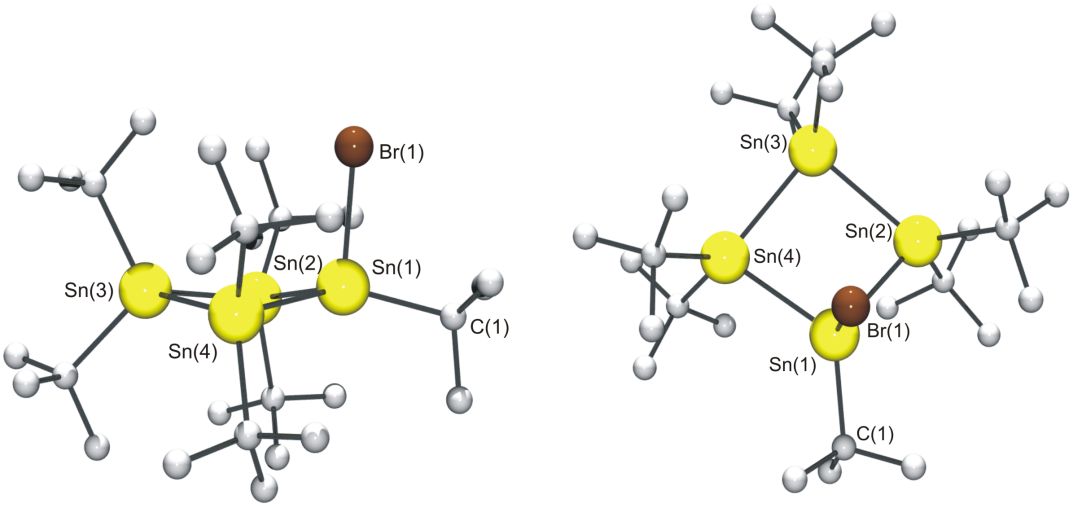

Figure 4.14: Crystal structure of **72** (Hydrogen atoms omitted for clarity) Selected bond lengths [Å] and angles [°] for **72**:Sn(1)-Br:2.5639(3); Sn(1)-C(1):2.196(2); Sn(1)-Sn(2):2.8143(2); Sn(1)-Sn(4):2.8123(2); Sn(2)-Sn(3):2.8831(2); Sn(3)-Sn(4):2.8975(2); Sn(4)-Sn(1)-Sn(2):94.514(6); Sn(1)-Sn(2)-Sn(3):85.779(5); Sn(2)-Sn(3)-Sn(4):91.260(6); Sn(1)-Sn(4)-Sn(3):85.543(6); C(1)-Sn(1)-Br:99.33(6);

The distances between Sn(1) to Sn(2/4) ranges from 2.813Å to 2.817Å for **71** and from 2.812Å to 2.814Å for **72**. The distances between Sn(3) to Sn(2/4) are to a certain extent longer in both molecules with values between 2.912Å and 2.887Å

for **71** and values between 2.883Å and 2.898Å for **72**. Again, the less sterical demand of the halogene compared to the $^{t}butyl$ group can be an explanation. The tin halogene distance is 2.4624Å for **71** and 2.5639Å for **72**. The Sn Br distance is somewhat larger than the Sn-Cl distance due to the larger covalence radius of bromine.

The inner cyclic angles of **71** range from 86.33° to 94.36°. Those of **72** range from 85.543° - 94.514°.

4.4.4 Comparisons of four membered tin ring described in literature

The most obvious structural difference between the monofunctional four membered tin ring systems and *octa-^{t}butyltetrastannacyclobutane* **61** is the difference in folding angles. For the methyl substituted ring **64** folding angles of 157.09° to 158.71° and for the *chloropropyl* **67** substituted ring a folding angle of 156.64° could be observed. For the *chloro* substituted ring **71**, a folding angle of 160.71° could be observed. *Bromo-hepta-^{t}butyltetrastannacyclobutane* **72** has the largest folding angle of 161.21°. Compared to that **61** is described as planar in literature(figure 4.15).

However, planar ring systems are far less common than puckered rings. Only for $[(Me_3Si)CH_2]_8Sn_4$ a similar planar arrangement could be found. Otherwise folding angles between 151.55° and 161.45° could be observed. Table 4.1 gives an overview of structurally characterized four membered tin rings.

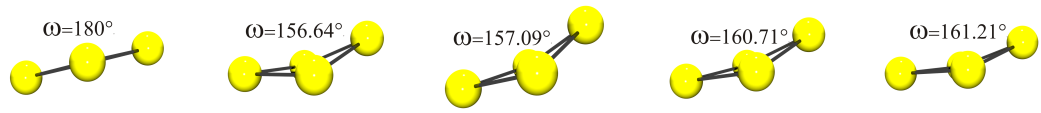

$^{t}Bu_8Sn_4$ **61**	$^{t}Bu_7Sn_4PrCl$ **67**	$^{t}Bu_7Sn_4Me$ **64**	$^{t}Bu_7Sn_4Cl$ **71**	$^{t}Bu_7Sn_4Br$ **72**

Figure 4.15: Visualisation of the torsion angle of the different crystal structure

Table 4.1: Structural data of different substituted tetrastannacyclobutanes

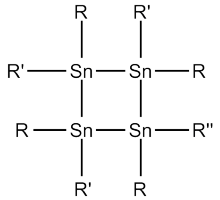

definition of the foldingangle

R	compound R'	R"	Sn-Sn distances [Å]	Sn-Sn-Sn angles [°]	Folding angle ω[°]	Ref.
	$^tBu_7MeSn_4$		2.811 - 2.884	85.67 - 92.76	157.09 – 158.71	*
^tBu	^tBu	Me				
	$^tBu_7Sn_4Cl$		2.813 - 2.912	86.33 - 94.36	160.71	*
^tBu	^tBu	Cl				
	$^tBu_7Sn_4Br$		2.814 - 2.898	85.54 - 91.26	161.21	*
^tBu	^tBu	Br				
	$^tBu_7(ClCH_2CH_2CH_2)Sn_4$		2.832 - 2.892	91.96-86.66	156.64	*
^tBu	^tBu	$3-Cl-propyl$				
	$^tBu_8Sn_4$		2.887	89.87-90.13	180	[41]
^tBu	^tBu	^tBu				
	$(1,1\text{-}Me_2Pr)_8Sn_4$		2.814 – 2.924	88.85 – 89.34	160.07	[41]
$1,1\text{-}Me_2Pr$	$1,1\text{-}Me_2Pr$	$1,1\text{-}Me_2Pr$				
	$[(Me_3Si)_3Si]_4Cl_4Sn_4$		2.803 – 2.915	88.14 – 90.37	161.45	[31]
$(Me_3Si)_3Si$	Cl	Cl				
	$[(Me_3Si)CH_2]_8Sn_4$		2.829 – 2.834	89.96 - 90.04	180	[3]
$(Me_3Si)CH_2$	$(Me_3Si)CH_2$	$(Me_3Si)CH_2$				
	$[2,6\text{-}Et_2\text{-}C_6H_3]_7BrSn_4$		2.818 – 2.931	87.54 – 92.91	155.40	[7]
$2,6\text{-}Et_2\text{-}C_6H_3$	$2,6\text{-}Et_2\text{-}C_6H_3$	Br				

* crystal structure first presented in this thesis

4.5 Reaction of dialkyldichlorostannanes with magnesium

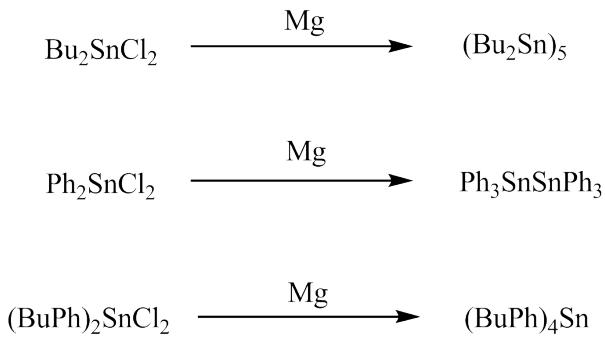

Figure 4.16: Reaction of dialkyldichlorostannanes with magnesium

Different types of *dialkyldichlorostannanes* were stirred overnight in the present of magnesium as done with *di^{t}butyldichlorostannane*. When using *dibutyldichlorostannane* as starting material, the reactions stops after the formation of the five membered ring. Apparently the *^{n}butyl* group cannot be abstracted.

Similar results when using *diphenyldichlorostannane* **43** were expected Puff et al. [40] claim that the reaction of **43** with *lithium* leads to *dodecaphenylhexastannacyclohexane* **47**. In addition, the abstraction of one hydrogen off a phenyl group is highly improbable. However, ^{119}Sn NMR of the reaction solution clearly display a signal at -144 ppm. This means that *phenyl* groups were exchanged and *hexaphenyldistannane* **46** was formed.

4.6 Reaction of *di^{t}butyldichlorostannane* with other metals

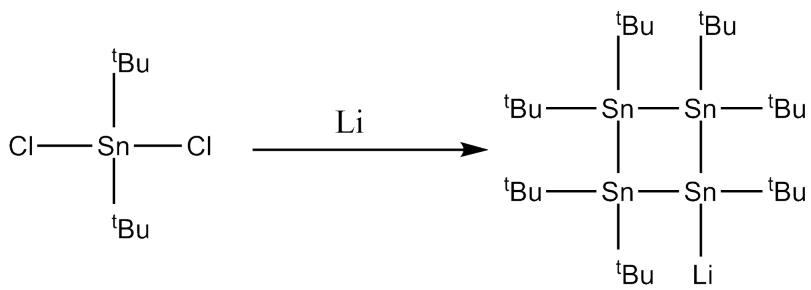

Figure 4.17: Reaction of *di^{t}butyldichlorostannane* with *lithium*

Di^{t}butyldichlorostannane reacts with lithium to form a dark red solution as known for magnesium. The mixture changes color after a few minutes which indi-

cates the start of the reaction. Different to magnesium no further heating is necessary. The reaction is finished after 30 minutes. ^{119}Sn NMR spectrum displaces a three signal pattern similarly to **62**. This strongly indicates that the according lithium species: 1, 1, 2, 2, 3, 3, 4-*hepta*^{t}*butyl*-4-*lithiotetrastannacyxclobutane* **63** was formed.

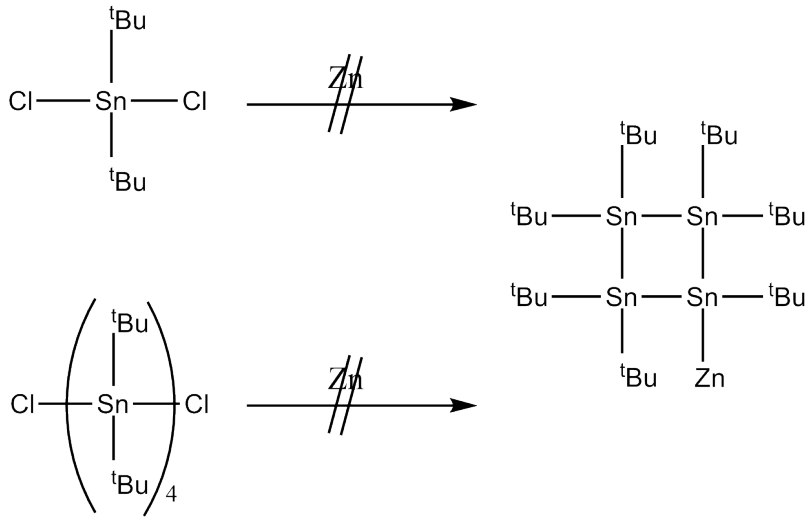

Figure 4.18: Reaction of *di*^{t}*butyldichlorostannane* and 1, 1, 2, 2, 3, 3, 4, 4-*octa*-^{t}*butyl*-1, 4-*dichlorotetrastannane* with *zinc*

The same progress was also done with zinc. However, no reaction took place. Also activation with heat and 1, 2-*dibromoethane* was unsuccessful. Furthermore 1, 4-*dichloro*-1, 1, 2, 2, 3, 3, 4, 4-*octa*-^{t}*butyltetrastannane* was stirred overnight in the presence of zinc. Also no reaction with zinc took place.

4.7 Disscusion of the NMR data

The ^{119}Sn NMR spectra of the monofunctionalized four membered tin ring system show three signal in a 1:2:1 ratio. Each signal has the characteristic pattern of ^{119}Sn–$^{119/117}$Sn coupling constants. The satellites of the ^{119}Sn–^{117}Sn coupling constant have a symmetrically arrangement around the central line, whereas the satellites of ^{119}Sn–^{119}Sn are not symmetrical. The ratio of the magnitude of the J(^{119}Sn–^{119}Sn) to J(^{119}Sn–^{117}Sn) ratio equals the ratio of the gyromagnetic ratio γ: $\gamma(^{119}Sn)/\gamma(^{117}Sn) \simeq 1.046$[10].

4.7.1 Comparision of the NMR data of the monofunctionalized tin ring systems

The ^{119}Sn NMR shifts of the monofunctionalised tetrastannacyclobutanes are listed in table 4.2. The magnesio and lithio substituted ring systems have very similar

Table 4.2: ^{119}Sn NMR shifts of different monofunctionalised tin rings

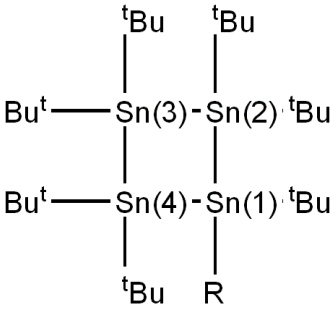

compound	δ Sn(3)[ppm]	δ Sn(2) [ppm]	δ Sn(1) [ppm]	ref
$^tBu_7Sn_4MgCl$ **62**	180	75	-6	[11]
$^tBu_7Sn_4Li$ **63**	179	75	-5	*
$^tBu_7Sn_4Me$ **64**	93	63	-49	[11]
$^tBu_7Sn_4Et$ **65**	96	63	-19	[11]
$^tBu_7Sn_4Pr$ **66**	94	58	-29	*
$^tBu_7Sn_4PrCl$ **67**	96	62	-26	*
$^tBu_7Sn_4PenCl$ **68**	97	61	-25	*
$^tBu_7Sn_4HexCl$ **69**	94	60	16	*
$^tBu_7Sn_4Cl$ **71**	85	92	202	[11]
$^tBu_7Sn_4Br$ **72**	82	102	236	*
$^tBu_8Sn_4$ **61**	80	80	80	[41]

* data first presented in this thesis

shifts. The differences between the shifts are only a few ppm.

The shifts of Sn(3) and Sn(2) of the alkyl and halogenoalkyl substituted ring systems are also quite similar. As expected only the shifts of Sn(1) differ considerably. The methyl substituted four membered ring system **64** has the lowest shift at -49 ppm, whereas the chlorohexyl substituted ring system **69** has the highest (16 ppm). Apparently there is no correlation between chain lengths and Sn(1) shift. However, substituents with an even number of carbon atoms tend to have higher shifts.

The Sn(1) shift of the propyl and the chloropropyl substituted ring system differ only in 3 ppm. Obviously, the chloro atom on the propyl group does not have a major influence on the ^{119}Sn NMR shift of Sn(1).

The ^{119}Sn NMR shifts of the halogeno subsituted four membered tin ring systems are shifted to high field. Sn(1) shift is 236 ppm for the chloro substituted ring system **71** and 202 ppm for the bromo substituted ring system **72**. Also the Sn(2/4) signals are the highest in comparison with other ring systems. They range from 92 ppm to 102 ppm, whereas the latter range from 75 ppm to 58 ppm.

4.7.2 Comparison of the coupling constants of various mono-functionalized tin ring systems

Table 4.3: ^{1}J and ^{2}J ^{117}Sn coupling constants of the Sn(1) signal of different mono-functionalised tin rings

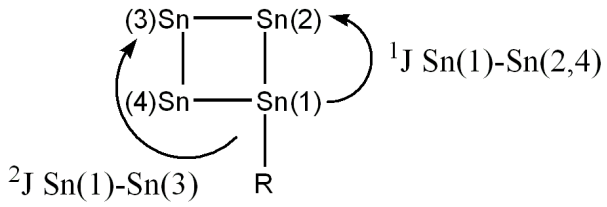

compound	^{1}J Sn(1)-^{117}Sn(2,4) [Hz]	^{2}J Sn(1)-^{117}Sn(3) [Hz]	ref
$^{t}Bu_7Sn_4MgCl$ **62**	6500	1564	[11]
$^{t}Bu_7Sn_4Me$ **64**	615	1850	[11]
$^{t}Bu_7Sn_4Et$ **65**	740	1460	[11]
$^{t}Bu_7Sn_4Pr$ **66**	727	1773	*
$^{t}Bu_7Sn_4PrCl$ **67**	762	1869	*
$^{t}Bu_7Sn_4PenCl$ **68**	743	1799	*
$^{t}Bu_7Sn_4Br$ **72**	1830	1892	*
$^{t}Bu_7Sn_4Cl$ **71**	1057	1952	[11]
$^{t}Bu_8Sn_4$ **61**	1195	1658	[41]

* data first presented in this thesis

The ^{1}J^{119}Sn(1)–^{117}Sn(2,4) coupling constant vary significantly depending on the substituent on the Sn(1) atom. The data is listed in table 4.3. **62** has a very large coupling constant ranging at 6500 Hz. Similar large coupling constants could be found for alkali substituted distannanes [16].

Smaller ^{1}J^{119}Sn(1)–^{117}Sn(2,4) coupling constants between 615 Hz and 762 Hz could be found for the alkyl- and chloroalkyl substituted tin ring systems. Larger coupling constants between 1057 Hz and 1830 Hz were found for the halogeno substituted ring systems.

The substituent on the Sn(1) atom does not have a major influence on the ^{2}J^{119}Sn(1)–^{117}Sn(3) coupling constant. They range from 1460 Hz to 1952 Hz. No obvious coherence between the nature of the substituent and the magnitude of the coupling constant could be found.

4.8 Calculation of four membered tin ring systems

4.8.1 Optimization of calculation method

A geometry method optimization for the monofunctionalized four membered tin rings were investigated. As the $^t butyl$ groups have large possibilities to move, convergence failures when using different methods, were quite common. In addition, the large number of atoms and the large tin atoms made structure optimization difficult. For optimization geometries calculations were carried out and compared with the structure of $^t Bu_7 Sn_4 Me$ **64** obtained by X-ray diffraction.

Methods, that made structure optimization possible are listed in table 4.4. CPU times over one day are quite common. Significantly shorter times where only achieved with STO-3G basis set, which is rather small.

Table 4.4: different calculation methods used for optimization of $^t Bu_7 Sn_4 Me$ which lead to an optimized geometry

basis sets		methode	CPU time [min]
Sn	C,H		
STO-3G	3-21G	B3LYP	1023
STO-3G	4-22GSP	B3LYP	2823
STO-3G	STO-3G	B3LYP	410
SDD	SDD	PBE1PBE	2894
SDD	SDD	HF	1132
STO-3G	STO-3G	HF	175

Structural data calculated with different methods are listed in tables 4.5 and 4.6. For all methods large differences in folding angles in comparison to the crystal structure could be observed. It can be assumed that the folding angle is highly influenced by the crystal packing. As only gas phase geometries can be calculated, this might be an explanation for the large differences.

Comparison of Hartree Fock (HF) methods to density functional theories (DFT) show that in general HF methods provide better results. The basis set SDD gives best results for the angles. Also the basis set STO-3G offer good results, but being very small it is generally not expected to give reliable results. Only DFT calculations with functional PBE1PBE and basis set SDD offer results as good as the HF SDD method. However, long CPU times are a disadvantage of this method.

Table 4.5: Comparison of various calculated structures of $^{t}Bu_7Sn_4Me$ with the crystal structure: bonding

calculation method	bonds [Å]				
	Sn(1)-Sn(2)	Sn(1)-Sn(4)	Sn(3)-Sn(2)	Sn(3)-Sn(4)	Sn(1)-C(1)
crystal structure	2.813	2.816	2.886	2.879	2.184
B3LYP: Sn:STO-3G; other:3-21G	2.869	2.863	2.932	2.927	2.020
B3LYP: Sn:STO-3G; other:4-22GSP	2.817	2.812	2.856	2.851	2.055
B3LYP: STO-3G;	2.717	2.723	2.769	2.772	2.137
PBE1PBE: SDD;	2.893	2.897	2.961	2.966	2.201
HF: SDD;	2.901	2.902	2.988	2.982	2.191
HF: STO-3G;	2.812	2.812	2.861	2.856	2.127

Table 4.6: Comparison of various calculated structures of $^{t}Bu_7Sn_4Me$ with the crystal structure: angles

calculation method	angles [°]			
	Sn(1)-Sn(2)-Sn(3)	Sn(1)-Sn(4)-Sn(3)	C(2)-Sn(1)-C(1)	folding angle
crystal structure	86.6	86.7	101.1	157.7
B3LYP: Sn:STO-3G; other:3-21G	88.2	88.4	105.5	162.8
B3LYP: Sn:STO-3G; other:4-22GSP	89.1	89.3	102.2	169.6
B3LYP: STO-3G;	88.7	89.1	101.1	165.0
PBE1PBE: SDD;	88.4	88.2	102.6	162.5
HF: SDD;	88.2	88.3	102.4	161.3
HF: STO-3G;	88.7	88.8	102.1	162.6

Chapter 5

Reaction of various tin hydrides with Bu_2Mg and Et_2Zn

5.1 Introduction

In 1961 Tamborski et al.[47] described the reaction of *triphenylchlorostannane* **12** with activated magnesium. They found out that the reaction follows a two step mechanism. In the first step, *hexaphenyldistannane* **46** precipitates. Afterwards, magnesium is inserted in the tin-tin bond to form a magnesium tin compound. The nature of the product was proved by hydrolysis, leading to *triphenylstannane* **45** in high yields.

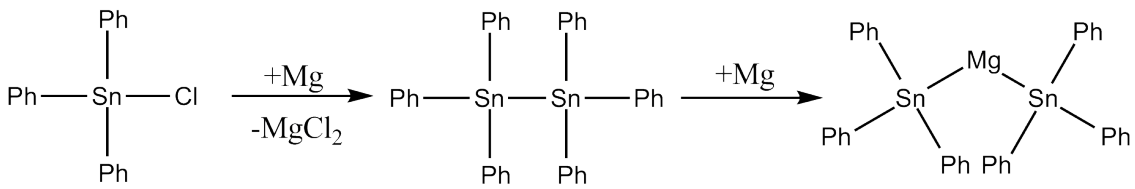

Figure 5.1: Reaction scheme of Ph_3SnCl **12** with magnesium described by Tamborski et al.[47]

Van der Kerk et al.[8] were the first to react **45** with a Grignard reagent. They used *triethylamine* for stabilization. Without this stabilization reagent decomposition took place and elemental tin was observed. An oily yellow compound was obtained which could not be recrystallized. They made various derivatisation reactions however, in order to prove the existence of a tin magnesium bond. They also found out that compared to the reaction described by Tamborski et al. no *hexaphenyldistannane* was formed.

In addition, Van der Kerk et al. made investigations concerning the formation of tin and group 12 element bonds using *triphenyltinhydride* **45**[12], as well as *triphenylchlorostannane* **12**[14] as starting materials. The group 12 elements

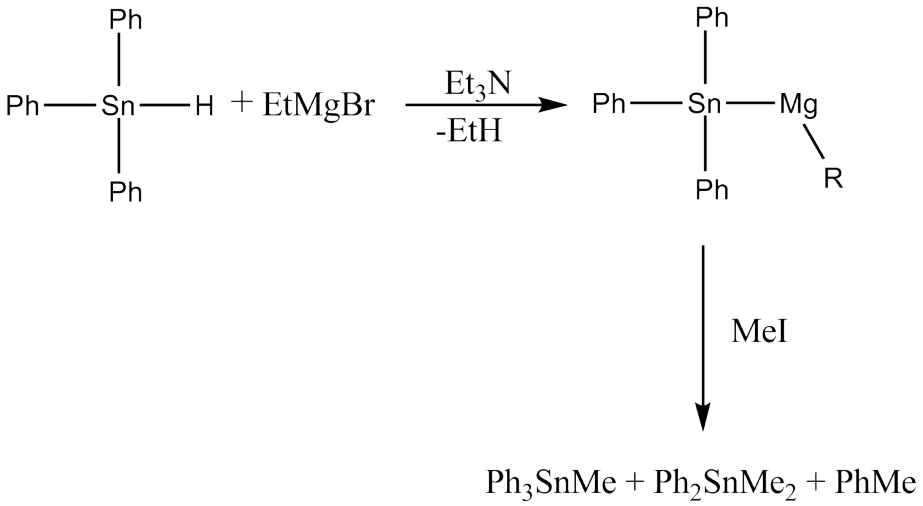

Figure 5.2: Reaction scheme of Ph_3SnH **45** with $EtMgBr$ by Van der Kerk et al.[8]

were added as dialkyl metal compound as done in the reaction with **9** mentioned above. In addition, they used various types of stabilization reagents and compared their yields[13]. Lateron some structural proposal were deduced out of derivatisation products and elemental analysis[15]. However, no crystal structure could be measured in order to confirm any of these theories. Despite their importance as mild stannilation product no further investigations on the formation of other compounds containing tin zinc bonds have been examined.

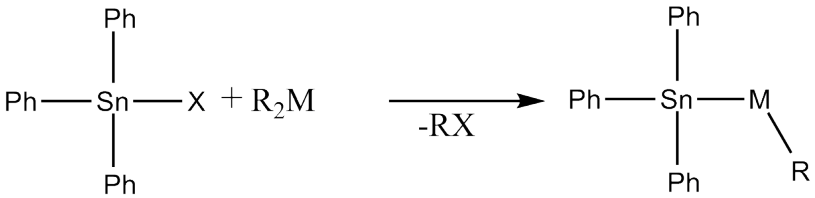

Figure 5.3: Reaction scheme of Ph_3SnX with R_2M by Van der Kerk et al.X: H[12], Cl[14]; M: Zn, Cd

In the late 1970s Lahournère and Valade published several papers on the formation of Bu_3SnMgR compounds out of tributylstannane and on their derivatisation [25][26][24]. In a first attempt, they used various types of Grignard reagents each forming the corresponding Sn-Mg compounds in about 70 % yields. *Hexabutyldistannane* was found as side product.

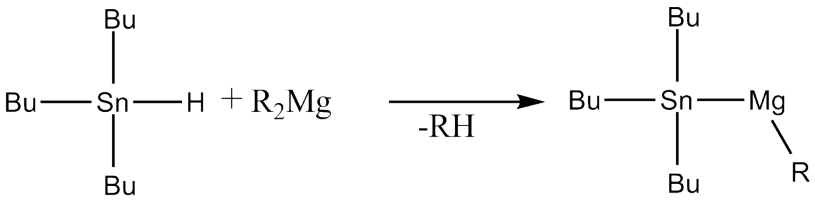

Figure 5.4: Reaction scheme of Bu_3SnH with R_2Mg by Lahournère and Valade [25][26][24]

5.2 Reaction of various R_3SnCl with magnesium: formation of Sn-Mg bonds

During this investigation, the reaction found out by Tamborski et al.[47] was redone. NMR samples of the two steps were taken. At first a signal at -144.3 ppm could be observed. Afterwards ^{119}Sn NMR chowed one signal at -100 ppm. It was found that the provided theory agrees with the experimental data.

Additionally *tri^{t}butylchlorostannane* **37** reacted with *magnesium*. The coupling of the two monostannes in order to form *hexa^{t}butyldistannane* could be confirmed by ^{119}Sn NMR investigations. No insertion of magnesium into the tin tin bond could be observed, however. Apparently, the sterical shielding of the tin tin bond by the large *^{t}butyl* groups hinders any further reaction.

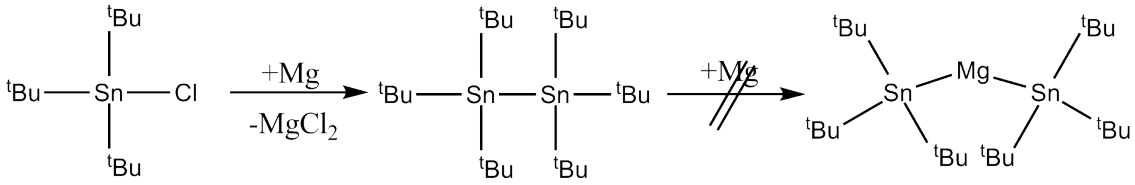

Figure 5.5: Reaction scheme of $^tBu_3SnCl$ with magnesium

5.3 Reaction of various R_3SnH with Bu_2Mg and Et_2Zn

5.3.1 Reaction of Bu_3SnH 32 with Bu_2Mg 9 and Et_2Zn 10

Tributylstannane **32** was stirred with *diethylzinc* **10** in a variety of solvent at room temperature. NMR investigations of the reaction product showed no reaction. Therefore mild heating (40°C) was used. Only decomposition and the formation of elemental tin was observed, however.

The reaction of **32** and *dibutylmagnesium* **9** leads to the same result. The butyl group lacks of electron stabilization. This might be the reason for this observation.

5.3.2 Reaction of Ph_3SnH 45 with Et_2Zn 10

The reaction of *triphenylstannane* **45** with *diethylzinc* **10** in THF has already been described by van Kerk et al.[12]. The reaction was redone in a variety of solvents. TMEDA was added afterwards for stabilization. Depending on the solvent different products could be obtained. The reaction with pentane resulted in a yellow solution. Without adding a stabilization reagent decomposition took place within 8 hours. In THF a white precipitation could be observed.

The reaction with diethylether as solvent leads to a yellow solution. Overnight two types of crystals precipitated. XRD measurement showed that one substance was *hexaphenyldistannane* **46**. Yet, the other substance was found to be a tristannane bounded to an *ethylzinc* fragment:$1,1,1,2,3,3,3$-*heptaphenyl*-2-(*ethylzincio*)*tristannane***TMEDA* **75**.

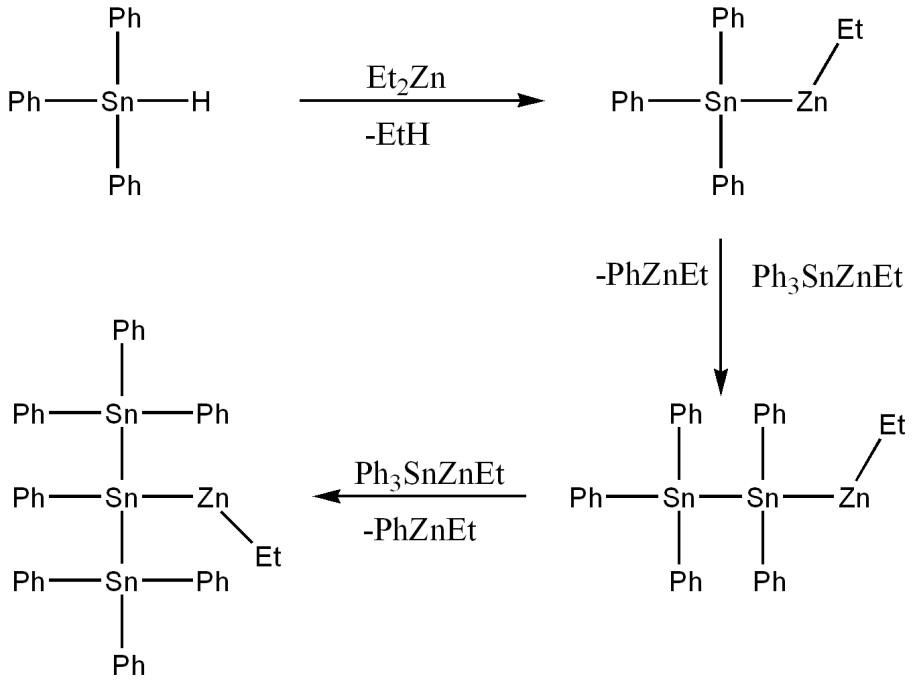

Figure 5.6: Proposed mechanism of the formation of zincotristannane in the reaction of Ph_3SnH **45** with Et_2Zn

^{119}Sn NMR measurements of the reaction mixtures showed different peaks, which could not be identified. Despite an analysis of the coupling pattern non of them could be clearly assigned to **75**. It can be assumed, however that in a first step *triphenyl*-(*ethylzincio*)*stannane* **73** is formed, as has already been described by van Kerk et al[12]. Since no stabilization reagent was added in the first place and diethylether is a weak coordinating solvent unstabilized product was able to react with one another in order to form $1,1,1,2,2$-*pentaphenyl*-1-(*ethylzincio*)*distannane*. In a next step another phenyl group was substitued by a triphenylstannane group. This mechanism is shown in figure 5.6. Although **75** was

isolated as crystal structure, it could not be excluded that the last phenyl group is not substituted.

Until now it is unsure weather two molecules of *triphenyl-(ethylzincio)stannane* **73** reacts with one another or **73** reacts with*triphenylstannane* **45** to form the ethylzinc substituted distannane. Since only unstabilized **73** undergoes this reaction, however the above proposed mechanism appears more likely.

5.3.3 Reaction of Ph_3SnH 45 with Bu_2Mg 9

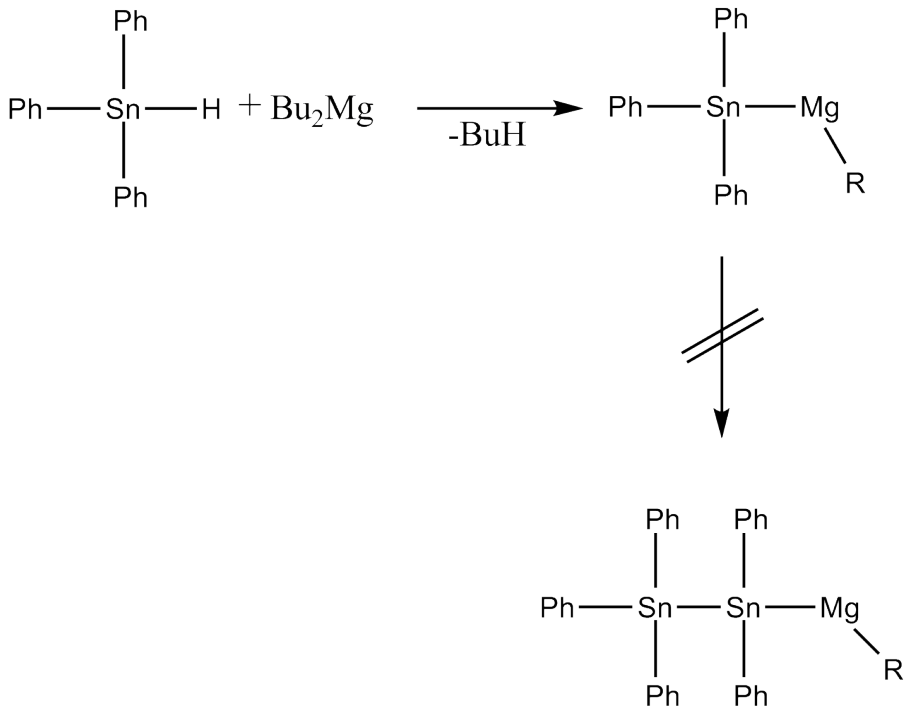

Figure 5.7: Reaction of Ph_3SnH **45** with Bu_2Mg **9**

Reaction of *dibutylmagnesium* **9** with *triphenylstannane* **45** in diethylether was investigated. After two hours a white precipitate could be observed. ^{119}Sn NMR investigation showed two signals: -151.6 ppm (main product) and -167.0 ppm. Literature[9] showed that the peak at -167.0 ppm is the educt. However, no possible product formed has a shift at about -152 ppm (table 5.1). ^{119}Sn NMR data of neither *triphenylstanyl-butylmagnesium* nor *bis(triphenylstanyl)magnesium* have not been reported so far. Therefore it can be assumed that a tin magnesium bond corresponding to one of the above mentiones compounds is formed.

After stirring the reaction mixture for 12 hours, another NMR sample was taken. However, no change in the NMR spectra could be observed. No onward reaction to a distannane or tristannane took place, as could be observed at the similar reaction with *diethylzinc*.

Table 5.1: ^{119}Sn NMR signals of possible products of the reaction of *triphenylstannane* **45** and *dibutylmagnesium* **9**

name	formular	δ [ppm]	ref
triphenylstannane	Ph_3SnH	-165	[9]
triphenylbutylstannane	Ph_3SnBu	-102	[54]
tetraphenylstannane	Ph_4Sn	-137	[9]
hexaphenyldistannane	$Ph_3SnSnPh_3$	-144	[9]

5.4 Reaction of various R_2SnH_2 with Bu_2Mg and Et_2Zn

5.4.1 Reaction of $^tBu_2SnH_2$ with Bu_2Mg 9 and Et_2Zn 10

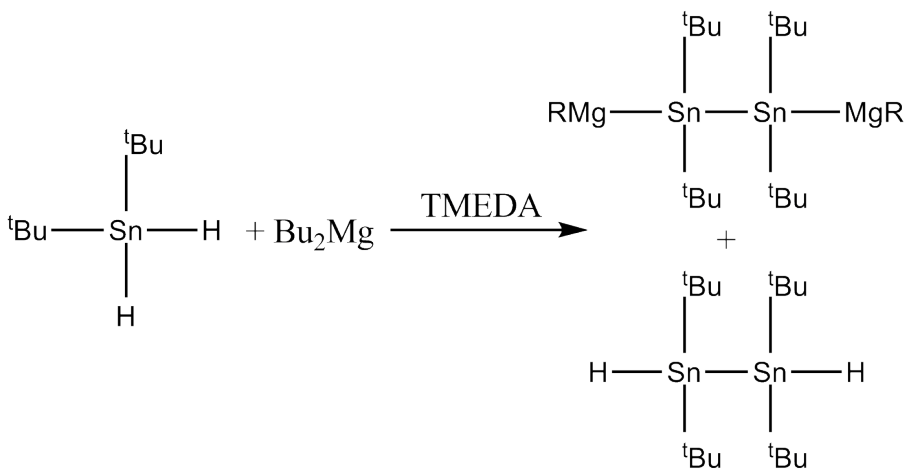

Figure 5.8: Reaction of $^tBu_2SnH_2$ **36** with Bu_2Mg **9**

Reaction of $^tBu_2SnH_2$ **36** with *dibutylmagnesium* **9** in the presence of TMEDA **31** was carried out. ^{119}Sn NMR shows one main signal at -77 ppm. A symmetric coupling pattern and small coupling constants of 303 Hz indicate that a symmetric substituted distannane was obtained. Another smaller signal at -83 ppm could be observed, too. According to literature [16] this is $1,1,2,2$-*tetra*^{t}*butyldistannane*. ^{1}H coupled measurement showed that the peak at -83 ppm is a douplet, whereas the peak at -77 ppm is not, suggesting the formation of $1,1,2,2-$ *tetra*^{t}*butyl*-1,2-*bis*(*butylmagnesio*)*distannane*.

When stirring **36** with *diethylzinc* in the presence of **31** over 4 days no reaction took place.

5.4.2 Reaction of Ph_2SnH_2 with Et_2Zn 10

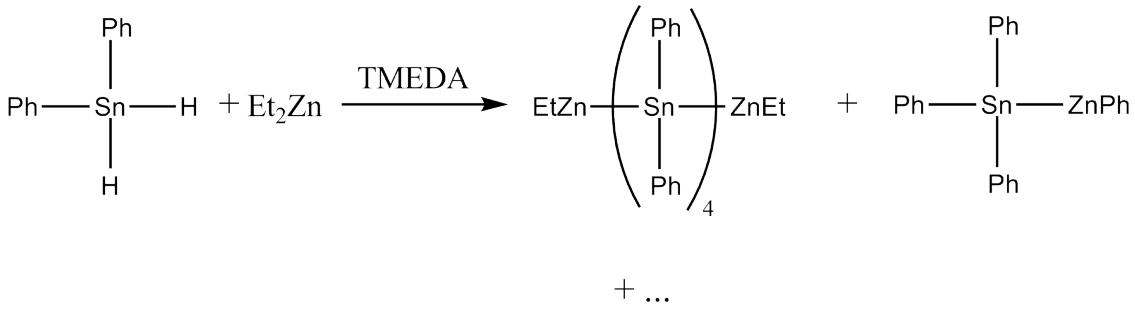

Figure 5.9: Reaction of Ph_2SnH_2 **44** with Et_2Zn **10**

Reaction of *diphenylstannane* **44** with *diethylzinc* **10** in diethylether at the presence of $TMEDA$ **31** leads to a yellow solution and a yellow precipitate. The precipitate was filtered and recrystallized in THF. Single crystals of $1,1,2,2,3,3,4$,4-*octa-phenyl-bis-*(*ethylzincio*)*tetrastannane**$2TMEDA$ **76** could be obtained, which are described later in chapter 5.6.2. It can be assumed that the reaction of **44** with **31** leads to a dehydrogenative coupling, as further shown in chapter 6. However, addition of **10** stops the polymerization immediately and leads to oligostannanes with tin zinc bonds.

The dehydrogenative coupling starts instantaneously which can be observed by a light yellow coloring of the reaction mixture. In order to slow down the polymerization, the reaction was performed at -40°C. To this reaction mixture **10** was added after 5 min, 15 min, 25 min , 35 min and 45 min. When adding **10** after 25 minutes a precipitate could be isolated, which was identified as **76** by X-ray analysis. No other product could be identified however, since ^{119}Sn NMR showed several peaks.

Out of one of the reaction mixture, also single crystals of *triphenyl-*(*ethylzincio*)-*stannane**$TMEDA$ **77** could be isolated. Although these crystals were only a side product, it clearly indicated that ligand exchange took place as well.

5.4.3 Reaction of Ph_2SnH_2 with Bu_2Mg 9

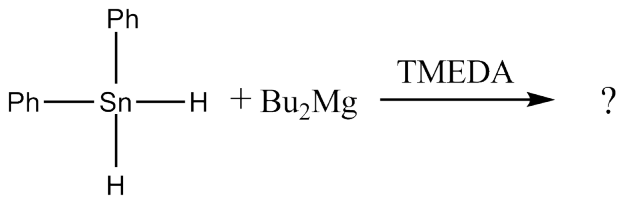

Figure 5.10: Reaction of Ph_2SnH_2 **44** with Bu_2Mg **9**

Reaction of *diphenylstannane* **44** with *dibutylmagnesium* **9** in the presence of $TMEDA$ **31** leads to brownish oily precipitate. The precipitate could be dissolved in THF. Contrary to the reaction with *diethylzinc*, ^{119}Sn NMR showed only one unidentified signal at -88 ppm.

Stirring **44** with **9** overnight without the presence of **31** leads to different products. ^{119} Sn NMR of the formed precipitate showed two signals: one at -209 and one at -223 ppm. Perphenylated six membered tin ring systems show ^{119}Sn NMR signals at approximately -208 ppm[9]. The obtained signal did not show any coupling pattern however, which contradicts the formation of a hexastannacyclohexane. The signal at -223 ppm could be identified as the educt.

5.4.4 Reaction of p-Tol_2SnH_2 50 with Bu_2Mg 9 and Et_2Zn 10

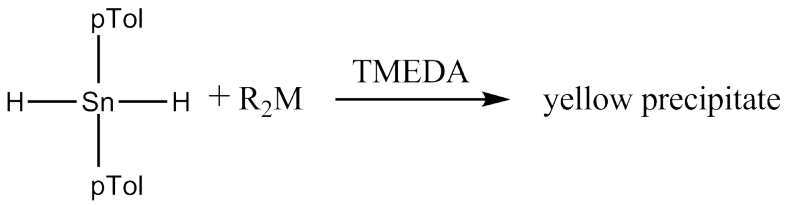

Figure 5.11: Reaction of p-Tol_2SnH_2 **50** with R_2M: Et_2Zn **10** and Bu_2Mg **9**

The reaction of *di-p-tolylstannanes* **50** with Bu_2Mg **9** in the presence of TMEDA **31** leads to a yellow precipitate and a dark orange solution. Different to the precipitate obtained when reacting **44** with **9** and **31**, this precipitate was insoluble in THF. ^{119}Sn NMR of the solution showed one unidentified signal at -104 ppm. It can be assumed that poldi-p-tolylstannane was obtained. The orange reaction solution did not show any signals in ^{119}Sn NMR. Single crystals of *di-p-tolylmagnesium**$TMEDA$ could be isolated however.

The reaction of **50** with **10** in the presence of **31**, leads to a yellow precipitate. The solution remained colourless and did not show any signal in the ^{119}Sn NMR. Again, formation of the polymer can be assumed.

5.4.5 Reaction of various stannanes with only $TMEDA$

The reactions of various dialkylstannanes with TMEDA **31** were investigated, too. Either cyclic oligomers or polymer chains could be observed. The products will be further described in chapter 6

Also *tributylstannane* **32** was stirred with **31** overnight. It was expected that the stannane reacts in a dehydrogenative coupling to form distannane. ^{119}Sn NMR investigations showed however, that no reaction took place. Further, *triphenylstannane* **45** was stirred with **31**. The result of no reaction was the same here.

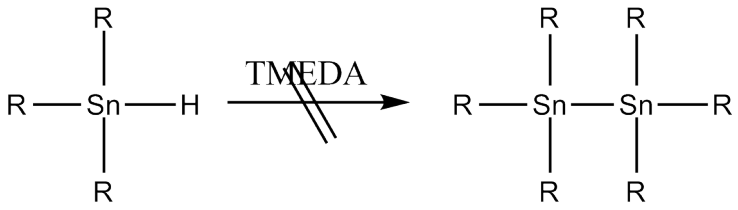

Figure 5.12: Reaction of R_3SnH with TMEDA

5.5 Discussion of the crystal structure of *di-p-tolyl-magnesium*TMEDA* 80 and comparison with similar structures described in literature

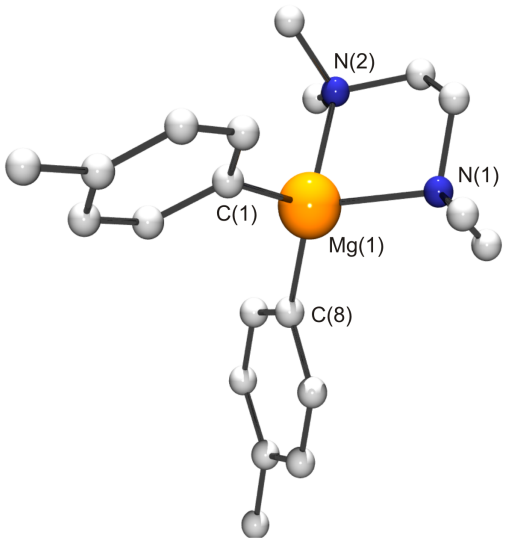

Figure 5.13: Crystal structure of **80**(Hydrogen atoms omitted for clarity) Selected bond lengths [Å] and angles [°] for **80**: Mg-C(1):2.1601(12); Mg-C(8):2.1539(12); Mg-N(1):2.2019(11); Mg-N(2):2.2114(10); C(1)-Mg-C(8):119.48(5); N(1)-Mg-N(2):82.41(4); N(1)-Mg-C(1):110.07(4); N(1)-Mg-C(8):112.86(5); N(2)-Mg-C(1):112.74(4); N(2)-Mg-C(8):113.37(5);

*Di-p-tolylmagnesium*TMEDA* **80** crystallizes in a monoclinic space group C2/c with 8 molecules in the unit cell. Mg-C distances range from 2.1539(12) Å to 2.1601(12) Å, which lies within the common C-Mg bond range. Mg-N distances range from 2.2019(11) Å to 2.2114(10) Å.

The magnesium atom has a tetrahedral coordination sphere with angles between

82.41(4)° and 119.48(5)°. The angle N(1)-Mg-N(2) (82.41(4)°) is the smallest. This is most probably due to the long Mg-N distances.

Crystal structures of several diarylmagnesium compounds are known. Their structural characteristics are listed in table 5.2. The most striking difference in those structures is the C-Mg-C angle which ranges from nearly linear 166.79° to 118.75°, which is only to a certain extend larger than a tetrahedral angle. This might depend on the coordination reagent. THF and TMEDA coordinated magnesium compounds tend to have smaller angles with a tetrahedral coordination sphere. If crown ether like coordination reagents are used, larger C-Mg-C angles could be observed. For *disupermesitylmagnesium* [50], which is not coordinated by TMEDA, THF or any similar coordination reagent a C-Mg-C angle of 158.34 could be observed.

Table 5.2: Structural data of various diarylmagnesium compounds

formula	coordination reagent	Mg-C [Å]	C-Mg-C angle[°]	CN of Mg	ref
$p\text{-}Tol_2Mg$	$TMEDA$	2.154-2.160	119.48	4	*
Ph_2Mg	$TMEDA$	2.167-2.170	119.22	4	[48]
Ph_2Mg	$C_8H_6O(OC_2H_2)_4$	2.190	163.75	4	[33]
$(p\text{-}^tBuPh)_2Mg$	$C_8H_6O(OC_2H_2)_4$	2.187-2.188	166.79	4	[34]
$(p\text{-}^tBuPh)_2Mg$	$O(C_2H_2OCH_3)_2$	2.157	112.58	4	[32]
Mes_2Mg	THF	2.165-2.182	118.75	4	[49]
$(iPr_3Ph)_2Mg$	THF	2.177-2.180	123.04	4	[49]
$(o\text{-}EtPh)_2Mg$	THF	2.135-2.137	127.73	4	[18]
Ph_2Mg	THF	2.128	122.45	4	[35]
$Supmes_2Mg$		2.118-2.120	158.34	2	[50]

* the crystall structure was first described in this work

5.6 Discussion of the crystal structures of compounds including a Sn-Zn bond

5.6.1 1, 1, 1, 2, 3, 3, 3-*Hepta-phenyl*-2-(*ethylzincio*)*tristannane** *TMEDA* **75**

1, 1, 1, 2, 3, 3, 3-*Hepta-phenyl*-2-(*ethylzincio*)*tristannane***TMEDA* **75** crystallizes in an orthorhombic space group Pna2(1). There are 8 molecules in the unit cell. Tin tin distances are between 2.79 Å and 2.82 Å, which lies within the average Sn-Sn distance. Sn-C distances range from 2.15 to 2.19 Å. The distance between Sn(3) and C(37) is the longest with 2.193 Å. Sn(3) - Zn distance is 2.68 Å.

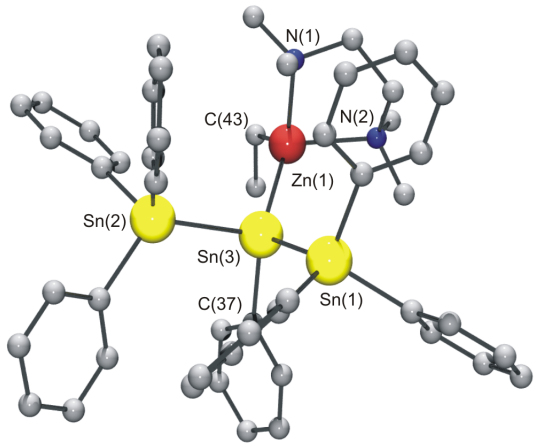

Figure 5.14: Crystal structure of **75** (Hydrogen atoms omitted for clarity) Selected bond lengths [Å] and angles [°] for **75**:Sn(3)-Sn(1):2.7923(3); Sn(3)-Sn(2):2.8165(3); Sn(3)-Zn:2.6790(4); Sn(3)-C(37):2.193(3); Sn(2)-C(1):2.165(2); Sn(2)-C(7):2.170(3); Sn(2)-C(13):2.170(3); Sn(1)-C(19):2.146(3); Sn(1)-C(25):2.161(3); Sn(1)-C(31):2.162(3); Zn-C(43):2.007(3); Zn-N(1):2.165(3); Zn-N(2):2.169(4); Sn(2)-Sn(3)-Sn(1):97.062(8); Sn(2)-Sn(3)-Zn:113.071(11); Sn(1)-Sn(3)-Zn:120.301(13); Sn(2)-Sn(3)-C(37):102.97(8); Sn(1)-Sn(3)-C(37):101.76(7); Zn-Sn(3)-C(37):118.36(8); Sn(3)-Zn-C(43):124.10(12); Sn(3)-Zn-N(1):107.46(7); Sn(3)-Zn-N(2):110.00(7); N(1)-Zn-N(2):83.75(13);

Sn(3) is coordinated in a tetrahedral way. However, the Sn(2)-Sn(3)-Sn(1) angle is significantly smaller than the expected tetrahedron angle of 109°, with 97.1°, whereas the angle Sn(2)-Sn(3)-Zn is 113.1° and the angle Sn(1)-Sn(3)-Zn is 120.3°, which is considerably larger than 109°. This is most probably due to a

higher p character of the Sn-Sn and the Sn-C bonding, whereas the Sn-Zn bond has a higher s character. The longer Sn(3)-C distance indicates this, too.

A similar contorted tetrahedral coordination sphere can be observed around the zinc atom. N(1)-Zn-N(2) is the smallest angle (83.8°). In addition, all other inner cyclic angles of the five membered ring Zn-N(1)-C(45)-C(46)-N(2) ranges from 104.7 Å to 112.0 Å. This effect can be explained by the long Zn-N distance (2.17 Å) compared to the other bonding of the ring which is about 1.5 Å. This indicates that no real Zn-N bonding is present. TMEDA is just coordinating on the zinc atom.

5.6.2 $1,1,2,2,3,3,4,4$-*Octa-phenyl*-$1,4$-*bis*-(*ethylzincio*)*tetrastannane**$2TMEDA$ **76**

$1,1,2,2,3,3,4,4$-*Octa-phenyl*-$1,4$-*bis*-(*ethylzincio*)*tetrastannane**$2TMEDA$ **76** crystallizes in the monoclinic space group P2(1)/c. There are 3 molecules in the unit cell. There is a centre of inversion in the middle of the central tin atoms Sn(2a) and Sn(2b).

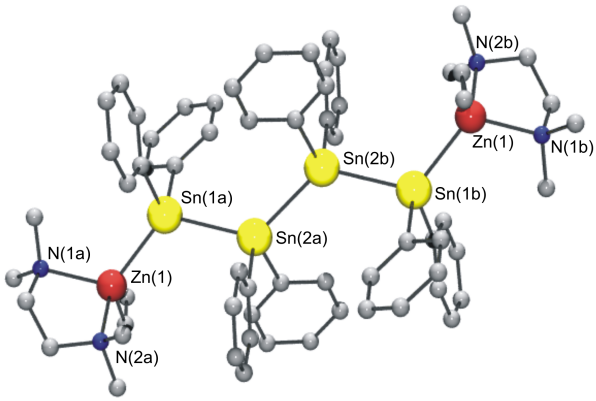

Figure 5.15: Crystal structure of **76** (Hydrogen atoms omitted for clarity) Selected bond lengths [Å] and angles [°] for **76**:Sn(1)-Sn(2):2.8155(3); Sn(1)-Zn:2.6416(5); Sn(2a)-Sn(2b):2.8085(4); Sn(1)-C(1):2.184(3); Sn(1)-C(7):2.180(3); Sn(2)-C(13):2.168(3); Sn(2)-C(19):2.166(3); Zn-C(25):2.023(6); Zn-N(1):2.168(4); Zn-N(2):2.186(3); Sn(1)-Sn(2a)-Sn(2b):124.892(13); Zn-Sn(1)-Sn(2):118.631(15); C(1)-Sn(1)-C(7):101.37(12); C(13)-Sn(2)-C(19):102.57(12); Sn(1)-Zn-N(1):113.36(11); Sn(1)-Zn-N(2):110.38(9); Sn(1)-Zn-C(25):122.7(2); N(1)-Zn-N(2):83.30(13); Zn-Sn(1)-Sn(2a)-Sn(2b):175.73; Sn(1a)-Sn(2a)-Sn(2b)-Sn(1b):180.0;

Tin Tin distances (Sn(1)-Sn(2):2.8155 Å and Sn(2a-Sn2b): 2.8085 Å) have approximately normal tin-tin distances. Also the Sn-C distances (2.166 Å- 2.184 Å) are between the usual tin carbon distances. The Sn(2) carbon distances are to a certain extend shorter than the corresponding Sn(1) carbon distances. This indicates that the Sn(1)-C bonding has a higher p character, which could be observed with **75**, too. However, this phenomenon is far less pronounced for **76** than in the case of **75**. The Sn-Zn distance is 2.6416 Å.

The tin atoms are in a tetrahedral coordination sphere. The Sn(1)-Sn(2a)-Sn(2b) angle, however is significantly larger (124.9°) than the expected tetrahedron angle. The Zn-Sn(1)-Sn(2) are 118.6°, which is also larger than the tetrahedral angle. In the contrary the C-Sn-C angles range from 101.4° to 102.6°.

The coordination sphere around the zinc atom amount to approximately about the same as described for 1, 1, 1, 2, 3, 3, 3-*hepta-phenyl*-2-(*ethylzincio*)*tristannane** *TMEDA* **75**. Only small differences in angles and distances could be observed.

5.6.3 *Triphenyl-(phenylzincio)stannane*TMEDA* 77

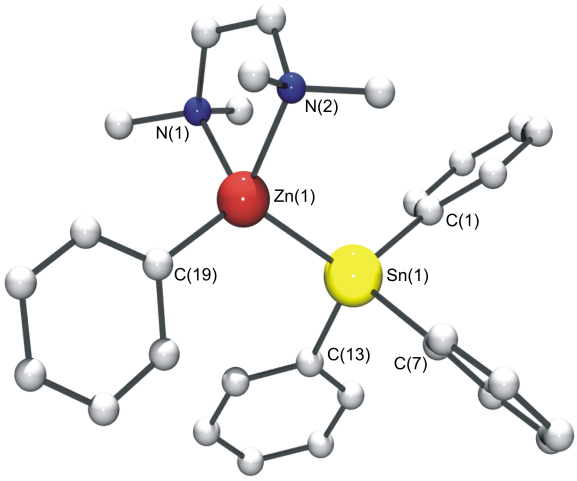

Figure 5.16: Crystal structure of **77** (Hydrogen atoms omitted for clarity) Selected bond lengths [Å] and angles [°] for **77**:Sn-Zn:2.6017(8); Sn-C(1):2.167(6); Sn-C(7):2.180(6); Sn-C(13):2.172(6); Zn-C(19):1.996(6); Zn-N(1):2.167(5); Zn-N(2):2.165(5); C(1)-Sn-Zn:120.81(16); C(7)-Sn-Zn:115.55(16); C(13)-Sn-Zn:112.35(19); C(1)-Sn-C(7):99.1(2); C(1)-Sn-C(13):102.3(2); C(7)-Sn-C(13):104.5(2); Sn-Zn-C(19):120.07(18); Sn-Zn-N(1):108.53(14); Sn-Zn-N(2):109.24(15); N(1)-Zn-N(2):84.15(18);

*Triphenyl-(phenylzincio)stannane*TMEDA* crystallizes in the monoclinic space

group P2(1)/c. There are 4 molecules in the unit cell. Tin carbon distances range from 2.167 Å to 2.180 Å, which lies within the usual Sn-C bonding. The Sn-Zn distance is 2.6017 Å.

The Sn atom has a tetrahedral coordination sphere. C-Sn-C angles are to a certain extend smaller than 109° ranging from 99° to 104°. C-Sn-Zn angles, however range from 121° to 112°.

The coordination sphere of the zinc atom is similar to the crystal structures discussed above (5.6.2 and 5.6.1). The zinc carbon distance is about the same, although the zinc is bonded to an phenyl group, in contrast to **75** and **76**, where zinc is bonded to an ethyl group.

5.6.4 Comparison with other crystal structures described in literature including a Sn-Zn bond

So far, only three different crystal structures including a Sn-Zn bond have been described. Formula and structural data are listed in table 5.3. The structures are shown in figure 5.17 Sn_9ZnPh was described by van Koten et al.[20] in 1990. Sn-Zn distances range from 2.740 Å to 2.787 Å. This is to some extend larger than comparable distances of the crystal structures described above (5.6.1, 5.6.2 and 5.6.3). This is caused by the considerably different tin structure bonded to the zinc atom: the former structure describes a Sn_9 cluster, whereas the latter are monostannanes (**77**) and oligostannanes (**75** and **76**). Sn-Zn distances of the other known crystal structures $[(Me_7Si_4)(TolN)_3Sn]_2Zn$ [30] and $(Ph_2C_3HO_2)_2Zn[C_3H_6N(CH_3)]_2Sn$ [22] are in the same range as the bond distances described in this thesis.

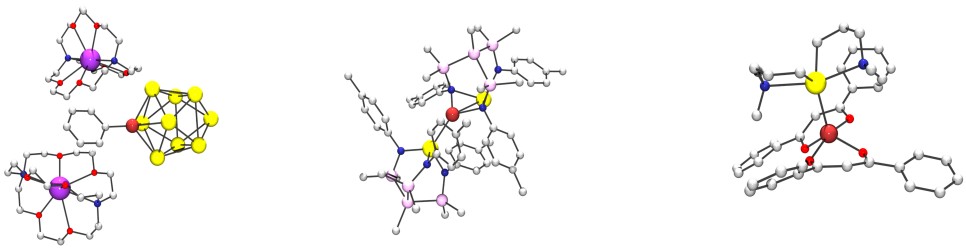

Sn_9ZnPh [20]	$[(Me_7Si_4)(TolN)_3Sn]_2Zn$ [30]	$(Ph_2C_3HO_2)_2Zn[C_3H_6N(CH_3)]_2Sn$ [22]

Figure 5.17: structure of compounds containing Sn-Zn bond, as described in literature

Table 5.3: Structural data of various compounds including a Sn-Zn bond

formula	Sn-Zn [Å]	Zn-C [Å]	Zn-N or Zn-O [Å]	CN of Zn	ref
Sn_9ZnPh	2.740-2.787	1.987		5	[20]
$[(Me_7Si_4)(TolN)_3Sn]_2Zn$	2.578		2.035-2.044	3	[30]
$(Ph_2C_3HO_2)_2Zn$ $[C_3H_6N(CH_3)]_2Sn$	2.634		1.997-2.065	5	[22]
Ph_7Sn_3ZnEt* $TMEDA$	2.679	2.007	2.165-2.169	4	*
$Ph_8Sn_4(ZnEt)_2$* $2TMEDA$	2.642	2.023	2.168-2.186	4	*
$Ph_3SnZnPh$* $TMEDA$	2.602	1.996	2.165-2.167	4	*

* the crystal structure was first described in this thesis

5.6.5 Comparison with ionic oligostannanes described in literature

Different to alkaline and earth alkaline metals, which have a low electro negativity, zinc has the same electro negativity than tin (table 5.4). Therefore compounds containing tin alkaline or tin earth alkaline bonds are expected to have a higher ionic character than those containing a tin zinc bond.

Table 5.4: Electro negativity of selected metals after Allred and Rochov

element	electro negativity
tin	1.7
zinc	1.7
lithium	1.0
potassium	0.9
magnesium	1.2
calcium	1.0
strontium	1.0

The most obvious difference between the tin zinc compounds and the compounds containing tin and an alkaline or an alkaline earth metal is that the latter have clearly separated ion pairs, whereas the former have a tin zinc distance which

is comparable to a covalent bonding. Taking into consideration the electonegativity, it is possible that tin zinc compounds do not form separated ion pairs even in solution.

In the ionic structures tin tin bonds are to a certain extend larger than usual Sn-Sn distances. In the contrary the Sn-Sn distances of the Sn-Zn compounds fall into the normal Sn-Sn bonding. This indicates that Sn-Zn compounds have far less ionic character. Table 5.5 below provides an overview of Sn-Sn bonding in various ionic tin structures.

Table 5.5: Structural data of various phenyl substituted ionic tin compounds including at least one Sn-Sn bond

formula	counter ion	Sn-Sn [Å]	ref
$(Ph_2Sn)_2$	$Li(NH_3)_4$	2.905	[44]
$(Ph_2Sn)_2$	$K(NH_3).crown2.6$	2.909	[53]
$(Ph_2Sn)_3$	$Li(NH_3)_4$	2.867-2.872	[52]
$(Ph_2Sn)_6$	$K_2(NH_3)_{12}$	2.869-2.821	[53]
$[Ph_3Sn]_3Sn$	$Ca[PO(N(CH_3)_2)_3]_2.crown.6.2$	2.820-2.835	[17]
$[Ph_3Sn]_3Sn$	$Sr[PO(N(CH_3)_2)_3]_2.crown.6.2$	2.811-2.836	[17]
$[Ph_3Sn]_3Sn$	$Li(NH_3)_4$	2.817-2.834	[17]

Chapter 6

Dehydrogenative coupling of diaryldihydrostannanes with a base

6.1 Reaction of various dialkylstannane with TMEDA

The reaction of $TMEDA$ **31** with dialkylstannanes leads to a dehydrogenative coupling. Different dialkyl- and diarylstannanes (listed in table 6.1)below were used for dehyrogenative coupling. Only the polydiarylstannanes, however, were further investigated. Reaction of *di*^{t}*butylstannane* with **31** leads to a light yellow precipitate, which could be identified as *octa*^{t}*butyltetrastannancyclobutane*. Reaction of *dibutylstannane* leads to a yellow precipitate, too. ^{119}Sn NMR of the reaction solution did not show any signals. Thus only non soluble polymerchains and no oligomeric ring systems were obtained.

6.2 Formation and characterization of the polymers

Table 6.1: Different alkyl groups of R_2SnH_2 used for polymerization

name	cyclic products	polymeric chains
n-butyl	-	x
^{t}butyl	x	-
phenyl	-	x
o-tolyl	-	x
p-butylphenyl	-	x

6.2.1 General characterization and comparison of the polymers

Optical description: Polydiphenylstannane and polydi-o-tolylstannane are yellow solids. They are hardly soluble in any solvent tested. On the contrary polybis (butylphenyl)stannane is a highly viscous orange-yellow liquid with a high solubility in diethylether, as well as THF. This is most probably due to the flexibility of the n-butyl group bound on the phenyl group. It inhibits a regular arrangement of the polymer chains in solid state and enhances the entropy when the polymer is dissolved.

Shearing: Each polymer was put on a slide and aligned with a spatula. Then the superficial material was removed with a razor blade in order to get a thin layer. The slide was investigated on a microscope with polarization filters (figure 6.1 and 6.2). In addition, VIS-measurement were carried out at different angles of the polarization filters. (figures 6.3, 6.4 and 6.5)

Both measurements clearly indicate that polydiphenylstanne is best aligned. Highest intensity differences at the measurement at different angles of polarisation can be observed. Polybis(-p-butylphenyl)stannane showed no alignment at all. No intensity difference in the VIS-measurements could be observed. Apparently, it is not viscous enough to stay in the aligned form. Concerning poly-di-o-tolylstannane it can be assumed that alignment of the polymer chains is partly inhibited due to sterical interference of the methyl group in ortho position.

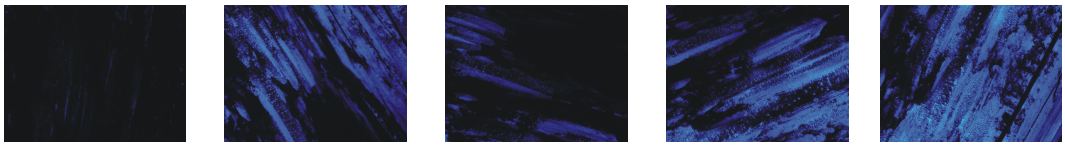

0°	40°	80°	120°	160°

Figure 6.1: Photos of aligned polydiphenylstannane under the microscope with polarisation filters at different angles

TGA measurements: The thermo stability of each polymer was tested with TGA measurements. (figures 6.6, 6.7 and 6.8). For polydiphenylstannane, as well as polybis(-p-butylphenyl)stannane one single loss of weight can be observed. Apparently, polydiphenylstannane is less stable since decomposition takes place at

0°	45°	90°	135°	180°

Figure 6.2: Photos of aligned polydi-o-tolylstannane under the microscope with polarization filters at different angles

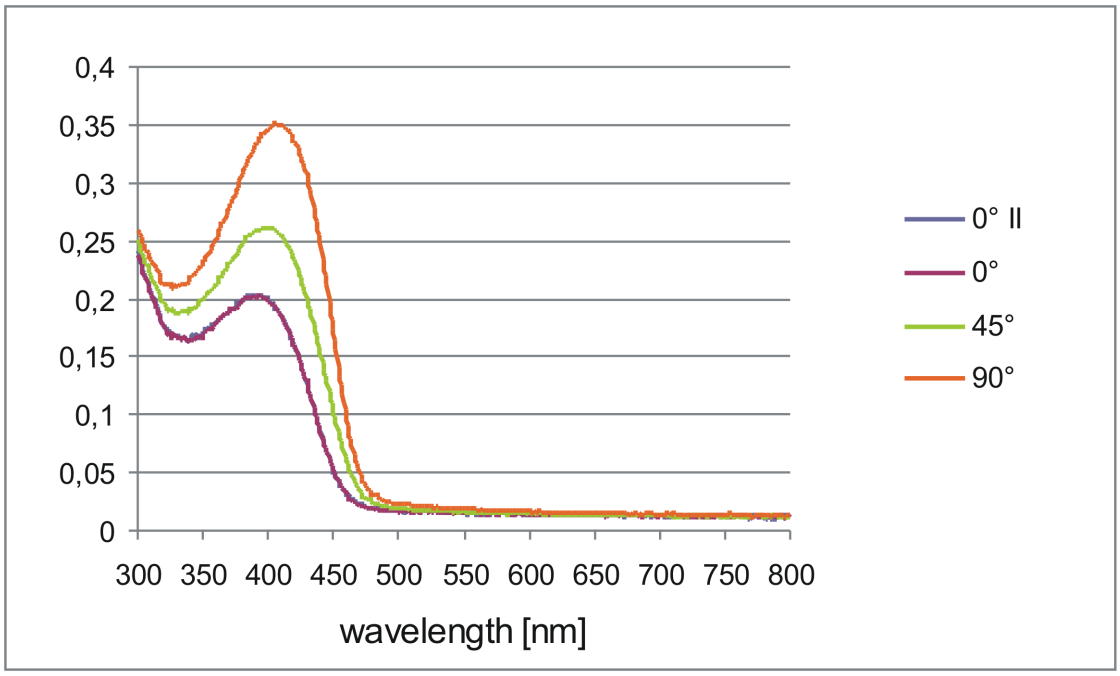

Figure 6.3: VIS measurement of polydiphenylstannane with polarisation filter at different angle. Absorption maximum is at 410 nm.

about 300°C which is 50°C less than was observed for polybis(-p-butylphenyl)stannane. For polydi-o-tolylstannane succesively decomposition takes place starting at about 300°C.

DSC measurements: DSC measurements were only made for polybis(butylphenyl)-stannane (figure 6.9). In the first run, a slight exothermic reaction could be observed at 60°C. However, this reaction was irreversible. No other reaction could be observed in between the temperature interval of -60°C to 150°C. In order to investigate this irreversible reaction some polybis(-p-butylphenyl)stannane was dissolved in ether and drops of the solution were put on a slide. After evaporating of the solvent a polymer film remained. The slide was gradually heated with a heat stage at a rate of 10°C per minute til 150°C and was then cooled down to room

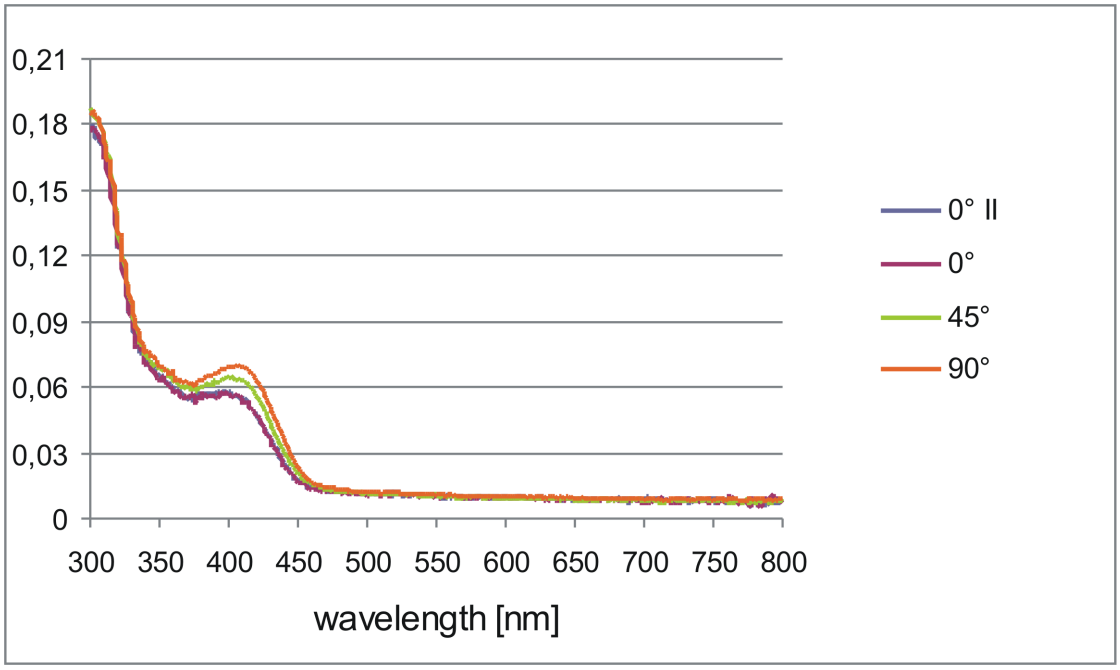

Figure 6.4: VIS measurement of polydi-o-tolylstannane with polarisation filter at different angle. Absorption maximum is at 410 nm.

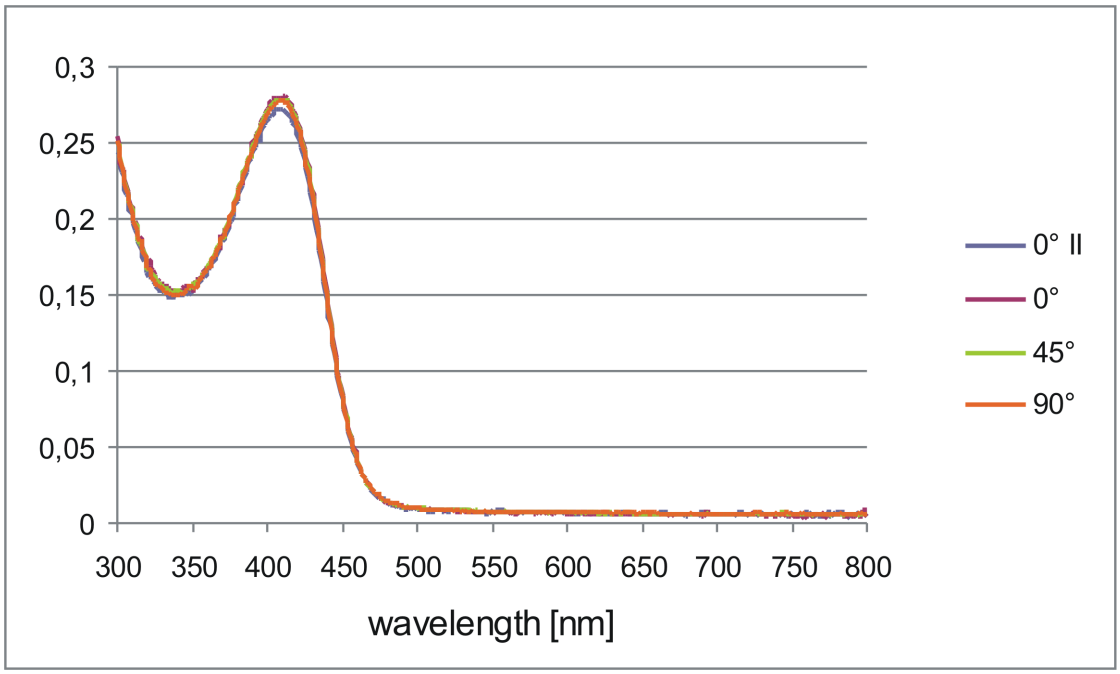

Figure 6.5: VIS measurement of polybis(-p-butylphenyl)stannane with polarisation filter at different angle. Absorption maximum is at 410 nm.

temperature. In the course of this heating step the film was constantly observed under the microscope and pictures were taken (figure 6.10).

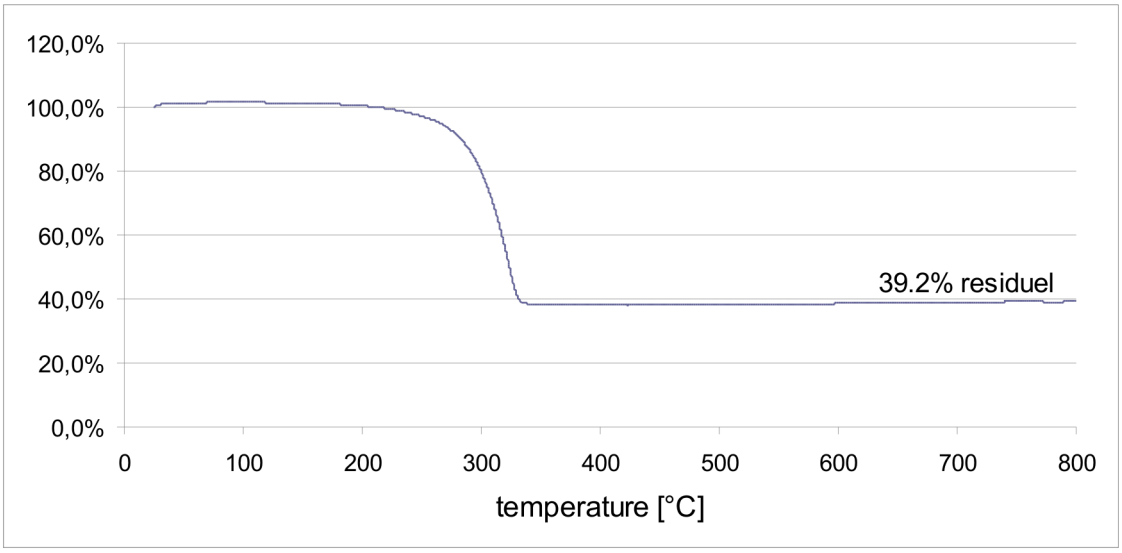

Figure 6.6: TGA measurement of polydiphenylstannane

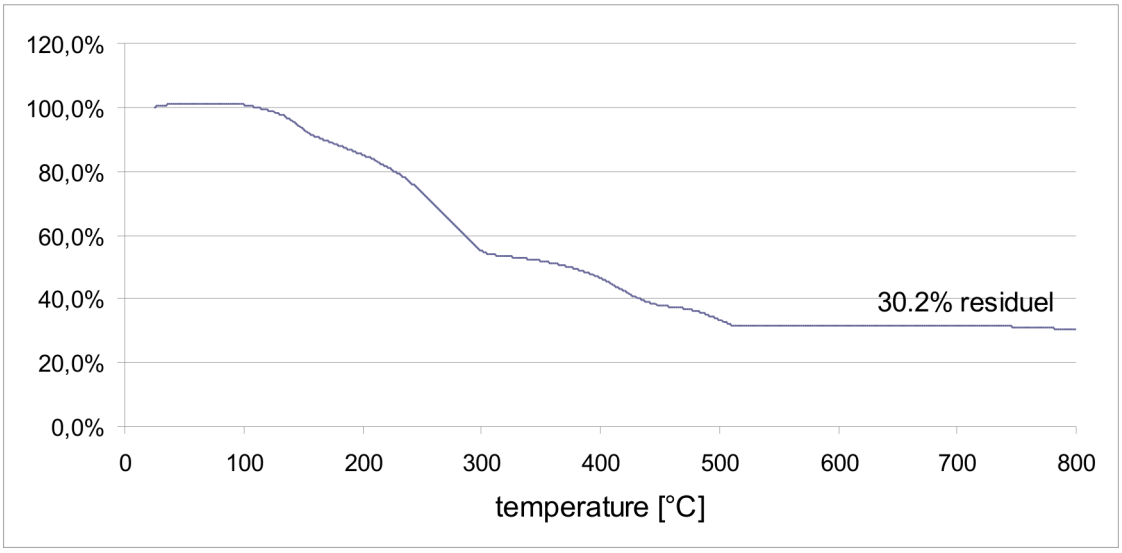

Figure 6.7: TGA measurement of polydi-o-tolylstannane

Above 60°C the color of the film slowly turned to gray. Apparently, a decomposition takes place as is indicated in the DSC spectra. The color of the film completely vanished after heating (figure 6.11). This white decomposition product is still non volatile however, since the TGA spectra did not show a loss of weight before 300°C.

Elemental analysis: Elemental analysis was made of all polymers (data listed in table 6.2). For polydiphenylstannane and polybis(-p-butylphenyl)stannane only small deviations from the expected values were found. The values for %C and %H found for poly-di-o-tolylstannane are far to low, However. On the contrary the %N

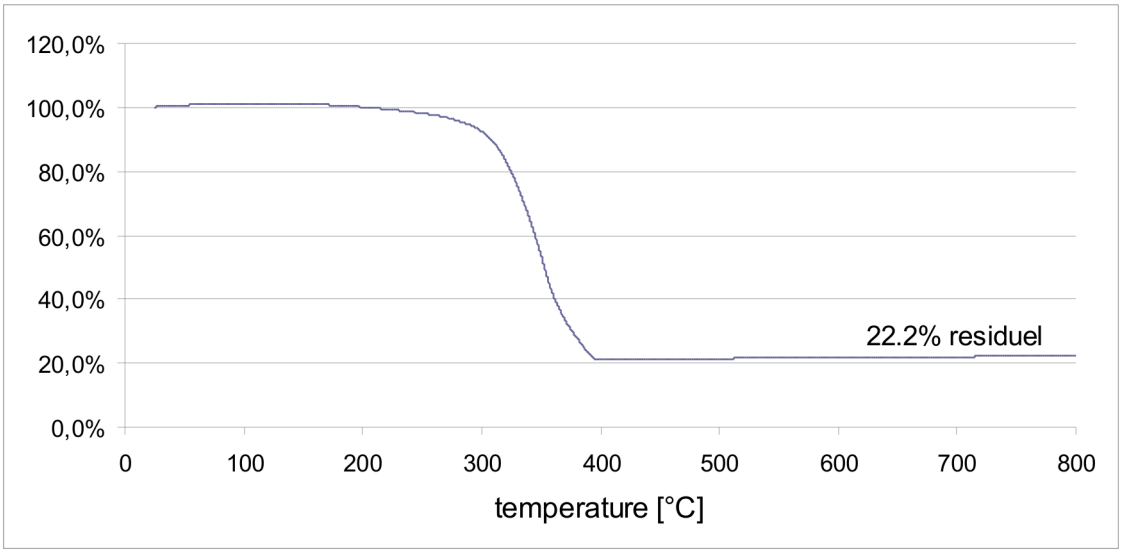

Figure 6.8: TGA measurement of polybis(-p-butylphenyl)stannane

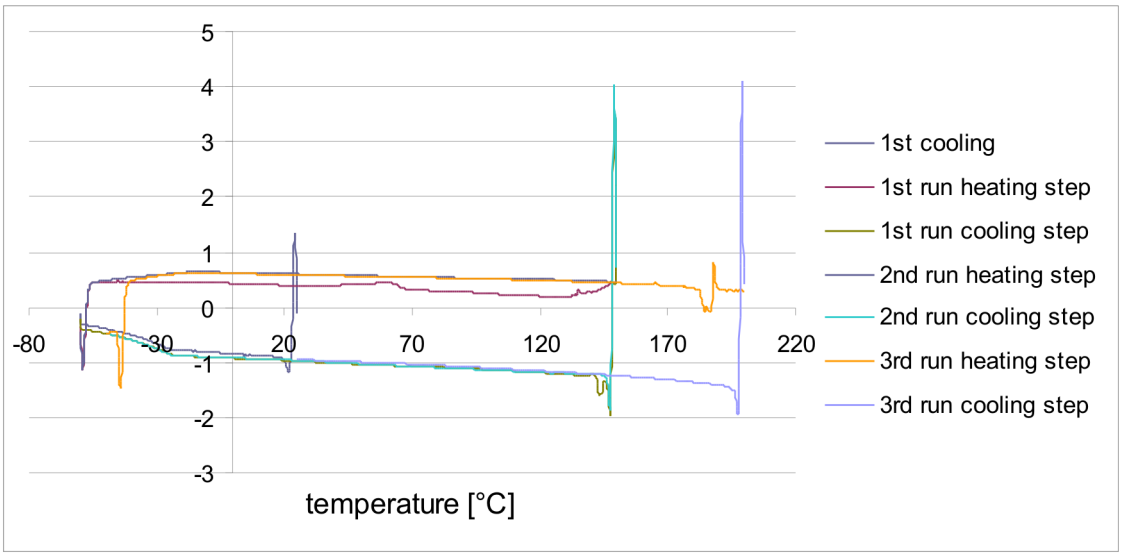

Figure 6.9: DSC measurement of polybis(-p-butylphenyl)stannane

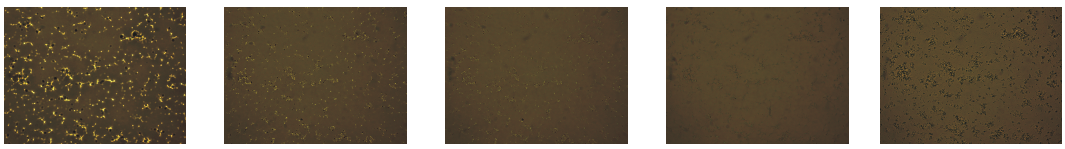

RT	55°C	85°C	115°C	150°C

Figure 6.10: Photos of polybis(-p-butylphenyl)stannane under the microscope at different temperatures

values are over 2 %, which can not be explained by deviation of the instrument. Since complete burning of the sample was assured, no explanation for this deviation

Figure 6.11: Photo of a polymer layer of polybis(-p-butylphenyl)stannane before and after heating above 150°C

can be provided.

Table 6.2: Elemental analysis data of polydiphenylstannane, polydi-o-tolylstannane and poly bis(butylphenyl)stannane

compound	%C		%H		% N	
	required	found	required	found	required	found
$[Ph_2Sn]_n$	52.81	50.55	3.69	3.9	0	0.22
$[o\text{-}Tol_2Sn]_n$	55.87	45.56	4.69	5.84	0	2.52
$[(BuPh)_2Sn]_n$	62.37	63.02	6.80	6.90	0	0.06

Head space analysis: A head space analysis of the reaction of *bis(butylphenyl)-stannane* with TMEDA was carried out, in order to find volatile side products. A significant amount of butylbenzene could be detected. This indicates the formation of side chains. This might be an explanation for the deviation of the required values at the elemental analysis.

Powder diffraction: X-ray powder diffraction was measured for both solid polymers: polydiphenylstannane and polydi-o-tolylstannane. The spectra showed that polydiphenylstannane is mostly amorphic. Only one peak could be observed (figure 6.12). However, polydi-o-tolylstannane has a high percentage of crystalline. Several distinct peaks could be observed (figure 6.13).

GPC measurments: Due to the bad solubility of polydiphenylstannane and polydi-o-tolylstannane no GPC measurements of these two compounds were possible. However, GPC measurements of polybis(-p-butylphenyl)stannane were made at different reaction condition. These measurements are later described in chapter

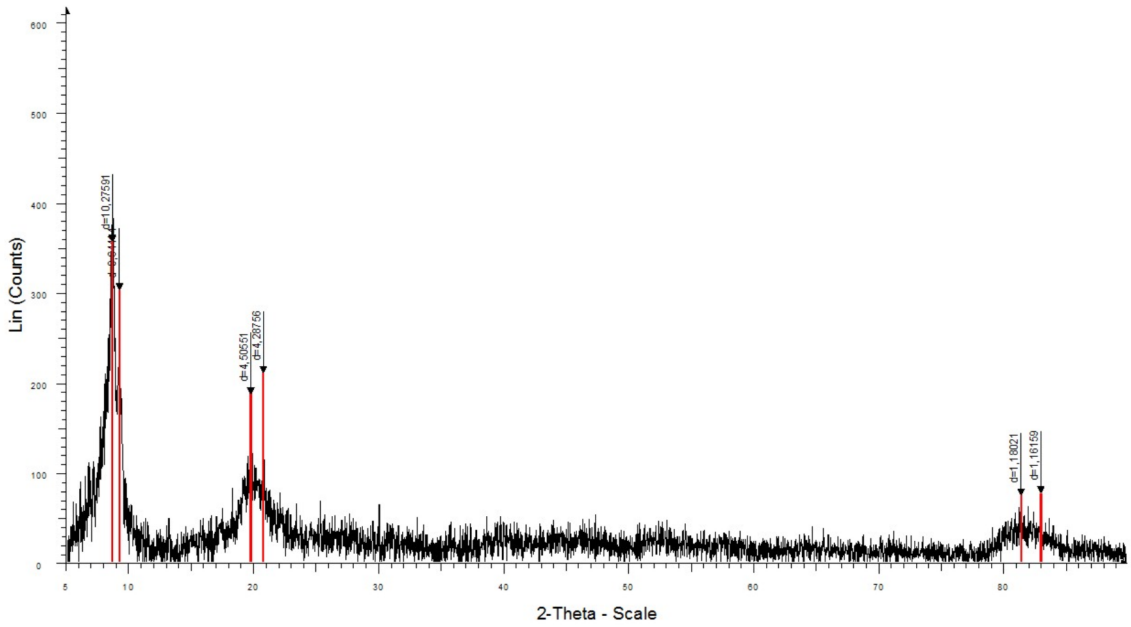

Figure 6.12: Powder diffraction of polydiphenylstannane

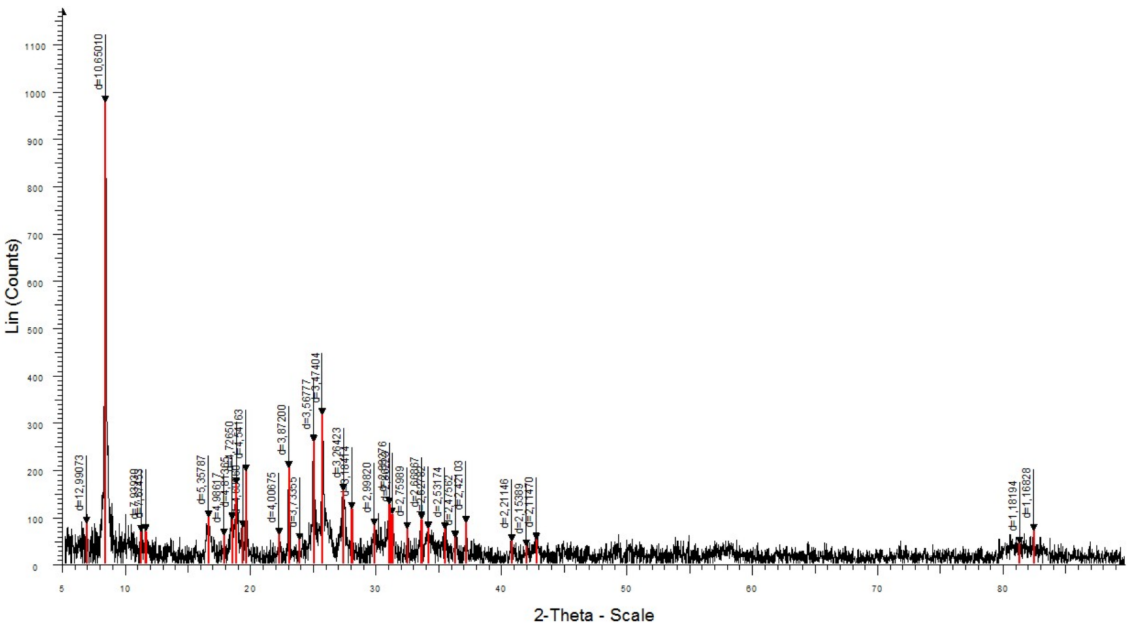

Figure 6.13: Powder diffraction of polydi-o-tolylstannane

6.2.3 and chapter 6.2.4. In general, polymer chains at the size of polystyrolpolymers with molar mass between 7000 Da and 40000 Da could be obtained. Two large polymer peaks could be observed in the measurement. The ratio between weight average molar mass and number average molar mass are between 3.4 and 1.2 depending on the reaction condition and reaction time. Generally, smaller ratios are found for longer reaction time, which indicates a small polymer mass distribution.

6.2.2 Stability of poly bis(p-butylphenyl)stannane

Polystannane are known to be unstable when exposed to light [10]. In genera,l polydialkylstannane are more light sensitive than polydiarylstannane. Also solvated polymers are more sensitive than the pure isolated product.

Stability tests were carried out on polybis(-p-butylphenyl)stannane. First polybis-(butylphenyl)stannane was exposed to light under inert atmosphere . The product remained yellow, which indicates that no decomposition took place. GPC measurements before and after the exposer confirmed this (figure 6.14). When solving the polymer in dried THF no decolorising took place for over one week. The same results were obtained when adding chlorine to the solution. Dissolving polybis(-p-butylphenyl)stannane in undried THF leads to a decolorising within 20 minutes, however. It is therefore assumed that for the decomposition process light, as well as humidity is necessary. Otherwise the product will remain stable.

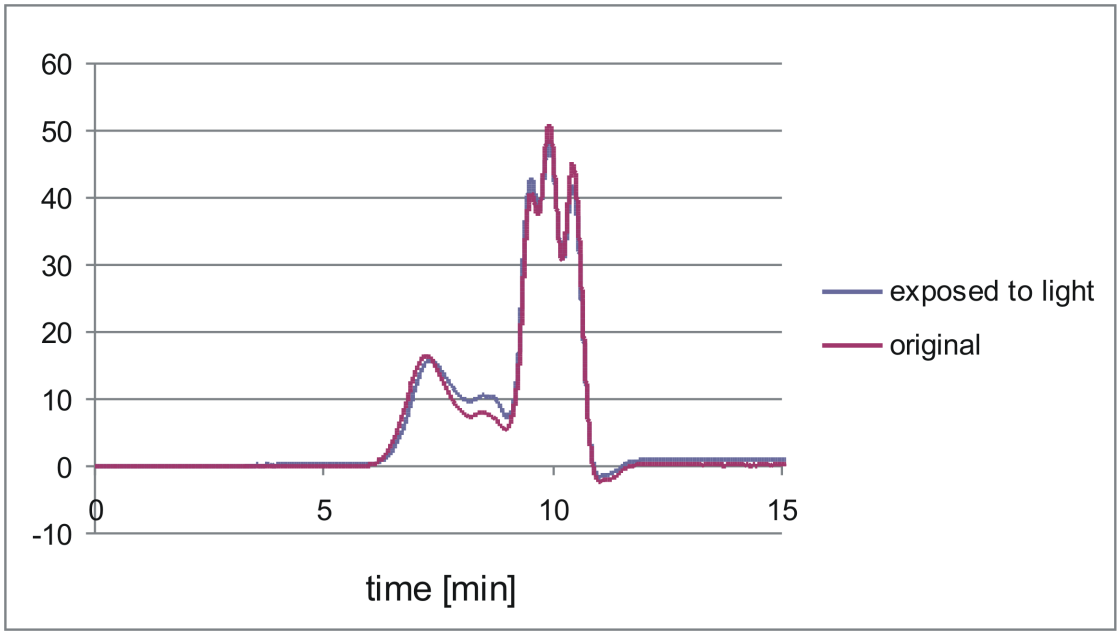

Figure 6.14: GPC measurement of polybis(-p-butylphenyl)stannane before and after exposure to light for 4 days

6.2.3 Polymerization with TMEDA 31: influent of different reaction parameters

The influence of different reaction parameters were investigated. For this investigation the reaction process was determined with GPC measurements at different reaction time. The molar mass of the first, as well as of the second peak of the measurement was compared. The signal was also adapted to the sample weight in order to compare the signal hight qualitatively.

To investigate the influence of the starting concentration, the reaction was carried out at three different starting concentrations: 10 g l^{-1}, 20 g l^{-1} and 40 g l^{-1}. Samples were taken after 3 hours, 21 hours and 45 hours. The signals are listed in table 6.3. The spectra for the measurement after 45 hours reaction time are shown in figure 6.15. The longest polymer chains were obtained after 3 hours. Apparently, the reaction was already finished at this stage. Afterwards decomposition took place. For the concentration 10 g l^{-1} the longest polymer chains were observed at all three reaction times. For 40 g l^{-1} the shortest chains were observed. Thus it clearly shows that the observed chain length is a direct functionality of the dilution.

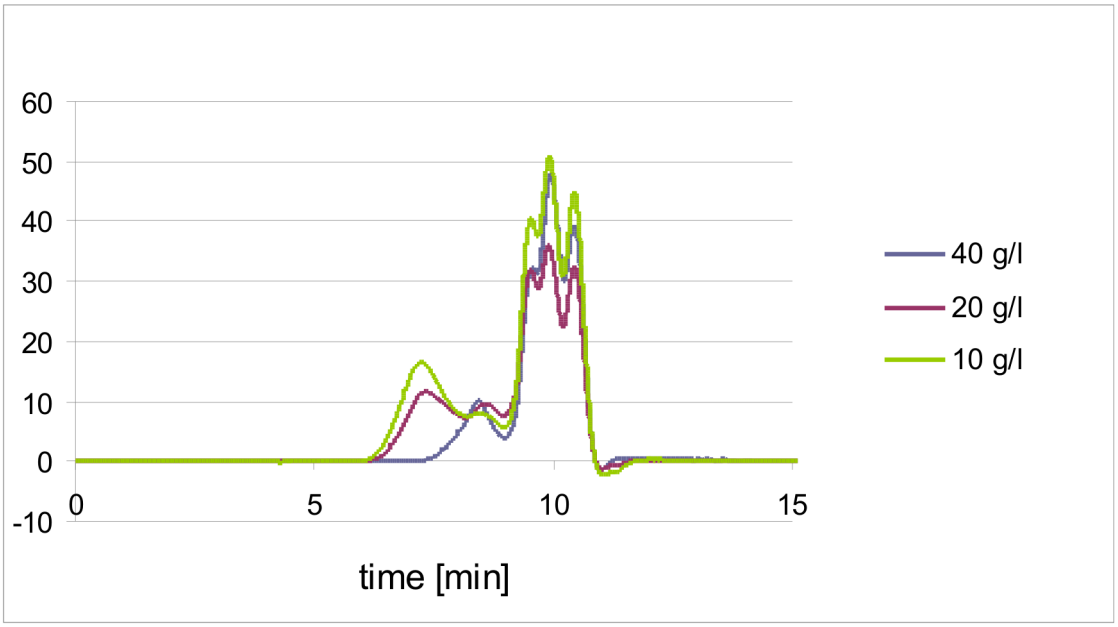

Figure 6.15: GPC measurement of polybis(-p-butylphenyl)stannane made out of different concentrated monomer solutions at 45 hours reaction time

The influence of the monomer to TMEDA ratio was also investigated (table 6.4). The monomer to TMEDA ratio of 1:1, 1:0.5 and 1:0.25 were used. Samples were taken after 20 minutes (figure 6.16) and 19 hours (figure 6.17). After 20 minutes lowest molecular masses could be observed for the 1:0.25 ratio. About the same molecular weights were observed for the 1:1 and the 1:0.5 ratio. After a reaction time of 19 hours however, the lowest molar masses for the 1:1 ratio could be observed. Apparently, the reaction time lengthened considerably when using less catalyst. Thus for every ratio there is a optimum reaction time, where molecular masses are at the highest. Afterwards, decomposition takes place. Since measurements were taken only after a short and a very long reaction time, nothing can be said about the ratio causing the highest molecular masses.

Table 6.3: Comparison of the first and second signal of the GPC measurement of polymerization with different monomer start concentration at different reaction time

concentration		3h		21h		45h	
		M_w	M_n	M_w	M_n	M_w	M_n
10 g l^{-1}	1st peak	17000	8000	14000	8000	15000	9000
	2nd peak	1000	1000	1500	1500	1500	1000
20 g l^{-1}	1st peak	13000	7000	13000	8000	12000	8000
	2nd peak	1500	1000	1500	1000	1500	1000
40 g l^{-1}	1st peak	6000	5000				
	2nd peak	1500	1500	3000	2000	2000	2000

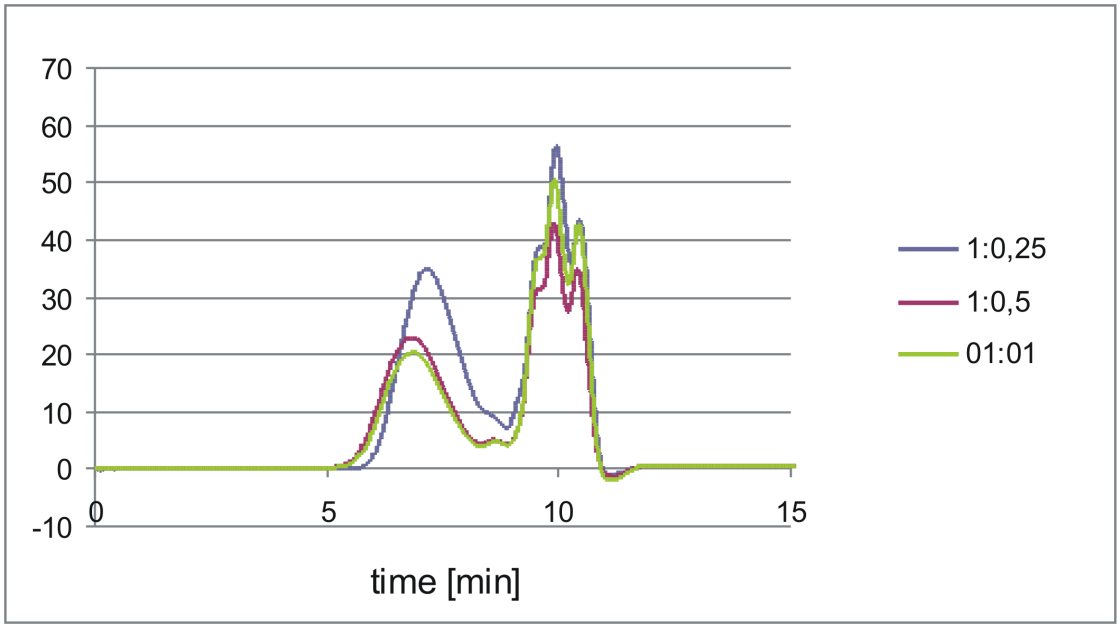

Figure 6.16: GPC measurement of polybis(-p-butylphenyl)stannane made with different monomer to TMEDA ratios at 20 minutes reaction time

6.2.4 Comparison of polymerization rate with different bases

The catalytic ability for the polymerization reaction was tested for different bases. Next to TMEDA also Et_3N, pyridine, as well as the non nitrogen base Li_2CO_3 was used. ^{119}Sn NMR samples of the reaction were taken after 1 day and after 2 days. For TMEDA as well as for Et_3N all monomer was converted into polymers after the first day. No cyclic oligomers could be observed. For pyridine no polymer could be observed after 1 day. After 2 days only slight conversion of the monomer to the polymer took place. No oligomeric products could be observed. When using

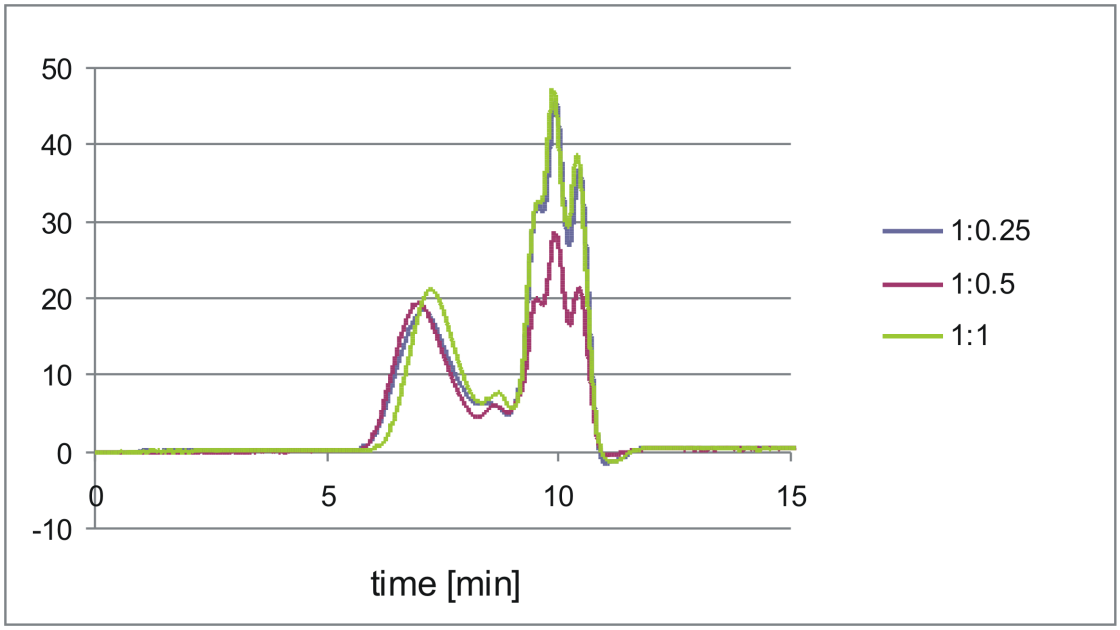

Figure 6.17: GPC measurement of polybis(-p-butylphenyl)stannane made with different monomer to TMEDA ratios at 19 hours reaction time

Table 6.4: comparison of the first and second signal of the GPC measurement of polymerization with different monomer to TMEDA ratio at different reaction time

concentration		20 min		19h	
		M_w	M_n	M_w	M_n
1 : 1	1st peak	35000	13000	15000	8000
	2nd peak	1000	1000	1000	1000
1 : 0.5	1st peak	39000	13000	24000	11000
	2nd peak	1000	1000	1000	1000
1 : 0.25	1st peak	19000	8000	22000	10000
	2nd peak	1000	1000	1000	1000

Li_2CO_3 as catalyst, no reaction took place. After 2 days only monomer could be observed in the ^{119}Sn NMR spectra. Bad solubility of Li_2CO_3, as well as the complete lack of coordination ability of the latter might be the reason for the failure to react.

Considering only the amine bases, pyridine has the lowest coordination ability, as well as the lowest pKs value. These two facts might be the reason for the bad catalytic activity.

In order to be able to compare TMEDA with Et_3N polymerization reaction with both bases were carried out, taking GPC samples every 10 minutes (figure 6.18 and figure 6.19). The resulting molar masses are listed in table 6.6. For Et_3N

Table 6.5: Qualitative comparison of polymerization rate of different bases after reaction of two days. The polymerization rate was detected by ^{119}Sn NMR

base	polymerization rate
TMEDA	++++
Et_3N	++++
pyridine	+
Li_2CO_3	none

highest molar masses (17000 Da) could be obtained after 10 minutes. Afterwards decomposition takes place and considerably lower molar masses about a few thousand Da could be obtained. For TMEDA highest molar masses (39000 Da) could be obtained after 20 minutes. Compared to the reaction with Et_3N only slight decomposition takes place afterwards.

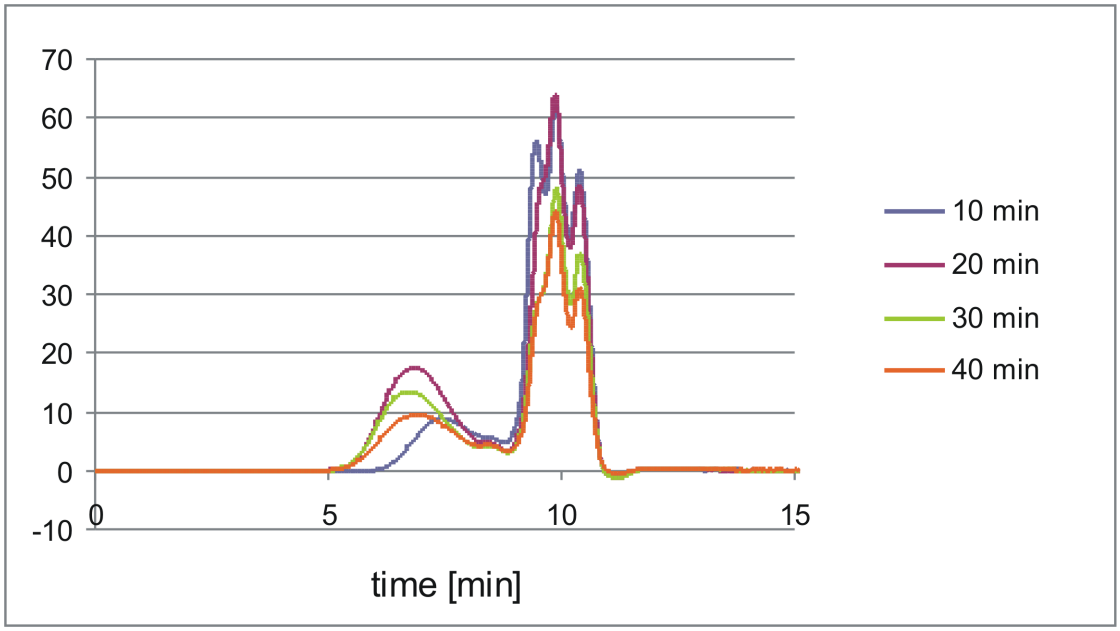

Figure 6.18: GPC measurement of polybis(-p-butylphenyl)stannane polymerized with $TMEDA$ at different reaction times

IR-measurements of the reaction mixture with TMEDA were done at the same intervals (figure 6.20). The reaction progress can be determined when observing the wavelength range about 1800 cm^{-1} as the Sn-H vibrational signal of *bis(butylphenyl)-stannane* is at 1850 cm^{-1}. Thus it could be concluded that nearly all educt was consumed after 30 minutes reaction time.

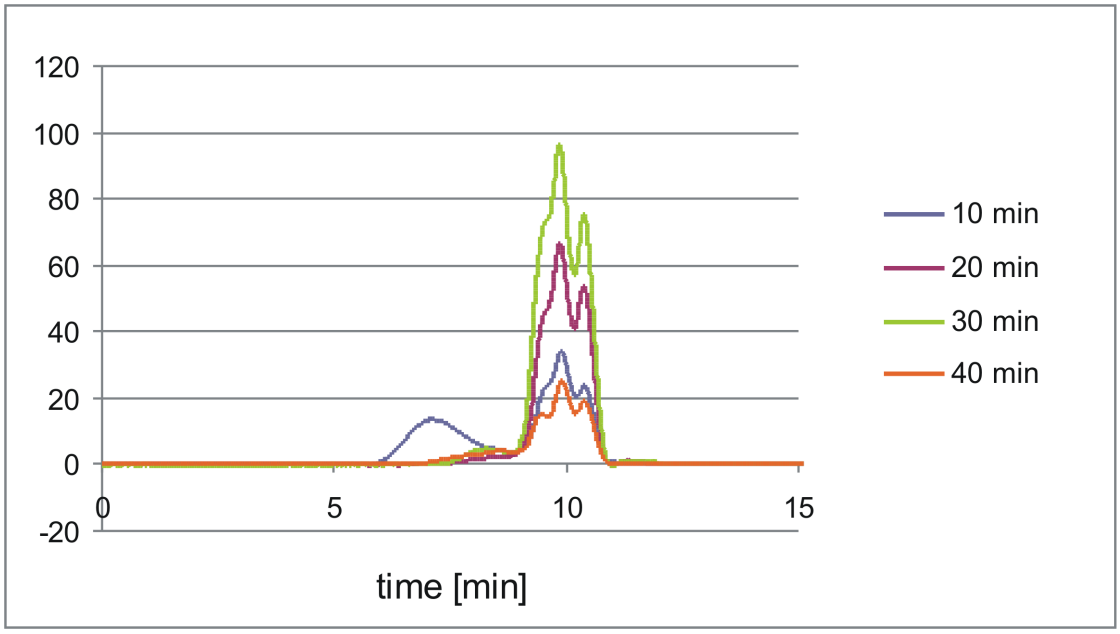

Figure 6.19: GPC measurement of polybis(-p-butylphenyl)stannane polymerized with Et_3N at different reaction times

Table 6.6: Molecular weight of the first two polymer peaks of the GPC analysis of polymerization with TMEDA and Et_3N at different reaction time

TMEDA				
reaction time	1st peak		2nd peak	
	M_w	M_n	M_w	M_n
10 min	13000	7000	1500	1500
20 min	39000	12000	1500	1500
30 min	46000	14000	1500	1500
40 min	41000	13000	1500	1500
Et_3N				
reaction time	1st peak		2nd peak	
	M_w	M_n	M_w	M_n
10 min	17000	5000		
20 min	5000	4000	1500	1000
30 min			3000	2000
40 min			1500	1000

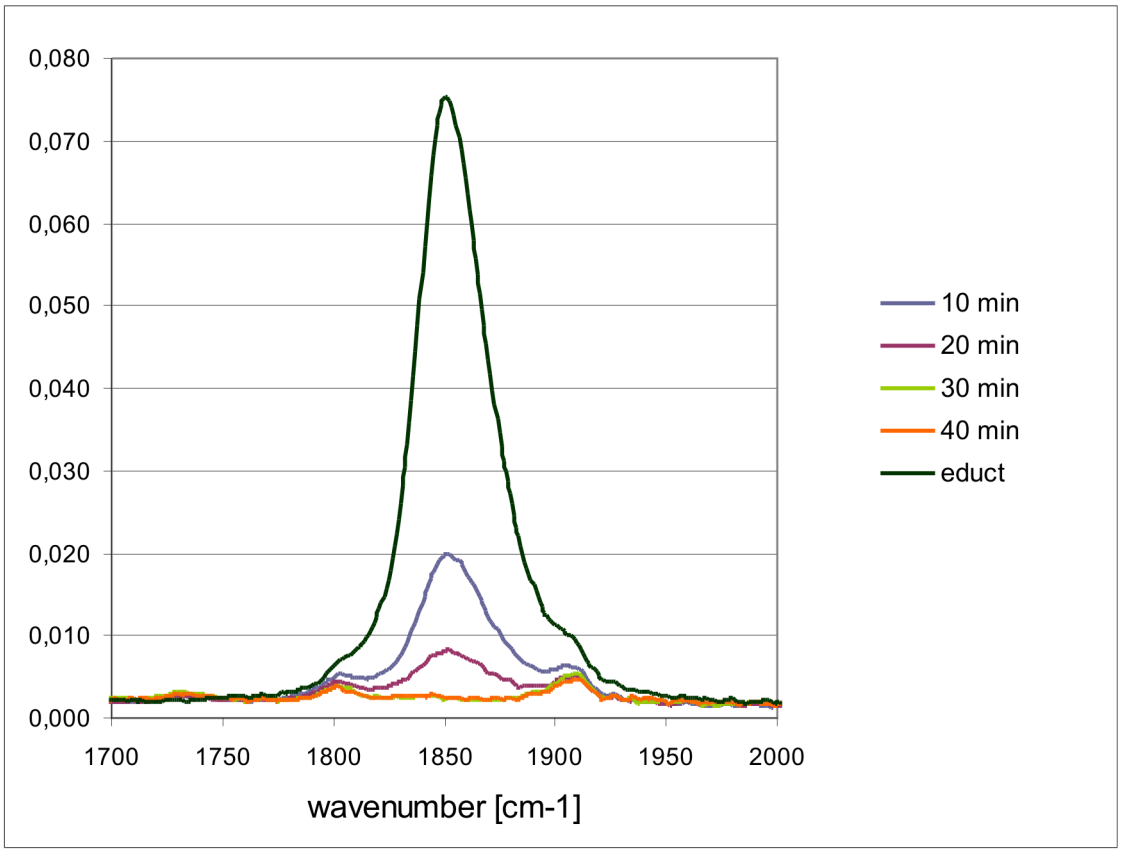

Figure 6.20: IR measurement of polybis(-p-butylphenyl)stannane polymerized with $TMEDA$ at different reaction times. The signal shown is the Sn-H vibration.

Chapter 7

Experimental

7.1 General methods

All reactions were carried out using an inert nitrogen atmosphere. Solvents were dried using an INNOVATIVE TECHNOLOGIES column solvent purification system. All chemicals were used as received from the respective chemical suppliers as listed in table C.2.

NMR-measurements: NMR spectra were measured on a Varian Mercury 300 spectrometer (operating at 300.2 MHz for ^{1}H, 111.96 MHz for ^{119}Sn and 75.5 for ^{13}C NMR measurements) using a standard 5 mm broad band probe. Samples for ^{119}Sn NMR spectra were either dissolved in deuterated chloroform ($CDCl_3$) or in cases of reaction samples and solutions of unstable products measured with a D_2O capillary in order to provide an external standard. NMR shifts were referenced to solvent residual peaks. Spectra were recorded at 25°C.

NMR spectra of chapter 6 were recorded on a Bruker UltraShield 300 MHz/54 mm Fourier transform spectrometer. Standard 5 mm broad band probe were used. All samples were dissolved in deuterated dichloromethane. In order to inhibit decomposition of the sample by day light all sample tubes were wrapped in aluminium foil, which was only removed before inserting the sample in the spectrometer.

XRD-measurements: XRD data collection was performed with a BRUKER-AXS KAPPA8 APEX II CCD diffractometer, using graphite monochromated Mo Ka α radiation (0.71073). Absorption corrections were performed using SADABS. The structures were solved with direct methods and the non-hydrogen atoms were refined anisotropically (full-matrix least squares on F2). All non-hydrogen atoms were refined employing anisotropic displacement parameters. Hydrogen atoms were located in calculated positions to correspond to standard bond lengths and angles. Crystallographic data for all compounds are given in chapter B.

Powder XRD-measurements: Powder XRD date collection was performed by a Bruker AXS D5005 powder diffractometer using graphite monochromated Cu K α radiation. The reflection goniometer has a theta/theta geometrie. Generator parameters are 45 kV and 35 mA. Sweep width is from 5 nm to 90 nm with an increment size of 0.02 nm.

Elemtal analysis: Elemental analyses were performed with a Heraeus VARIO ELEMENTAR EL analyzer.

The elemental analysis described in chapter 6 were performed by the Microelemental Analysis Laboratory of the Department of Chemistry at ETH Zürich.

Head space analysis: Head space analysis: GC: HP 5890 SERIES II;

first column: length: 30 m, inner diameter: 0.53, film thickness: 1.8 μm, GS-Q, J8W scientific;

second column: length: 30m, inner diameter: 0.25μm, film thickness: 0.25μm, ZB-FFAP, Zebron;

Column pressure: $5 * 10^4$ Pa

Oven program: Initial Temperature: 40°C; initial time: 10.00 min; run time: 43.86 min;

Table 7.1: Head space analysis parameters

level	rate[°C min^{-1}]	final temperature[°C]	final time [min]
1	70.00	100	3.00
2	10.00	200	20.00
3	0.00	200	

MS: HP 5951A; mode: TIC (total ion chrom.); m/z = 10-100;

Gel permeations chromatography: Gel permeations chromatography was performed with a GPC from Viscotek VE7510 with degasser, VE1121 solvent pump, VE520 autosampler and Model 301 triple detector array. A PL gel 5 μm Mixed-D column from Polymer Laboratories Ltd. (Shropshire, United Kindom) was used. THF was used as eluent. For calibration atactic-poly(styrene) standards from Fluka were employed. Samples were dissolved in THF with 2.5 v/v toluene which served as marker. The eluent flow was at 1 ml min^{-1}.

Microscope photographs: For the microscope photos a Leica DMRX polarizing microscope was used. For measurements with variable temperature a Linkam THMS 600 heating-/cooling stage was employed. 20 fold magnification was used.

VIS measurements: Polarizing VIS measurements were performed with a Perkin Elmer Lambda 900 spectrophotometer equipped with rotating polarizers.

IR measurements: Infrared spectra were recorded with a Bruker Vertex 70 FTIR spectrometer with the attenuated total reflection (ATR) technique by using a Si-crystal. The sample was directly deposited to the crystal with a spatula.

Thermal gravimetric analysis and differential scanning calorimetry: Thermal analysis was performed by differential scanning calorimetry with a DSC822e instrument (Mettler Toledo, Greifensee, Switzerland) equipped with an intracooler and thermal gravimetric analysis with a TGA/SDTA851e from Mettler Toledo under nitrogen atmosphere.

Heating rate for the thermal gravimetric analysis were at 5°C min^{-1}.

Heating and cooling rate for the differential scanning calorimetry were at 5°C min^{-1}.

Calculations: All calculations were done with gaussian 03 program: Gaussian 03, Revision B.03, M. J. Frisch, G. W. Trucks, H. B. Schlegel, G. E. Scuseria, M. A. Robb, J. R. Cheeseman, J. A. Montgomery, Jr., T. Vreven, K. N. Kudin, J. C. Burant, J. M. Millam, S. S. Iyengar, J. Tomasi, V. Barone, B. Mennucci, M. Cossi, G. Scalmani, N. Rega, G. A. Petersson, H. Nakatsuji, M. Hada, M. Ehara, K. Toyota, R. Fukuda, J. Hasegawa, M. Ishida, T. Nakajima, Y. Honda, O. Kitao, H. Nakai, M. Klene, X. Li, J. E. Knox, H. P. Hratchian, J. B. Cross, C. Adamo, J. Jaramillo, R. Gomperts, R. E. Stratmann, O. Yazyev, A. J. Austin, R. Cammi, C. Pomelli, J. W. Ochterski, P. Y. Ayala, K. Morokuma, G. A. Voth, P. Salvador, J. J. Dannenberg, V. G. Zakrzewski, S. Dapprich, A. D. Daniels, M. C. Strain, O. Farkas, D. K. Malick, A. D. Rabuck, K. Raghavachari, J. B. Foresman, J. V. Ortiz, Q. Cui, A. G. Baboul, S. Clifford, J. Cioslowski, B. B. Stefanov, G. Liu, A. Liashenko, P. Piskorz, I. Komaromi, R. L. Martin, D. J. Fox, T. Keith, M. A. Al-Laham, C. Y. Peng, A. Nanayakkara, M. Challacombe, P. M. W. Gill, B. Johnson, W. Chen, M. W. Wong, C. Gonzalez, and J. A. Pople, Gaussian, Inc., Pittsburgh PA, 2003.

7.2 Preparation of different compounds

7.2.1 Preparation of the educts

Preparation of tetraarylstannane: Arylbromide was reacted with 1.2 molar excess magnesium in a Grignard reaction to form arylmagnesiumbromide. THF was used as solvent. The reaction was refluxed for 1 hour.

$SnCl_4$ **11** was suspended in 200 mL THF. Arylbromide to **11** ratio was 1:0.8. While cooling with ice the arylmagnesiumbromide solution was added dropwise via a cannula. The reaction mixture was refluxed for one hour. THF was removed afterwards. The product was extracted with hexane via a soxhlet extractor.

Alternative synthesis of tetraarylstannane: Arylmagnesiumbromide was synthesis as described above. **11** was diluted with hexane and added to the reaction mixture via a dropping funnel. The reaction was refluxed for one hour. Water was added in order to hydrolize excess of grignard reagent and dissolve the salts formed during the reaction. The organic phase was seperated and dried with $CaCl_2$ and concentrated to half the volume. The tetraarylstannane was recrystalized out of the reaction mixture.

Tetrakis-p-butylphenylstannane **57:** *Tetrakis-p-butylphenylstannane* is a colorless liquid which solidifies below - 50°C. The product was cleaned by drying on vacuum for 6 hours.

^{1}H NMR (299.948 MHz, $CDCl_3$): δ = 0.4-1.0 ppm [t, 12 H], 1.3-1.5 ppm [m, 8 H], 1.6-1.7 ppm [m, 8 H], 2.55-2.6 ppm [t, 8 H], 7.2-7.3 ppm [d, 8 H], 7.8-7.9 [d, 8 H].

^{13}C NMR (75.50 MHz, $CDCl_3$): δ = 13.93 ppm [s, 4 C], 22.45 ppm [s, 4 C], 33.73 ppm [s, 4 C], 35.82 ppm [s, 4 C], 135.2 ppm [s, 4 C], 129.0 ppm [s, 8 C], 137.5 ppm [s, 8 C], 143.7 ppm [s, 4 C].

^{119}Sn NMR (111.96 MHz, $CDCl_3$): δ = -125 ppm

Preparation of diaryldichlorostannane: Tetraarylstannane and $SnCl_4$ **11** were put in a flask in a ratio of 1:1. The reaction was heated until the mixture liquidified. Then it was cooled down to about 50 °C and heptane was added. The reaction mixture was refluxed for 2 hours. The hot solution was filtered in order to remove inorganic side products. The product crystallized straight from the reaction solution.

Di-p-tolyldichlorostannane **48:** After cooling the reaction mixture to -80°C white crystals were formed. No melting point could be determined as the crystals melted below room temperature and no melting point apparatus for temperature below 20°C were avaible.

^{1}H NMR (299.948 MHz, $CDCl_3$): δ = 2.42 ppm [t, 6 H], 7.34-7.36 ppm [d, 4 H], 7.57-7.60 ppm [d, 4 H].

^{13}C NMR (75.50 MHz, $CDCl_3$): δ = 21.87 ppm [s, 2 C], 133.7 ppm [s, 2 C], 130.6 ppm [s, 4 C], 135.1 ppm [s, 4 C], 142.5 ppm [s, 2 C].

^{119}Sn NMR (111.96 MHz, $CDCl_3$): δ = -44.3 ppm

CHN analysis: Found: C,45.07%; H, 3.77%; $C_{14}H_{14}SnCl_2$ (MM: 371.88g mol$^-$1) required: C, 45.22%; H, 3.79%;

Di-m-tolyldichlorostannane **51:** Light brown crystals could be isolated.

Mp: 43°C

^{1}H NMR (299.948 MHz, $CDCl_3$): δ = 2.41 ppm [t, 6 H], 7.34-7.36 ppm [d, 2 H], 7.40-7.46 ppm [t, 2 H], 7.48-7.51 ppm [d, 2 H], 7.64 ppm [s, 2 H].

^{13}C NMR (75.50 MHz, $CDCl_3$): δ = 21.78 ppm [s, 2 C], 129.7 ppm [s, 2 C], 132.2 ppm [s, 2 C], 132.8 ppm [s, 2 C], 135.7 ppm [s, 2 C], 137.0 ppm [s, 2 C], 139.9 ppm [s, 2 C].

^{119}Sn NMR (111.96 MHz, $CDCl_3$): δ = -38.6 ppm

CHN analysis: Found: C,42.58%; H, 2.89%; $C_{14}H_{14}SnCl_2$ (MM: 371.88g mol$^-$1) required: C, 45.22%; H, 3.79%;

Bis-p-butylphenyldichlorostannane **56:** The reaction mixture was refluxed for about 6 hours in order to ensure the completeness of the reaction. Then heptane was removed and the product was cleaned by drying in vacuum for 6 hours.

^{1}H NMR (299.948 MHz, $CDCl_3$): δ = 0.94-1.01 ppm [t, 6 H], 1.2-1.4 ppm [m, 4 H], 1.5-1.6 ppm [m, 4 H]; 2.5 ppm [t, 4 H]; 7.1-7.2 ppm [d, 4 H]; 7.6 [d, 4 H].

^{119}Sn NMR (111.96 MHz, $CDCl_3$): δ = -19.6 ppm

Bis(3, 5-*dimethylphenyl*)-*dichlorostannane* **59:** Although not altering the reaction condition (3, 5-*dimethylphenyl*)-*trichlorostannane***acetone* **60** crystallized instead of **59**.

Mp: 32°C

^{1}H NMR (299.948 MHz, $CDCl_3$): δ = 2.17 ppm [s, 6 H], 2.39 ppm [s, 6 H], 7.21-7.23 ppm [s, 2 H]; 7.26 ppm [s, 1 H].

^{13}C NMR (75.50 MHz, $CDCl_3$): δ = 21.60 ppm [s, 2 C], 31.16 ppm [s, 2 C], 132.6 ppm [s, 1 C], 131.5 ppm [s, 2 C], 135.1 ppm [s, 2 C], 140.5 ppm [s, 1 C].

^{119}Sn 1H NMR (111.96 MHz, $CDCl_3$): δ = -64.5 ppm

CHN analysis: Found: C,42.82%; H, 4.27%; $C_{12}H_{15}SnCl_3O$ (MM: 388.30g mol^{-}1) required: C, 34.03%; H, 3.89%;

In a second attempt **59** could be isolated.

^{1}H NMR (299.948 MHz, $CDCl_3$): δ = 2.10-2.12 ppm [s, 6 H], 7.21-7.24 ppm [s, 4 H]; 7.08-7.11 ppm [s, 2 H].
^{13}C NMR (75.50 MHz, $CDCl_3$): δ = 21.56 ppm [s, 4 C], 136.81 ppm [s, 2 C], 132.62 ppm [s, 4 C], 133.74 ppm [s, 4 C], 139.55 ppm [s, 2 C].
^{119}Sn NMR (111.96 MHz, $CDCl_3$): δ = -26.1 ppm

CHN analysis: Found: C,42.82%; H, 4.27%; $C_{16}H_{18}SnCl_2$ (MM: 399.93g mol^{-}1) required: C, 48.05%; H, 4.54%;

Preparation of diaryldihydrostannane: Diethylether was degassed. LAH was suspended with the degassed ether. An equimolar amount of diarylstannane was put in a dropping funnel and dissolved in degassed ether. The solution was added drop wise while cooling to 0°C. The reaction mixture was stirred for one hour. Unreacted LAH was neutralized with degassed water. The organic phase was separated with a cannula and washed with a degassed aqueous sodiumtatrate solution. Afterwards the organic phase was dried with $CaCl_2$. Ether was removed and the product was cleaned by drying in vacuum for 1 hour. The product was stored in brown colored septum vials at 4 °C.

Bis-p-butylphenylstannane **58:** ^{1}H NMR (299.948 MHz, D_2O): δ = 0.94-0.99 ppm [t, 6 H], 1.3-1.4 ppm [m, 4 H], 1.5-1.6 ppm [m, 4 H]; 2.5-2.6 ppm [t, 4 H]; 7.2 ppm [d, 4 H]; 7.6 [d, 4 H], 6.3 [s, 2 H, ^{1}J(H-^{119}/^{117}Sn) = 1907/1821 Hz].
^{119}Sn NMR (111.96 MHz, D_2O): δ = -234.3 ppm [s, 1 Sn].

Preparation of dialkyldihydrostannane: Dialkylstannanes were prepared similar to diarylstannanes, but the ether was removed by destillation at 50°C. The product was recondensated afterwards.

7.2.2 Preparation of different tin ring systems

Synthesis of 1, 1, 2, 2, 3, 3, 4-*hepta-^{t}butyl*-4-*chloromagnesiotetrastannacyclobutane* **62:** *Dichlorodi^{t}butylstannane* (5g, 16mmol) was dissolved in 100ml THF in a 250

ml flask. 3.8g (160mmol) magnesium was added. The solution was stirred overnight at 30°C. Subsequently, the solution was separated from magnesium with a cannula.

Alternative synthesis of **62**: *Octa*^{t}*butyltetrastannacyclobutane* (0.5g, 0.9mmol) and 0.2 g (9 mmol) Magnesium was placed in a flask. 5 ml of dry THF and 0.1 ml of ^{t}*butylchloride* were added with a syringe. In order to start the reaction 0.1 ml of $Br_2C_2H_4$ were added. The reaction was stirred overnight. A dark read solution was obtained containing the product **62**.

Synthesis of $1,1,2,2,3,3,4$-*hepta*-^{t}*butyl*-4-*lithiotetrastannacyclobutane* **63:** *Dichlorodi*^{t}*butylstannane* (1g, 3.3 mmol) was dissolved in 100ml THF in a 250 ml flask. 0.2g (33mmol) lithium was added. The solution was stirred 30 minutes. Subsequently, the solution was separated from lithium with a cannula.

The product could not be isolated. No ^{1}H NMR and ^{13}C NMR were obtained. Due to instability no overnight measurements were possible.

^{119}Sn NMR (111.96 MHz, D_2O): δ = 179.47 ppm [s, 1 Sn(3)], 75.26 ppm [s, 2 Sn(2,4)], -4.69 ppm [s, 1 Sn(1)].

Alkylation of $1,1,2,2,3,3,4$-*hepta*-^{t}*butyl*-4-*chloromagnesiotetrastannacyclobutane* **62:** To the solution of **62** an equimolare amount of alkylation reagent was added. THF was removed. To the remaining solid pentane was added. The solution was filtered and pentane was removed. The product was recrysatllized from THF.

$1,1,2,2,3,3,4$-*Hepta*-^{t}*butyl*-4-*methyltetrastannacyclobutane* **64:** *Dimethylsulfate* **14** was added as reagent.

Mp:194°C

CHN analysis: Found: C, 40.06%; H, 7.52%; $C_{29}H_{66}Sn_4$ (MM: 889.53 g mol$^-$1) required: C, 39.16%; H, 8.01%;

$1,1,2,2,3,3,4$-*Hepta*-^{t}*butyl*-4-*ethyltetrastannacyclobutane* **65:** *Bromoethane* **16** was added as reagent.

The obtained crystals were not sufficiently arranged in a crystal lattice to give a reliable crystal structure.

Dt:190 °C

CHN analysis: Found: C,39.76%; H, 7.53%; $C_{30}H_{68}Sn_4$ (MM: 903.71g mol$^-$1) required: C, 39.87%; H, 7.36%;

$1,1,2,2,3,3,4$-*Hepta-*^{t}*butyl-4-propyltetrastannacyclobutane* **66:** 1-*Chloropropane* **18** was added as reagent.

The obtained crystals were not sufficiently arranged in a crystal lattice to give a reliable crystal structure.

Dt: 198°C

^{1}H NMR (299.948 MHz, $CDCl_3$): δ = 1.39–1.54 ppm [m, 70 H]

^{13}C NMR (75.50 MHz, $CDCl_3$): δ = 48.6 ppm [s, 1 C], 37.1 ppm [s, 1 C], 31.9 ppm [s, 1 C], 33.6–35.2 ppm [m, 28 C].

^{119}Sn NMR (111.96 MHz, $CDCl_3$): δ = 94 ppm [s, 1 Sn(3), ^{1}J(^{119}Sn(3)-^{119}/^{117}Sn(2,4)) = 1021/1009 Hz, ^{2}J(^{119}Sn(3)-^{117}Sn(1)) = 1831 Hz], 58 ppm [s, 2 Sn(2,4), ^{1}J(^{119}Sn(2,4)-^{119}/^{117}Sn(3)) = 1024/979 Hz, ^{1}J(^{119}Sn(2,4)-^{119}/^{117}Sn(1)) = 759/727 Hz, ^{2}J(^{119}Sn(2,4)-^{117}Sn(2,4)) = 1476 Hz], -29 ppm [s, 1 Sn(1), ^{1}J(^{119}Sn(1)-^{119}/^{117}Sn(2,4)) = 759/727 Hz, ^{2}J(^{119}Sn(1)-^{119}/^{117}Sn(3)) = 1773 Hz].

CHN analysis: Found: C, 39.81%; H, 7.50%; $C_{31}H_{70}Sn_4$ (MM: 917.738 g mol$^-$1) required: C, 40.57%; H, 7.69%;

$1,1,2,2,3,3,4$-*Hepta-*^{t}*butyl-4-chloropropyltetrastannacyclobutane* **67:** $1,3$-*Dichloropropane* **21** was added as reagent.

Mp:92°C

^{1}H NMR (299.948 MHz, $CDCl_3$): δ = 1.23-1.56 ppm [m, 63 H]

^{13}C NMR (75.50 MHz, $CDCl_3$): δ =68.25 ppm [s, 1 C], 25.82 ppm [s, 1 C], 33.96 ppm [s, 1 C], 29.9 - 35.2 ppm [m, 28 C].

^{119}Sn NMR (111.96 MHz, $CDCl_3$): δ = +96 ppm [s, 1 Sn(3), ^{1}J(^{119}Sn(3)-^{119}/^{117}Sn(2,4)) = 982/ 938 Hz, ^{2}J(^{119}Sn(3)-^{117}Sn(1)) = 1906 Hz], 62 ppm [s, 2 Sn(2,4), ^{1}J(^{119}Sn(2,4)-^{117}Sn(3)) = 939 Hz, ^{1}J(^{119}Sn(2,4)-^{119}/^{117}Sn(1)) = 809/ 763 Hz, ^{2}J(^{119}Sn(2,4)-^{117}Sn3/1) =1417], -23 ppm [s, 1 Sn(1), ^{1}J(^{119}Sn(1)-^{119}/^{117}Sn(2,4)) = 795/762 Hz, ^{2}J(^{119}Sn(1)-^{117}Sn(3)) = 1869 Hz].

CHN analysis: Found: C, 39.80%; H, 7.30%; $C_{31}H_{69}ClSn_4$ (MM: 952.18 g mol$^-$1) required: C, 39.10%; H, 7.30%;

$1,1,2,2,3,3,4$-*Hepta-*^{t}*butyl-4-chloropentyltetrastannacyclobutane* **68:** $1,5$-*Dichloropentane* **23** was added as reagent. The product could not be recrystalized.

^{1}H NMR (299.948 MHz, $CDCl_3$): δ = 0.85-0.92 ppm [t, 2 H], 1.2-2.35 ppm [m, 69 H], 3.5-3.55 ppm [t, 2, H].

^{13}C NMR (75.50 MHz, $CDCl_3$): δ = 45.38 ppm [s, 1 C], 29.47-36.75 ppm [s, 32 C].

^{119}Sn NMR (111.96 MHz, $CDCl_3$): δ = 97.39 ppm [s, 1 Sn(3), ^{1}J(^{119}Sn(3)-^{119}/^{117}Sn(2,4)) = 1020/973 Hz, ^{2}J(^{119}Sn(3)-^{119}/^{117}Sn(1)) = 1931/1799 Hz], 60.92 ppm [s, 2 Sn(2,4), ^{1}J(^{119}Sn(2,4)-^{119}/^{117}Sn(3)) = 976/934 Hz, ^{1}J(^{119}Sn(2,4)-^{119}/^{117}Sn(1)) = 780/742 Hz, ^{2}J(^{119}Sn(2,4)-^{117}Sn(2,4)) = 1463 Hz], -24.87 ppm [s, 1 Sn(1), ^{1}J(^{119}Sn(1)-^{119}/^{117}Sn(2,4)) = 774/743 Hz, ^{2}J(^{119}Sn(1)-^{119}/^{117}Sn(3)) = 1927/1799 Hz].

CHN analysis: Found: C, 35.51%; H, 6.4%; $C_{33}H_{73}ClSn_4$ (MM: 980.23 g mol$^-$1) required: C, 40.44%; H, 7.51%;

$1,1,2,2,3,3,4$-*Hepta-*^{t}*butyl-4-bromohexyltetrastannacyclobutane* **69:** $1,6$-*Dibromohexane* **24** was added as reagent. Each signal in the ^{119}Sn NMR spectra was paired. $1,6-bis-(hepta-^t\,butyltetrastannacyclobutanyl)hexane$ **70** is assumed to be the second product. They could not be separated by crystallization.

^{119}Sn NMR (111.96 MHz, $CDCl_3$): δ = 93.51 ppm [s, 1 Sn(3)], 60.26 ppm [s, 2 Sn(2,4)], 15.83 ppm [s, 1 Sn(1)].

1-*Chloro-*$1,2,2,3,3,4,4$-*hepta-*^{t}*butyltetrastannacyclobutane* **71:** $1,2$-*Dichloropropane* **19** was used as reagent.

Dt: 184°C

1-*Bromo-*$1,2,2,3,3,4,4$-*hepta-*^{t}*butyltetrastannacyclobutane* **72:** $1,2$-*Dibromopropane* **20** was added as reagent.

Dt: 174°C

^{1}H NMR (299.948 MHz, $CDCl_3$): δ = 1.25-1.66 ppm [m, 63 H]

^{13}C NMR (75.50 MHz, $CDCl_3$): δ = 29.5-35.2 ppm [m, 28 C].

^{119}Sn NMR (111.96 MHz, $CDCl_3$): δ = 85.2 ppm [s, 1 Sn(3), ^{1}J(^{119}Sn(3)-^{117}Sn(2,4)) = 1079 Hz, ^{2}J(^{119}Sn(3)-^{117}Sn(1)) = 1953/1899 Hz], 91.9 ppm [s, 2 Sn(2,4), ^{1}J(^{119}Sn(2,4)-^{117}Sn(3)) = 1079/1034 Hz, ^{1}J(^{119}Sn(2,4)-^{119}/^{117}Sn(1)) =

1865/1830 Hz, ^{2}J(^{119}Sn(2,4)-^{117}Sn(2,4) = 857 Hz], 202.1 ppm [s, 1 Sn(1), ^{1}J(^{119}Sn(1)-^{119}/^{117}Sn(2,4)) = 1951/1830 Hz, ^{2}J(^{119}Sn(1)-^{117}Sn(3)) = 2018/1892 Hz].

CHN analysis: Found: C, 35.25%; H, 5.91%; $C_{28}H_{63}BrSn_4$ (MM: 954.55 g mol$^-$1) required: C, 35.23%; H, 6.65%;

Reaction of 62 with $1,4$-*dichlorobutine* **22:** To a solution of **62**, **22** was added equimolare. The reaction was the same as described for the other halogenoalkyls.

^{119}Sn NMR showed following signals: 235.2 ppm, 201.5 ppm, 102.6 ppm, 91.8 ppm, 85.1 ppm, 81.6 ppm, 70.3 ppm. The signals at 235.2 ppm, 102.6 ppm and 81.6 ppm might be **71**.

Reaction of 62 with $1,2$-*dibromoethane* **15:** To a solution of **62**, **15** was added in surplus. The reaction was the same as described for the other halogenoalkyls. According to ^{119}Sn NMR 1-*bromo*-$1,2,2,3,3,4,4$-*hepta-*^{t}*butyltetrastannacyclobutane* **72** was built as main product. Other ^{119}Sn NMR signals at 113 ppm, 102 ppm, 93 ppm, 77 ppm, -5 ppm, -7 ppm and -9 ppm could be observed.

Cleavage of 64 Gaseous chlorine was induced into 100 mL *tetrachloromethane* in a flask. The weight of the flask before and after the induction of chlorine was measured and the concentration of chlorine was calculated. **64** was out in a flask. An equimolar amount of chlorine was added while cooling to 0°C.

^{119}Sn NMR showed signals at: 127.2 ppm, 125.7 ppm, 121.0 ppm, 120.3 ppm, 119.2 ppm, 114.9 ppm, 113.6 ppm, 111.4 ppm, 105.8 ppm, 57.8 ppm, 57.7 ppm, 54.0 ppm, 53.4 ppm, 42.5 ppm, 41.3 ppm, 34.6 ppm, 15.8 ppm, 11.2 ppm, 11.0 ppm, 7.9 ppm, -1.6 ppm, -4.0 ppm, -7.3 ppm, -31.9 ppm, -38.1 ppm, -75.2 ppm, -79.1 ppm, -81.6 ppm, -83.0 ppm, -86.1 ppm, -105.2 ppm, -121.1 ppm

Reaction of dialkyldichlorostannanes with magnesium 1: Dialkyldichlorostannane was dissolved in THF. An excess of magnesium was added. The reaction was stirred overnight at 30°C.

Reaction of *dibutyldichlorostannane* **39 with 1** ^{119}Sn NMR showed one signal at -203 ppm, presumably *decabutylpentastannacyclopentane* **42**.

Reaction of *diphenyldichlorostannane* **43 with 1** ^{119}Sn NMR showed one signal at -144.05 ppm, presumably *hexa-phenyldistannane* **46**.

Reaction of *bis-p-butylphenyl-dichlorostannane* **with 1** ^{119}Sn NMR showed one signal at -126.15 ppm, presumably *tetrakis-p-butylphenylstannane* **57**.

7.2.3 Preparation of compounds containing a Sn Zn or Sn Mg bond

Reaction of trialkylchlorostannanes with magnesium 1: Trialkylchlorostannane was dissolved in 50 mL THF. An excess of **1** was added. 0.1 mL *dibromoethane* was added as a starter. The reaction was exotherm and gas formation could be observed. The mixture was stirred overnight.

Reaction of *triphenylchlorostannanes* **12 with 1:** ^{119}Sn NMR measurement showed one signal at -100 ppm. Presumably a magnesium tin bond was established.

Reaction of *tri^{t}butylchlorostannanes* **37 with 1:** ^{119}Sn NMR signal at -3.75 ppm, presumably *hexa^{t}butyldistannane* **38**.

Reaction of trialkylstannanes with *dibutylmagnesium* **9:** Trialkylstannane was dissolved in 20 mL diethylether. An equimolar amount of **9** dissolved in heptane was added. The mixture was stirred overnight. TMEDA was added as stabilization reagent.

Reaction of *triphenylstannane* **45 with 9:** ^{119}Sn NMR showed two unidentified signals: 151.6 ppm, 167.0 ppm.

Reaction of *tributylstannane* **32 with 9:** The reaction mixture was heated at 40°C for 4 days. ^{119}Sn NMR showed one signal at -90.21 ppm, presumably the educt.

Reaction of trialkylstannanes with *diethylzinc* **10:** Trialkylstannane was dissolved in 20 mL diethylether. An equimolar amount of **10** dissolved in hexane was added. The mixture was stirred overnight. TMEDA was added as stabilization reagent.

Reaction of *triphenylstannane* **45 with 10:** ^{119}Sn NMR showed different peaks, which could not be identified. Different products crystallized from the reaction mixture. Amoung them was *hexaphenyldistannane* and $1,1,1,2,3,3,3$-*hepta-phenyl-(ethylzincio)tristannane*$^*TMEDA$.

^{119}Sn NMR data showed signals at -115.5 ppm, -117.0 ppm, -135.8 ppm, -138.1 ppm, -139.8 ppm, -447.1 ppm, -449.5 ppm

The reaction was repeated in THF and pentane. In THF, a white solid precipitated. ^{119}Sn NMR data showed signals at -115.6 ppm, -117.0 ppm, -135.8 ppm, -147.9 ppm, -205.9 ppm, -449.4 ppm.

In pentane, the reaction solution turned yellow. Over night the product decomposed and elemental tin could be observed.

^{119}Sn NMR data showed signals at -115.1 ppm, -116.7 ppm, -135.7 ppm, -139.6 ppm, -144.0 ppm, -206.5 ppm, -449.3 ppm.

Reaction of *tributylstannane* **32 with 10:** The reaction mixture was heated to 40°C for 4 days. ^{119}Sn NMR showed one signal at -90.23 ppm, presumably the educt.

Reaction of dialkylstannanes with *dibutylmagnesium* **9:** Dialkylstannanes was dissolved in 20 mL diethylether. An equimolar amount of TMEDA was added. An equimolar amount of **9** dissolved in heptane was added. The mixture was stirred overnight.

Reaction of *di^{t}butylstannane* **36 with 9:** According to ^{119}Sn NMR two products were formed. One signal was at 83.51 ppm, presumably 1, 1, 2, 2-*tetra^{t}butylstannane*. The other signal is at 76.65 ppm presumably 1, 1, 2, 2-*tetra^{t}butyl*-1, 2-*bis*(*butylmagnesio*)*distannane* **78**.

^{119}Sn NMR (111.96 MHz, D_2O): δ = 76.65 ppm [s, 1 Sn, ^{1}J(^{119}Sn-^{117}Sn) = 303.41 Hz]

Reaction of *diphenylstannane* **44 with 9:** A yellow precipitate was obtained after several minutes. The precipitate turned orange overnight. The precipitate was dissolved in THF. ^{119}Sn NMR spectra showed one peak at -88.04 ppm.

Reaction of *di-p-tolylstannane* **50 with 9:** A dark orange solution and a yellow precipitate were obtained. The precipitate was hardly soluble in THF. ^{119}Sn NMR showed one signal at 103.99 ppm. The solution did not show any signal in ^{119}Sn NMR. *Di-p-tolylmagnesium*TMEDA* crystallized from the reaction mixture. Due to instability, no NMR data of the crystals could be obtained.

Reaction of dialkylstannanes with *diethylzinc* **10:** Dialkylstannanes was dissolved in 20 mL diethylether. An equimolar amount of TMEDA was added. An equimolar amount of **10** dissolved in hexane was added. The mixture was stirred overnight at room temperature.

Reaction of *di^{t}butylstannane* **36 with 10:** ^{119}Sn NMR showed one signal at -116.68 ppm presumably the educt.

Reaction of *diphenylstannane* **44 with 10:** A yellow precipitate was obtained. The precipitate was filtered and dissolved in THF. The ^{119}Sn NMR spectra showed several unidentified peaks: -110.1 ppm, -125.2 ppm, -172.2 ppm, -205.9 ppm, -215.8 ppm.

$1,1,2,2,3,3,4,4$-*octa-phenyl*-$1,2$-*bis*-(*ethylzincio*)*tetrastannane* *$2TMEDA$ crystallized from the THF solution. Due to instability no NMR data of the crystal structure could be obtained.

Reaction of *di-p-tolylstannane* **50 with 10:** A yellow precipitate was obtained. The solution did not show any signal in ^{119}Sn NMR.

7.2.4 Dehydrogenative coupling of stannanes

Reaction of trialkylstannane with TMEDA 31: Trialkylstannane was dissolved in 30 mL diethylether. An equimolar amount of **31** was added. The reaction was stirred overnight at room temperature.

Tributylstannane **13:** ^{119}Sn NMR showed one signal at -90.35 ppm presumably the educt.

Triphenylstannane **45:** ^{119}Sn NMR showed one signal at -165.43 ppm presumably the educt.

Dehydrogenative coupling of dialkylstannanes with TMEDA 31: 0.1g dialkylstannane was dissolved in 10 mL ether. TMEDA was added equimolar. The reaction was stirred for 2 hours. The solvent was evaporated and the remaining product was cleaned by drying in vacuum for 12 hours.

Di^{t}butylstannane: A light yellow precipitate was observed. There were no signals in ^{119}Sn NMR spectra.

Dibutylstannane: A light yellow precipitate was observed. There were no signals in ^{119}Sn NMR spectra.

Diphenylstannane: A yellow precipitate was observed. There were no signals in ^{119}Sn NMR spectra.

CHN analysis: Found: C, 50.55%; H, 3.9%; $(C_{12}H_{10}Sn)_n$ (MM: 272.92*n g mol$^-$1) required: C, 52.81%; H, 3.69%;

Di-o-tolylstannane: An orange precipitate was observed. There were no signals in ^{119}Sn NMR spectra.

CHN analysis: Found: C, 45.56%; H, 5.84%; $(C_{14}H_{14}Sn)_n$ (MM: 300.98*n g mol^{-}1) required: C, 55.87%; H, 4.69%;

Bis-(butylphenyl)-stannane: The solution turned yellow. After removing the solvent a highly viscous oil was obtained.

^{119}Sn NMR (111.96 MHz, $CDCl_3$): δ = -196.7 ppm

CHN analysis: Found: C, 63.02%; H, 6.90%; $(C_{20}H_{26}Sn)_n$ (MM: 385.14*n g mol^{-}1) required: C, 62.37%; H, 6.80%;

Appendix A

Abbreviations

A.1 Abbreviations

d	days
h	hours
min	minutes
EA	elemental analysis (carbon, hydrogen, nitrogen)
MM	molar mass
IR	infra red
VIS	visible light
UV	ultra violet
MS	mass spectroscopy
M/z	mass per charge
GPC	gel permeation chromatography
TGA	thermal gravimetric analysis
DSC	differential scanning calorimetry
XRD	X-ray diffraction
ESR/EPR	electronic paramagnetic resonance
NMR	nuclear magnetic resonance spectroscopy
δ	chemical shift
${}^{n}J$	coupling constant through n bondings
Hz	Herz
mHz	Megaherz
ppm	parts per million
s	singlet (NMR)
d	duplet (NMR)
t	triplet (NMR)
q	quadruplet (NMR)

m	multiplet (NMR)
mp	melting point
bp	boiling point
Dt	decomposition temperature
rt	room temperature
°C	degree Celsius
max	maximum
Pa	pascal
ID	identification number
μm	micrometer
g	gramme
l	liter
ml	milliliter
R	alkyl
Ar	aryl
LAH	lithiumalluminumhydride
CN	coordination number
cf	convergence failure
DFT	density functional theorie
HF	Hartree Fock

A.2 Chemical short names

abrevision	fragmentname	fragmentpicture
Me	methyl	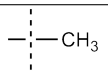
Et	ethyl	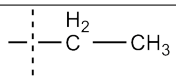
nPr	propyl	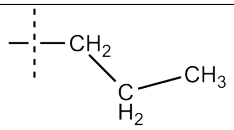
iPr	iso-propyl	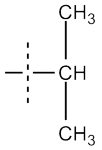
nBu	butyl	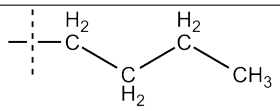
^{t}Bu	^{t}butyl	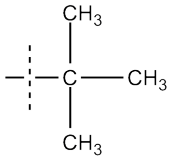

abrevision	fragmentname	fragmentpicture
^{t}Am	^{t}amyl	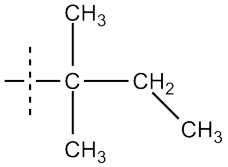
nHe	hexyl	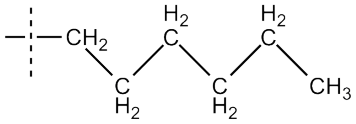
Ph	phenyl	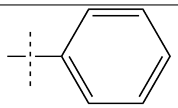
p-Tol	para-tolyl	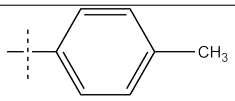
m-Tol	metha-tolyl	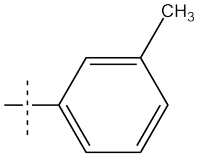
o-Tol	ortho-tolyl	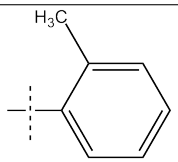
Mes	mesityl	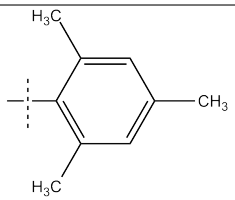
Supmes	supermesityl	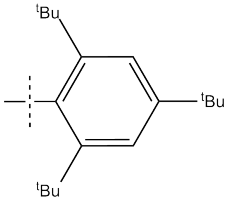
Phen	phenantryl	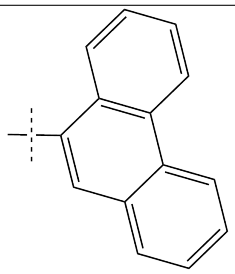

abrevision	fragmentname	fragmentpicture
TMS	trimethylsilyl	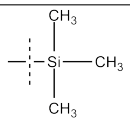
TMEDA	tetramethylethylenediamine	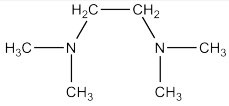

Appendix B

Crystal tabular

B.1 Crystal structures of chapter

Table B.1: Crystal structure data of *di-p-tolyldichlorostannane* **48**, *di-m-tolyldichlorostannane* **51** and 3, 5-*dimethylphenyltrichlorostannane*acetone* **60**

compound	$p-Tol_2SnCl_2$	$m-Tol_2SnCl_2$	$Me_2PhSnCl_3$ $^*C_3H_6O$
empirical formula	$C_{14}H_{14}SnCl_2$	$C_{14}H_{14}SnCl_2$	$C_{11}H_{15}OSnCl_3$
formula weight	371.86	371.86	388.30
temperature	$100(2)K$	$293(2)K$	$100(2)K$
wavelength	0.71073	0.71073	0.71073
crystal system	monoclinic	orthorhombic	monoclinic
space group	C2/c	Pbca	P2(1)/c
Unit cell dimensions	$a = 19.4075(8)$	$a = 9.5456(6)$	$a = 13.5503(9)$
	$b = 6.6000(3)$	$b = 9.2428(6)$	$b = 8.7844(6)$
	$c = 23.1379(10)$	$c = 32.636(2)$	$c = 13.0869(9)$
	$\alpha = 90°$	$\alpha = 90°$	$\alpha = 90.00°$
	$\beta = 94.406(2)°$	$\beta = 90°$	$\beta = 109.919(2)°$
	$\gamma = 90°$	$\gamma = 90°$	$\gamma = 90.00°$
Volume	$2955.0(2)^3$	$2879.4(3)^3$	$1464.56(17)^3$
Z	8	8	4
Density (calculated)	$1.672Mgm^{-3}$	$1.716Mgm^{-3}$	$1.761Mgm^{-3}$
Absorption coefficient	$2.067mm^{-1}$	$2.121mm^{-1}$	$2.270mm^{-1}$
F(000)	1456	1456	760
Crystal size	$0.36x0.27x0.12$ mm^3	$0.45x0.07x0.06$ mm^3	$0.84x0.63x0.47$ mm^3
Theta range for data collection	1.77 to 34.99°	2.47 to 30.00°	1.60 to 30.00
Index ranges	$-31 \leq h \leq 31$, $-7 \leq k \leq 10$, $-37 \leq l \leq 37$	$-13 \leq h \leq 13$, $-13 \leq k \leq 12$, $-45 \leq l \leq 45$	$-19 \leq h \leq 19$, $-12 \leq k \leq 12$, $-18 \leq l \leq 18$

compound	$p-Tol_2SnCl_2$	$m-Tol_2SnCl_2$	$Me_2PhSnCl_3{*}C_3H_6O$
Reflections collected	13988	37038	57166
Independent reflections	944 [R(int) = 0.0232]	4205 [R(int) = 0.0498]	4281 [R(int) = 0.0352]
Completeness to θ_{max}	100.0%	100.0%	100.0%
Absorption correction	SADABS multi-scan	SADABS multi-scan	SADABS multi-scan
Refinement method	Full-matrix least-squares on F^2	Full-matrix least-squares on F^2	Full-matrix least-squares on F^2
Data / restraints / parameters	944 / 0 / 154	4205 / 0 / 156	4281 / 0 / 150
Goodness-of-fit on F2	1.100	1.055	1.246
Final R indices [I>2sigma(I)]	R1 = 0.0104, wR2 = 0.0251	R1 = 0.0310, wR2 = 0.0577	R1 = 0.0192, wR2 = 0.0472
R indices (all data)	R1 = 0.0106, wR2 = 0.0252	R1 = 0.0439, wR2 = 0.0621	R1 = 0.0205, wR2 = 0.0476
Largest diff. peak and hole	3.561 and -1.154 $e^{\circ}-3$	0.853 and -0.669 $e^{\circ}-3$	0.618 and -0.558 $e^{\circ}-3$

B.2 Crystal structures of chapter

Table B.2: Crystal structure data of $1,1,2,2,3,3,4$-*hepta*^{t}*butyl*-4-*methyltetrastannacyclobutane* **64** and $1,1,2,2,3,3,4$-*hepta*^{t}*butyl*-4-*chloroporpyltetrastannacyclobutane* **67**

compound	$^tBu_7Sn_4Me$	$^tBu_7Sn_4C_3H_6Cl$
empirical formula	$C_{29}H_{66}Sn_4$	$C_{31}H_{69}ClSn_4$
formula weight	889.58	952.18
temperature	$100(2)K$	$193(2)K$
wavelength	0.71073 .	0.71073
crystal system	triclinic	monoclinic
space group	P-1	P2(1)/n
Unit cell dimensions	$a = 17.1953(7)$	$a = 11.2394(4)$
	$b = 17.4677(15)$	$b = 16.9307(7)$
	$c = 21.5922(9)$	$c = 21.6409(9)$
	$\alpha = 105.242(2)^{\circ}$	$\alpha = 90^{\circ}$
	$\beta = 111.8510(10)^{\circ}$	$\beta = 100.670(2)^{\circ}$
	$\gamma = 99.053(2)^{\circ}$	$\gamma = 90^{\circ}$
Volume	$5567.0(6)^3$	$4046.9(3)^3$
Z	6	4

compound	$^tBu_7Sn_4Me$	$^tBu_7Sn_4C_3H_6Cl$
Density (calculated)	$1.592Mgm^{-3}$	$1.564Mgm^{-3}$
Absorption coefficient	$2.674mm^{-1}$	$2.522mm^{-1}$
F(000)	2640	1892
Crystal size	$0.60x0.43x0.28mm^3$	$0.25x0.20x0.10mm^3$
Theta range for data collection	1.26 to 30.00°	1.54 to 23.57°.
Index ranges	$-24 \leq h \leq 24$, $-23 \leq k \leq 24$, $-30 \leq l \leq 30$	$-12 \leq h \leq 12$, $-18 \leq k \leq 18$, $-24 \leq l \leq 24$
Reflections collected	128359	121428
Independent reflections	32387 [R(int) = 0.0340]	5953 [R(int) = 0.0864]
Completeness to θ_{max}	99.7%	98.7%
Absorption correction	SADABS multi-scan	SADABS multi-scan
Refinement method	Full-matrix least-squares on F^2	Full-matrix least-squares on F^2
Data / restraints / parameters	32387 / 0 / 958	5953 / 0 / 346
Goodness-of-fit on F2	1.087	1.059
Final R indices [I>2sigma(I)]	R1 = 0.0363, wR2 = 0.0848	R1 = 0.0227, wR2 = 0.0402
R indices (all data)	R1 = 0.0482, wR2 = 0.0958	R1 = 0.0364, wR2 = 0.0457
Largest diff. peak and hole	3.119 and -1.607 $e.^{-3}$	0.401 and -0.433 $e.^{-3}$

Table B.3: Crystal structure data of 1-*chloro*-1, 2, 2, 3, 3, 4, 4-*hepta*^{t}*butyltetrastannacyclobutane* **71** and 1-*bromo*-1, 2, 2, 3, 3, 4, 4-*hepta*^{t}*butyltetrastannacyclobutane* **72**

compound	$^tBu_7Sn_4Cl$	$^tBu_7Sn_4Br$
empirical formula	$C_{28}H_{63}ClSn_4$	$C_{28}H_{63}BrSn_4$
formula weight	909.99	954.44
temperature	$100(2)K$	$100(2)K$
wavelength	0.71073	0.71073
crystal system	monoclinic	monoclinic
space group	P21	P21

compound	$^tBu_7Sn_4Cl$	$^tBu_7Sn_4Br$
Unit cell dimensions	$a = 11.0241(10)$	$a = 11.0225(6)$
	$b = 15.8630(10)$	$b = 15.8499(9)$
	$c = 11.7906(10)$	$c = 11.7801(7)$
	$\alpha = 90°$	$\alpha = 90.00°$
	$\beta = 116.608(4)°$	$\beta = 116.722(2)°$
	$\gamma = 90°$	$\gamma = 90.00°$
Volume	$1843.5(3)^3$	$1838.25(18)^3$
Z	2	2
Density (calculated)	$1.639Mgm^{-3}$	$1.724Mgm^{-3}$
Absorption coefficient	$2.764mm^{-1}$	$3.786mm^{-1}$
F(000)	896	932
Crystal size	$0.22x0.21x0.16mm^3$	$0.15x0.14x0.08mm^3$
Theta range for data collection	2.07 to 30.00°	1.94 to 30.00°
Index ranges	$-13 \leq h \leq 15$,	$-15 \leq h \leq 15$,
	$-22 \leq k \leq 21$,	$-22 \leq k \leq 22$,
	$-16 \leq l \leq 16$	$-16 \leq l \leq 16$
Reflections collected	31089	10628
Independent reflections	10284[R(int) = 0.0226]	10336 [R(int) = 0.0306]
Completeness to θ_{max}	99.9%	99.8%
Absorption correction	SADABS multi-scan	SADABS multi-scan
Refinement method	Full-matrix least-squares on F^2	Full-matrix least-squares on F^2
Data / restraints / parameters	10284/1/320	10628 / 1 / 320
Goodness-of-fit on F2	1.036	1.014
Final R indices [I>2sigma(I)]	R1 = 0.0190, wR2 = 0.0452	R1 = 0.0155, wR2 = 0.0372
R indices (all data)	R1 = 0.0195, wR2 = 0.0454	R1 = 0.0166, wR2 = 0.0375
Largest diff. peak and hole	1.775 and -0.748 $e.^{-3}$	0.802 and -0.843 $e.^{-3}$

B.3 Crystal structures of chapter

Table B.4: Crystal structure data of *di-p-tolylmagnesium**$TMEDA$ **80**

compound	p-Tol_2Mg*$TMEDA$
empirical formula	$C_{20}H_{30}MgN_2$
formula weight	322.78
temperature	$104(2)K$
wavelength	0.71073
crystal system	monoclinic
space group	C2/c
Unit cell dimensions	$a = 19.1148(7)$
	$b = 12.7490(5)$
	$c = 16.3176(6)$
	$\alpha = 90.00°$
	$\beta = 92.009(2)°$
	$\gamma = 90.00°$
Volume	$3974.1(3)^3$
Z	8
Density (calculated)	$1.079Mgm^{-3}$
Absorption coefficient	$0.091mm^{-1}$
F(000)	1408
Crystal size	$0.40x0.38x0.26mm^3$
Theta range for data collection	1.92 to 30.00°
Index ranges	$-26 \leq h \leq 26$,
	$-17 \leq k \leq 17$,
	$-22 \leq l \leq 22$
Reflections collected	66520
Independent reflections	5792 [R(int) = 0.0322]
Completeness to θ_{max}	99.8%
Absorption correction	SADABS multi-scan
Refinement method	Full-matrix least-squares on F^2
Data / restraints / parameters	5792 / 0 / 215
Goodness-of-fit on F2	1.018
Final R indices [I>2sigma(I)]	R1 = 0.0430, wR2 = 0.1140
R indices (all data)	R1 = 0.0601, wR2 = 0.1277
Largest diff. peak and hole	0.417 and -0.253 $e.^{-3}$

Table B.5: Crystal structure data of $1,1,1,2,3,3,3$-*heptaphenyl-(ethylzincio)-tristannane*$*TMEDA$ **75**, $1,1,2,2,3,3,4,4$-*octaphenyl-bis-(ethylzincio)tetrastannane*$*2TMEDA$ **76** and *tripheny-(ethylzincio)stannane*$*TMEDA$ **77**

compound	$(Ph_3Sn)_2PhSnZnEt$ $*TMEDA$	$Ph_8Sn_4Zn_2Et_2*$ $2TMEDA$	$Ph_3SnZnPh*$ $TMEDA$
empirical formula	$C_{50}H_{56}N_2Sn_3Zn$	$C_{64}H_{82}N_4Sn_4Zn_2$	$C_{30}H_{36}N_2SnZn$
formula weight	1106.53	1513.00	608.73
temperature	$100(2)K$	$100(2)K$	$100(2)K$
wavelength	0.71073	0.71073	0.71073
crystal system	orthorhombic	monoclinic	monoclinic
space group	Pna2(1)	P2(1)/c	P2(1)/c
Unit cell dimensions	$a = 25.6055(15)$	$a = 10.2112(9)$	$a = 17.3427(15)$
	$b = 11.2156(7)$	$b = 16.1023(16)$	$b = 11.6801(10)$
	$c = 16.4924(10)$	$c = 21.587(2)$	$c = 16.8004(15)$
	$\alpha = 90°$	$\alpha = 90°$	$\alpha = 90.00°$
	$\beta = 90°$	$\beta = 90.690(4)°$	$\beta = 110.549(3)°$
	$\gamma = 90°$	$\gamma = 90°$	$\gamma = 90.00°$
Volume	$4736.3(5)^3$	$3549.1(6)^3$	$3186.6(5)^3$
Z	8	3	4
Density (calculated)	$1.643Mgm^{-3}$	$1.557Mgm^{-3}$	$1.419Mgm^{-3}$
Absorption coefficient	$2.593mm^{-1}$	$2.129mm^{-1}$	$1.564mm^{-1}$
F(000)	2320	1740	1400
Crystal size	$0.16x0.14x0.07$ mm^3	$0.45x0.07x0.06$ mm^3	$0.34x0.12x0.08$ mm^3
Theta range for data collection	2.34 to 28.35°	1.89 to 29.62°	2.15 to 25.00
Index ranges	$-34 \leq h \leq 34$, $-14 \leq k \leq 14$, $-20 \leq l \leq 21$	$-11 \leq h \leq 13$, $-22 \leq k \leq 22$, $-29 \leq l \leq 29$	$-0 \leq h \leq 20$, $-13 \leq k \leq 0$, $-19 \leq l \leq 18$
Reflections collected	76110	70404	5269
Independent reflections	11315 [R(int) = 0.0331]	9745 [R(int) = 0.0198]	5269 [R(int) = 0.0672]

compound	$(Ph_3Sn)_2PhSnZnEt$ *$TMEDA$	$Ph_8Sn_4Zn_2Et_2$* 2$TMEDA$	$Ph_3SnZnPh$* $TMEDA$
Completeness to θ_{max}	99.3%	97.5%	99.8%
Absorption correction	SADABS multi-scan	SADABS multi-scan	SADABS multi-scan
Refinement method	Full-matrix least-squares on F^2	Full-matrix least-squares on F^2	Full-matrix least-squares on F^2
Data / restraints / parameters	11315 / 1 / 511	9745 / 2 / 387	5269 / 0 / 357
Goodness-of-fit on F2	0.986	1.090	1.062
Final R indices [I>2sigma(I)]	R1 = 0.0240, wR2 = 0.0519	R1 = 0.0347, wR2 = 0.0905	R1 = 0.0565, wR2 = 0.1038
R indices (all data)	R1 = 0.0308, wR2 = 0.0548	R1 = 0.0451, wR2 = 0.1000	R1 = 0.0980, wR2 = 0.1127
Largest diff. peak and hole	0.818 and -0.652 $e.^{-3}$	2.601 and -1.575 $e.^{-3}$	0.953 and -0.822 $e.^{-3}$

Appendix C

Reagents, products and solvents

C.1 Solvents

name	short	formula	vendor
tetrahydrofurane	THF	C_4H_8O	Fischer Sci
diethylether	Et_2O	$C_2H_5OC_2H_5$	Roth
pentane	*pentane*	C_5H_{12}	Roth
hexane	*hexane*	C_6H_{14}	Roth
heptane	*heptane*	C_7H_{16}	Roth
toluene	*toluene*	C_6H_5Me	Brenntag
acetone	*acetone*	C_3H_6O	Brenntag
ethanol	$EtOH$	C_2H_5OH	Roth
chloroform	$CHCl_3$	$CHCl_3$	Fluka
tetrachloromethane	CCl_4	CCl_4	Merck
d-chloroform	$CDCl_3$	$CDCl_3$	deutero
heavy water	D_2O	D_2O	deutero

C.2 Reagents

ID	name	formula	vendor
1	*magnesium*	Mg	Aldrich
2	*lithium*	Li	Aldrich
3	*zinc*	Zn	Riedel de Häen
4	*calciumchloride*	$CaCl_2$	Riedel de Häen
5	*sodiumtatrate*	$Na_2C_4H_6O_6$	Merck
6	*lithiumaluminimhydride*	$LiAlH_4$	Aldrich
7	^{t}*butyllithium*	^tBuLi	Aldrich

ID	name	formula	vendor
8	*butyllithium*	$BuLi$	Aldrich
9	*dibutylmagnesium*	Bu_2Mg	Acros
10	*diethylzinc*	Et_2Zn	Aldrich
11	*tetrachlorostannane*	$SnCl_4$	Riedel de Häen
12	*triphenylchlorostannane*	Ph_3SnCl	Aldrich
13	*tributylstannane*	Bu_3SnH	Fluka
14	*dimethylsulfate*	Me_2SO_4	Aldrich
15	$1,2$-*dibromoethane*	$C_2H_4Br_2$	Merck
16	*bromoethane*	C_2H_5Br	Fluka
17	3-*bromopropene*	C_3H_5Br	Merck
18	1-*chloropropane*	C_3H_7Cl	Riedel de Häen
19	$1,2$-*dichloropropane*	$C_3H_6Cl_2$	ACROS
20	$1,2$-*dibromopropane*	$C_3H_6Br_2$	Merck
21	$1,3$-*dichloropropane*	$C_3H_6Cl_2$	Fluka
22	$1,4$-*dichlorobutine*	$C_4H_4Cl_2$	Fluka
23	$1,5$-*dichloropentane*	$C_5H_{10}Cl_2$	Aldrich
24	$1,6$-*dibromohexane*	$C_6H_{12}Cl_2$	Aldrich
25	^{t}*butylchloride*	^tBuCl	Fluka
26	4-*bromotoluene*	C_7H_7Br	Aldrich
27	3-*bromotoluene*	C_7H_7Br	Aldrich
28	2-*bromotoluene*	C_7H_7Br	Aldrich
29	1-*bromo*-$3,5$-*dimethylbenzene*	C_8H_9Br	Aldrich
30	1-*bromo*-4-*butylbenzene*	$C_{10}H_{13}Br$	Aldrich
31	*tetramethylethylenediamine*	$Me_4N_2C_2H_4$	Aldrich
32	*pyridine*	C_5H_5N	Acros
33	*triethylamine*	C_6H_15N	Merck
34	*lithiumcarbonate*	Li_2CO_3	Merck

C.3 list of chemical compounds

ID	name	formula	compound
35	*di-^{t}butyl-dichlorostannane*	$^tBu_2SnCl_2$	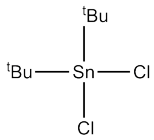
36	*di-^{t}butylstannane*	$^tBu_2SnH_2$	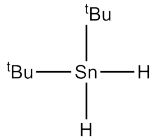
37	*tri-^{t}butyl-chlorostannane*	$^tBu_3SnCl$	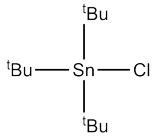
38	*hexa-^{t}butyldistannane*	$^tBu_6Sn_2$	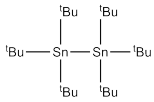
39	*di-butyldichlorostannane*	Bu_2SnCl_2	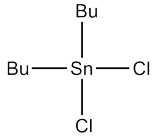
40	*di-butylstannane*	Bu_2SnH_2	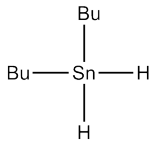
41	$1,1,2,2$-*tetra-^{t}butyldistannane*	$^tBu_4Sn_2H_2$	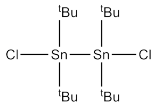
42	*deca-butyl-penta-stannacyclopentane*	$Bu_{10}Sn_5$	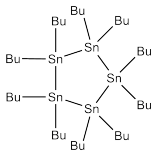
43	*di-phenyl-dichlorostannane*	Ph_2SnCl_2	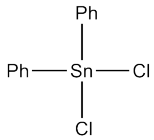

ID	name	formula	compound
44	*di-phenylstannane*	Ph_2SnH_2	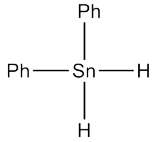
45	*tri-phenylstannane*	Ph_3SnH	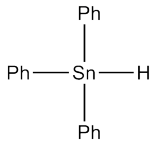
46	*hexa-phenyldistannane*	Ph_6Sn_2	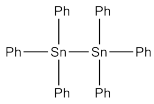
47	*dodeca-phenylhexastannacyclohexane*	$Ph_{12}Sn_6$	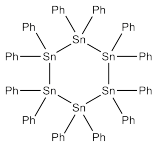
48	*di-p-tolyl-dichlorostannane*	$p-Tol_2SnCl_2$	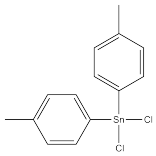
49	*tetra-p-tolylstannane*	$p-Tol_4Sn$	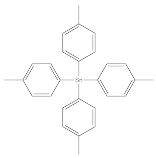
50	*di-p-tolylstannane*	$p-Tol_2SnH_2$	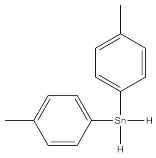
51	*di-m-tolyldichlorostannane*	$m-Tol_2SnCl_2$	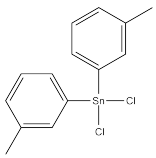
52	*tetra-m-tolylstannane*	$m-Tol_4Sn$	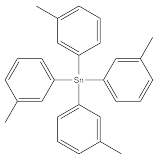

ID	name	formula	compound
53	*di-o-tolyldichlorostannane*	$o-Tol_2SnCl_2$	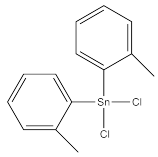
54	*tetra-o-tolylstannane*	$o-Tol_4Sn$	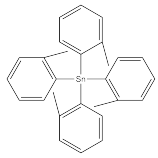
55	*di-o-tolylstannane*	$o-Tol_2SnH_2$	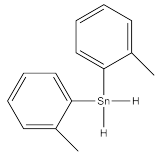
56	*bis-(p-butylphenyl)-dichlorostannane*	$(BuPh)_2SnCl_2$	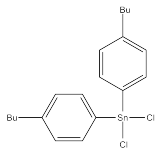
57	*tetrakis-(p-butylphenyl)-stannane*	$(BuPh)_4Sn$	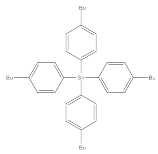
58	*bis-(p-butylphenyl)-stannane*	$(BuPh)_2SnH_2$	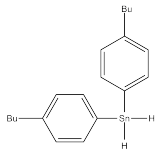
59	*bis-(3,5-dimethylphenyl)-dichlorostannane*	$(Me_2Ph)_2SnCl_2$	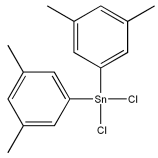
60	*3,5-dimethylphenyldichloro-stannane*acetone*	$(Me_2Ph)SnCl_3$* *acetone*	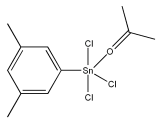
61	*octa-^{t}butyl-tetrastannacyclobutane*	$^tBu_8Sn_4$	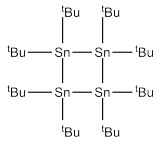

ID	name	formula	compound
62	1, 1, 2, 2, 3, 3, 4-*hepta-*^{t}*butyl-4-chloromagnesiotetrastanna-cyclobutane*	$^tBu_7Sn_4MgCl$	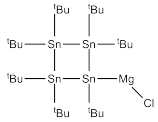
63	1, 1, 2, 2, 3, 3, 4-*hepta-*^{t}*butyl-4-lithiotetrastannacyclobutane*	$^tBu_7Sn_4Li$	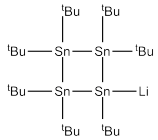
64	1, 1, 2, 2, 3, 3, 4-*hepta-*^{t}*butyl-4-methyltetrastannacyclobutane*	$^tBu_7Sn_4Me$	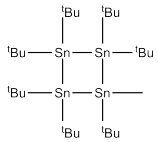
65	1, 1, 2, 2, 3, 3, 4-*hepta-*^{t}*butyl-4-ethyltetrastannacyclobutane*	$^tBu_7Sn_4Et$	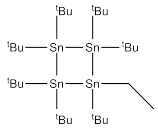
66	1, 1, 2, 2, 3, 3, 4-*hepta-*^{t}*butyl-4-propyltetrastannacyclobutane*	$^tBu_7Sn_4Pr$	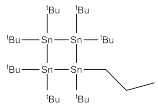
67	1, 1, 2, 2, 3, 3, 4-*hepta-*^{t}*butyl-4-chloropropyltetrastanna-cyclobutane*	$^tBu_7Sn_4C_3H_6Cl$	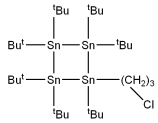
68	1, 1, 2, 2, 3, 3, 4-*hepta-*^{t}*butyl-4-chloropentyltetrastanna-cyclobutane*	$^tBu_7Sn_4C_5H_{10}Cl$	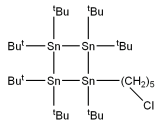
69	1, 1, 2, 2, 3, 3, 4-*hepta-*^{t}*butyl-4-chlorohexyltetrastanna-cyclobutane*	$^tBu_7Sn_4C_6H_{12}Cl$	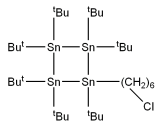
70	1, 6-*bis-*(1, 1, 2, 2, 3, 3, 4-*hepta-*^{t}*butyltetrastanna-cyclobutanyl)-hexane*	$(^tBu_7Sn_4)_2C_6H_{12}$	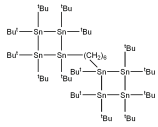

ID	name	formula	compound
71	1-*chloro*-1, 2, 2, 3, 3, 4, 4-*hepta-* ^{t}*butyltetrastannacyclobutane*	$^{t}Bu_7Sn_4Cl$	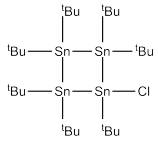
72	1-*bromo*-1, 2, 2, 3, 3, 4, 4-*hepta-* ^{t}*butyltetrastannacyclobutane*	$^{t}Bu_7Sn_4Br$	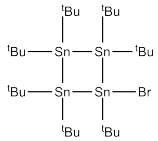
73	*triphenyl-(ethylzincio)stannane*	$(Ph_3Sn)ZnEt$	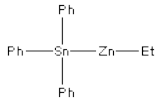
74	1, 1, 2, 2, 2-*penta-phenyl*-1-(*ethylzincio*)-*distannane***TMEDA*	$Ph_3SnPh_2SnZnEt$* $TMEDA$	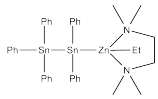
75	1, 1, 1, 2, 3, 3, 3-*hepta-phenyl*-2-(*ethylzincio*)-*tristannane***TMEDA*	$(Ph_3Sn)_2PhSnZnEt$* $TMEDA$	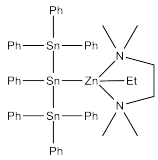
76	1, 1, 2, 2, 3, 3, 4, 4-*octa-phenyl*-1, 2-*bis*-(*ethylzincio*)*tetra-stannane**2*TMEDA*	$(Ph_2Sn)_4(ZnEt)_2$* 2$TMEDA$	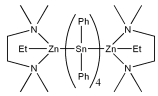
77	*triphenyl-(phenylzincio)stannane** $TMEDA$	$Ph_3SnZnPh$*$TMEDA$	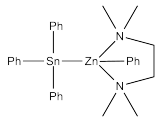
78	1, 2-*bis*-(*butylmagnesio*)-1, 1, 2, 2-*tetra*^{t}*butyldistannane*	$(^{t}Bu_4Sn_2(BuMg)_2$	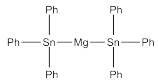
79	*bis*-(*triphenylstannyl*)-*magnesium*	$(Ph_3Sn)_2Mg$	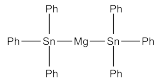
80	*di-p-tolylmagnesium** $TMEDA$	$p - Tol_2Mg$* $TMEDA$	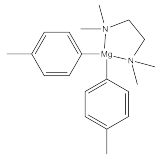

List of Figures

List of Tables

Bibliography

[1] J R Babcock and L R Sita. *Journal of American Chemical Society*, 118:12481–12482, 1996.

[2] R Becerra, P P Gaspar, C R Harrington, W J Leigh, I Vargas-Baca, R Walsh, and D Zhou. *Journal of American Chemical Society*, 127:17469–17478, 2005.

[3] V K Belsky, N N Zemlyansky, N D Kolosova, and L V Borisova. *Journal of Organometallic Chemistry,*, 215:41–48, 1981.

[4] P Braunstein and X Morise. *Organometallics*, 17:540–550, 1998.

[5] P Brown, M F Mahon, and K C Molloy. *Journal of Organometallic Chemistry*, 435:265–273, 1992.

[6] T L Brown and G L Morgan. *Inorganic Chemistry*, 2(4):736–740, 1962.

[7] C J Cardin, D J Cardin, M A Convery, M M Devereux, and N B Kelly. *Journal of Organometallic Chemistry*, 414:C9–C11, 1991.

[8] H M J C Creemers, J G Noltes, and G J M Van der Kerk. *Journal of Organometallic Chemistry*, 14:217–221, 1968.

[9] A G Davies, editor. Wiley-VCH Verlag GmbH & Co., Weinheim, 2004.

[10] A G Davies, M Gielen, K H Pannell, and E R Tiekink, editors. John Wiley & Sons, Ltd, Chichester, West Sussex, PO19 8SQ, United Kingdom, 1st edition, 2008.

[11] K Decker. PhD thesis, Graz University of Technologie, 2007.

[12] F J A Des Tombe and G J M Van der Kerk. *Chemical communications*, 24:914–915, 1966.

[13] F J A Des Tombe, G J M Van der Kerk, H M J C Creemers, N A D Carey, and J G Noltes. *Journal of Organometallic Chemistry*, 44:247–252, 1972.

[14] F J A Des Tombe, G J M Van der Kerk, and J G Noltes. *Journal of Organometallic Chemistry*, 13:P9–P12, 1968.

[15] F J A Des Tombe, G J M Van der Kerk, and J G Noltes. *Journal of Organometallic Chemistry*, 43, 1972.

[16] U Englich, U Hermann, I Prass, T Schollmeier, K Ruhlandt-Senge, and F Uhlig. *Journal of Organometallic Chemistry*, 646:271–276, 2002.

[17] U Englich, K Ruhlandt-Senge, and F Uhlig. *Journal of Organometallic Chemistry*, 613:139–147, 2000.

[18] H Eriksson, M Örtendahl, and M Hå kansson. *Organometallics*, 15:4823–4831, 1996.

[19] W V Farrar and H A Skinner. *Journal of Organometallic Chemistry,*, 1:434–436, 1964.

[20] J M Goicoechea and S C Sevov. *Organometallics*, 25:4530–4536, 2006.

[21] P T Greene and R F Bryan. *Inorganic physical theory*, A:2549–2554, 1971.

[22] J T B H Jastrzebski, H A J Sypkens, F J A des Tombe, P A van der Schaaf, J Boersma, and G van Koten. *Journal of Organometallic Chemistry*, 396:25–31, 1990.

[23] K A Kocheshkov and A N Nesmeyanov. *Journal of Russian Physical-Chemical Society*, 62:1795–1812, 1930.

[24] J C Lahournère and J Valade. *Journal of Organometallic Chemistry,*, 22:C3–C4, 1970.

[25] J C Lahournère and J Valade. *Journal of Organometallic Chemistry,*, 33:C7–C10, 1971.

[26] J C Lahournère and J Valade. *Journal of Organometallic Chemistry,*, 33:C4–C6, 1971.

[27] M-L Lechner, K Fürpass, J Sykora, R C Fischer, Albering J, and F Uhlig. *Journal of Organometallic Chemistry*, 694:4209–4215, 2009.

[28] V Y Lu and T D Tilley. *Macromolecules*, 29:5763–5764, 1996.

[29] V Y Lu and T D Tilley. *Macromolecules*, 33:2403–2412, 2000.

[30] M Lutz, B Findeis, M Haukka, R Graff, T A Pakkanen, and L H Gade. *Journal of Europien Chemistry*, 8(14):3269–3276, 2002.

[31] S P Mallela, Y Saar, S Hill, and R A Geanangel. *Inorganic Chemistry*, 38:2957–2960, 1999.

[32] P R Markies, O S Akkerman, and F Bickelhaupt. *Organometallics*, 13(2616-2627), 1994.

[33] P R Markies, T Nomoto, O S Akkerman, and F Bickelhaupt. *Journal of American Chemical Society*, 110:4845–4846, 1988.

[34] P R Markies, T Nomoto, G Schat, O S Akkerman, and F Bickelhaupt. *Organometallics*, 10:3826–3837, 1991.

[35] P R Markies, G Schat, O S Akkerman, and F Bickelhaupt. *Organometallics*, 9:2243–2247, 1990.

[36] S Masamune and L R Sita. *Journal of American Chemical Society*, 107:6390–6391, 1985.

[37] W P Neumann and J Fu. *Journal of Organometallic Chemistry*, 273:295–302, 1984.

[38] W P Neumann, J Pedain, and R Sommer. *Justus Liebigs Annalen der Chemie*, 694:9 – 18, 1966.

[39] M Okano, N Matsumoto, M Arakawa, T Tsuruta, and H Hamano. *Chemical Communications*, 17:1799–1800, 1998.

[40] H Puff, C Bach, H Reuter, and W Schuh. *Journal of Organometallic Chemistry*, 277:17 – 28, 1984.

[41] H Puff, C Bach, W Schuh, and R Zimmer. *Journal of Organometallic Chemistry*, 312:313–322, 1986.

[42] H Puff, B Breuer, W Schuh, R Sievers, and R Zimmer. *Journal of Organometallic Chemistry*, 332:279–288, 1987.

[43] H Puff, W Schuh, W Wald, and G Weidenbrück. *Journal of Organometallic Chemistry*, 363:265–280, 1989.

[44] N Scotti, U Zachwieja, and H Jacobs. *Zeitschrift für anorganische und allgemeine Chemie*, 623:1503–1505, 1997.

[45] H K Sharma, F Cervantes-Lee, J S Mahmoud, and K H Pannell. *Organometallics*, 18:399–403, 1999.

[46] L R Sita and I Kinoshita. *Journal of American Chemical Society*, 114(18):7024–7029, 1992.

[47] C Tamborski and E J Soloski. *Journal of American Chemical Society*, 83:3734, 1961.

[48] D Thoennes and E Weiss. *Chemische Berichte*, 111(10):3381–3384, 1978.

[49] K M Waggoner and P P Power. *Organometallics*, 11(10):3209–3214, 1992.

[50] R J Wehmschulte and P P Power. *Organometallics*, 14:3264–3267, 1995.

[51] M Weidenbruch, K Schäfers, S Pohl, W Saak, K Peters, and H G von Schnering. *Journal of Organometallic Chemistry*, 346:171–180, 1988.

[52] K Wiesler and N Korber. *Zeitschrift Kristallografie*, 220:188–191, 2005.

[53] K Wiesler, C Suchentrunk, and N Korber. *Helvetica Chimica Acta*, 89:1158–1168, 2006.

[54] B Wrackmeyer. *Annual reports on NMR Spectroscopie*, 16:73–186, 1985.